CHALMERS
UNIVERSITY OF TECHNOLOGY

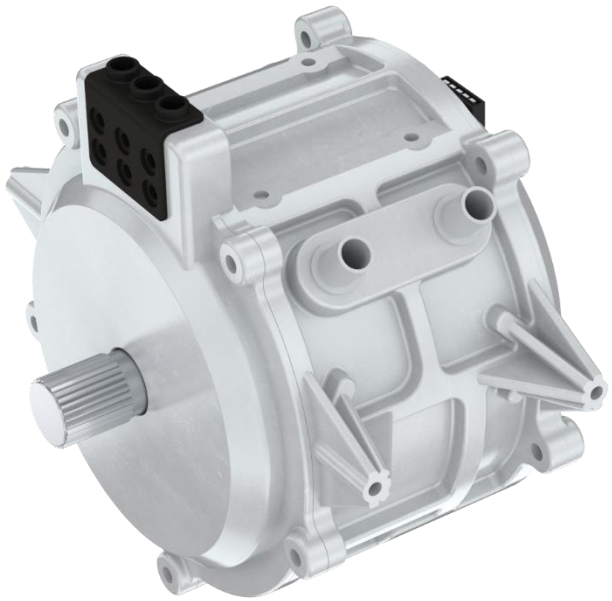

A Scalable Life Cycle Inventory of an Electrical Automotive Traction Machine

Technical and Methodological Description, version 1.01

ANDERS NORDELÖF
EMMA GRUNDITZ
ANNE-MARIE TILLMAN
TORBJÖRN THIRINGER
MIKAEL ALATALO

Divisions of Environmental Systems Analysis & Electric Power Engineering
CHALMERS UNIVERSITY OF TECHNOLOGY
Gothenburg, Sweden 2017
Report No. 2016:4 (1.01)

Report 2016:4 (1.01)

A Scalable Life Cycle Inventory of an Electrical Automotive Traction Machine

Technical and Methodological Description, Version 1.01

ANDERS NORDELÖF
Division of Environmental Systems Analysis
Chalmers University of Technology
anders.nordelof@chalmers.se

EMMA GRUNDITZ
Division of Electric Power Engineering
Chalmers University of Technology

ANNE-MARIE TILLMAN
Division of Environmental Systems Analysis
Chalmers University of Technology

TORBJÖRN THIRINGER
Division of Electric Power Engineering
Chalmers University of Technology

MIKAEL ALATALO
Division of Electric Power Engineering
Chalmers University of Technology

Department of Technology Management and Economics
Division of Environmental Systems Analysis
CHALMERS UNIVERSITY OF TECHNOLOGY
Gothenburg, 2017

A Scalable Life Cycle Inventory of an Electrical Automotive Traction Machine

Technical and Methodological Description, version 1.01

ANDERS NORDELÖF, EMMA GRUNDITZ, ANNE-MARIE TILLMAN,
TORBJÖRN THIRINGER & MIKAEL ALATALO

© ANDERS NORDELÖF, 2017.

Report 2016:4 (1.01)
Department of Technology Management and Economics
Division of Environmental Systems Analysis
Chalmers University of Technology
412 96 Gothenburg
Sweden
Phone + 46 (0)31-772 1000

This project was supported by the Swedish Electric and Hybrid Vehicle Centre (SHC), as a part of the thematic research area "Electrical machines and drives".

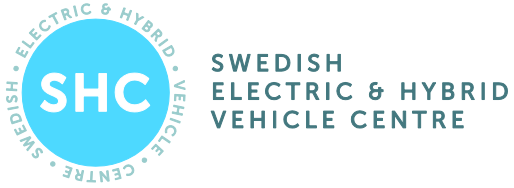

Chalmers Reproservice
Gothenburg, Sweden, 2017

Context

This report is one of four coupled publications. It describes the technical and methodological selections, and the data collection made to develop of a scalable life cycle inventory (LCI) model of an electrical automotive traction machine. It also presents the essential electrical machine theory background for the work. The report is intended to be used as a reference book for the scalable LCI model when detailed information and explanations are sought. Therefore, no summary or abstract has been included.

The scalable LCI model covers both design and production data of a permanent magnet synchronous machine (PMSM). The resulting LCI model, in the form of a Microsoft Excel Macro-Enabled Worksheet file (Nordelöf, 2016, 2017), can be downloaded from the Swedish Life Cycle Center as a part of the SPINE@CPM LCA Database[1].

Furthermore, a series of two peer reviewed articles presents the LCI model based on this report. The first article, part I (DOI: 10.1007/s11367-017-1308-9), describes how the LCI model was established and the type of results it provides, including the underlying PMSM design and the structure of the LCI data model based on mainly chapters 2 and 4 of this report. Additionally to what is included here, it also contains an evaluation of the mass estimations made by the model through comparison with data for seven existing PMSMs for vehicles from established brands, published from 2013 or later.

The second article, part II (DOI: 10.1007/s11367-017-1309-8), presents an overview of new primary production data and how literature data was revised to cover the complete PMSM motor manufacturing chain, including magnet fabrication, electrical steel production and a comprehensive survey of an electric motor factory. More in depth information about all production procedures, and how the data was established, is presented in Chapter 5 of this report. Part II of the article series also discusses the selected system boundaries and explains how to link the gate to gate inventory to the Ecoinvent database version 3 (Weidema et al., 2013), based on Chapter 2 of this report.

[1] Provided by the Swedish Life Cycle Center at http://cpmdatabase.cpm.chalmers.se

Revision history

Version 1.0 – original publication

Version 1.01
Update made in Table 25, section 5.1.3, for the dysprosium oxide input during magnet fabrication.

Table of Contents

Context ..... **iii**

Revision history ..... **iv**

1 Introduction **1**

1.1 Background 1

1.2 Purpose and intended application of the inventory model 1

1.3 Aim and structure of this report 2

2 Methodological approach **3**

2.1 Model structure, data collection and scaling 3

2.2 Assessment system boundaries 4

2.3 Representation of flows in Ecoinvent 6

2.4 User options, technical scope and uncertainty 7

3 Technical overview of electrical machine design **9**

3.1 Basic principles and prerequisites 9

3.2 Fundamental electrical machine parameters 9

3.3 PMSMs in comparison to induction machines 11

3.4 Engineering approach and variability in design 11

3.5 The function of different subparts 11

4 Design of the reference machines **14**

4.1 Stator package 14

4.1.1 Electrical steel composition 14

4.1.2 Stator core design 14

4.1.3 Magnet wire 16

4.1.4 Winding configuration 16

4.1.5 Insulation and impregnation 18

4.2 Rotor package 21

4.2.1 Rotor core design 21

4.2.2 Permanent magnet composition 23

4.2.3 The motor shaft 25

4.3 Integration, protection and monitoring 26

4.3.1 Housing 26

4.3.2 Bearings 30

4.3.3 Resolver 30

4.3.4 Terminal block, bolts, nuts and paint 31

4.4 The assembled unit 33
4.4.1 Summary of design parameters 33
4.4.2 Machine efficiency and performance 33

5 Assessment of production procedures 36
5.1 Magnet production chain 36
5.1.1 Coupling rare earth oxides to upstream data 36
5.1.2 From rare earth oxides to rare earth metals 37
5.1.3 Fabrication of magnets 38
5.2 Manufacture of steel, copper and aluminum subparts 43
5.2.1 Alloying silicon steel 43
5.2.2 General processing of steel parts 44
5.2.3 Electrical steel sheet production 45
5.2.4 Die casting of aluminum parts 47
5.2.5 Production efforts for copper parts 48
5.3 Preparation of parts with coatings, plastics, elastomers and resins 49
5.3.1 Enameling of the copper wire 49
5.3.2 Subparts with molded plastics 49
5.3.3 Extrusion of foils and cable tubes 50
5.3.4 Other insulation and coating materials 51
5.4 At the motor factory 51
5.4.1 Process overview 51
5.4.2 From steel sheets to core stacks 51
5.4.3 Installing and securing the winding 54
5.4.4 Impregnation procedure 55
5.4.5 Shaft preparation 56
5.4.6 Rotor assembly 59
5.4.7 Preparation of die cast housing parts 60
5.4.8 Wire termination, unit assembly and painting 63
5.4.9 Technical building services 65

References 68

Appendix A: Qualitative uncertainty assessment 79

1 Introduction

1.1 Background

Few well populated and transparent inventory datasets have been published for electric vehicle powertrain components, both regarding the composition of materials and production processes (Hawkins et al., 2012). Existing component datasets are often presented with fixed values for mass, material composition and performance parameters (Del Duce et al., 2014, Weidema et al., 2013). However, varying powertrain requirements implies a modification of component dimensions and design, i.e. changes in terms of weight and composition of subparts. At the same time, useful and flexible cradle-to-gate life cycle inventories of automotive components, including upstream production efforts, build on relatively detailed data for weight and composition, which often is difficult to obtain. Instead, more easily acquired engineering parameters, for example in the form of open automotive powertrain specifications, are commonly expressed in terms of torque or power.

Moreover, there is a general need for more thorough investigations of vehicle production data (Del Duce et al., 2014, Hawkins et al., 2012). In particular, updated and more detailed data for the manufacturing of electric powertrain components is needed since procedures are changing as the technology area matures, at the same time as the relative importance of production, compared to the vehicle use phase, increase with vehicle electrification (Nordelöf et al., 2014). Commonly used datasets for the production of electrical vehicles parts are in some cases very roughly approximated or outdated (ABB, 2002, Arnell, 2012, Del Duce et al., 2014, Habermacher, 2011, Weidema et al., 2013, Överstam, 2013).

Concluding, there is lack of life cycle inventory data for electric powertrain components which can be directly calculated from basic parameters in powertrain specifications, such as torque or power. There is also a lack of comprehensive inventory data both for the design and production of electrical machines which calls for new data collection.

1.2 Purpose and intended application of the inventory model

The goal of this project was to establish a general and scalable life cycle inventory (LCI) data model for a permanent magnet synchronous electric motor (PMSM), designed for electric vehicle propulsion. The aim was to provide mass composition and manufacturing data for a typical electrical machine design. The model generates data on motors ranging in power from 20-200 kW and in torque from 48-477 Nm, i.e. from a small electric passenger vehicle up to, for example, an electrically propelled bus. The purpose of the model is to complement the few existing datasets and assist LCA evaluation of electric powertrains through generation of data for different sized electrical machines. The resulting datasets represent gate-to-gate production of the motor, from materials to complete motor. The inventory model is available as a spreadsheet file in Microsoft Excel, which can be downloaded as from the SPINE@CPM LCA Database[2], together with this model report.

The material composition is generated by means of a scalable model of a PMSM, which can be used as an estimate of any PMSM designed for electric propulsion if it falls within the range for power and torque requirements for which the model is valid. Two reference machine designs have been established and evaluated for electrical and magnetic properties using engineering software tools. Specific design selections were adopted for a single motor all-electric vehicle application. For a starting point, the authors observed existing electrical traction machine designs, both personally and in published reports, e.g. benchmarking literature (Burress and Campbell, 2013, Burress et al., 2011, Miller, 2013b, Ozpineci, 2014). The data for the electromagnetically active parts (see Section 3.1 for an explanation of the different motor parts) has then been complemented with data for catalogued subparts and engineering estimates of less detail, in order to model a complete machine.

Subsequently, the model for the calculation of the PMSM material composition was combined with LCI data for the manufacturing stages, necessary to produce a motor from the materials. The manufacturing data presented is to a large extent new original LCI data, collected directly from production site documentation

[2] Provided by the Swedish Life Cycle Center at http://cpmdatabase.cpm.chalmers.se/Scripts/sheet.asp?ActId=JT-2016-06-21-39

including a site visit, several expert interviews, machine specifications and textbook descriptions of alternative manufacturing procedures. In addition to being used as a part of the over-all data model, the manufacturing data can also be used in its own right, in LCA studies where the material composition of the motor is known from other sources.

Finally, an important objective was to make the model easy to use by LCA practitioners. For this reason, the manufacturing processes have been followed upstream to a point where LCI data for material production exist in the Ecoinvent database version 3 (Weidema et al., 2013).

1.3 Aim and structure of this report

The aim of this report is to explain and describe the theory and data processing that has led to the inventory details presented in the spreadsheet calculation file coupled to this report. It is expected that the target audience (typically LCA practitioners) have basic engineering knowledge but little or no experience of electrical machine technology. The report has been divided into four parts after this introduction. Chapter 2 discusses the working procedures and LCA methodology behind the model; Chapter 3 presents basic terminology and theory of PMSM electrical machines; Chapter 4 explains the design selections in detail and the resulting composition of the machine; and Chapter 5 describes the necessary motor and subpart production procedures along with the LCI data collection for each process.

2 Methodological approach

2.1 Model structure, data collection and scaling

This project was conducted as a collaboration between researchers with different expertise, both LCA methodology and electrical machine design. Component design data was compiled from theory books, technology benchmarking literature, experts in industry and product descriptions. Additionally, production data has been collected from industry in form of documents, site visit notes, more expert interviews, machine specifications, instruction films and textbook descriptions. These two different types of data has then been combined into one scalable LCI model. It request the user to enter a value for maximum power, and optionally the torque (allows for an adjustment of the operation voltage). In return, it provides a gate to gate life cycle inventory for the production of an internal permanent magnet synchronous electrical machine, together with the mass configuration of the machine and a recommended representation for the input and output flows in Ecoinvent's database version 3 (Weidema et al., 2013). The basic structure of the LCI model is shown in Figure 1.

Two motors, referred to as the "small" and the "large" reference machines, were constructed in ANSYS Maxwell (ANSYS, 2015), a software tool for computational design and evaluation of electrical machine performance. The two cross section geometries have the same basic form but differ in the diameter and size of the slots in the machine cores. This principal design was selected based on observations of electrical machines in different automotive traction applications made both during disassembly and in benchmarking literature, to be as generic as possible for a PMSM, as judged by the authors.

The design tool calculations delivered a key link between the mass of the electromagnetically active parts in the design and the ability of the machine to deliver a specific maximum torque and power. Hence, this mass is referred to as "active" and consists of the amount of electrical steel in the stator and rotor cores, the amount of copper in the stator slots and the amount of magnets in the rotor, to provide the required electromagnetic properties of the motor. However, these masses are just a portion of the total machine weight. Consequently, additional data on weight and composition of the passive components (e.g. insulation, shaft, bearings, housing etc.) was collected from electrical machine design literature, industrial benchmarking reports, subpart catalogues and expert interviews, and combined with the experience and engineering judgement of the authors, to complement the reference machines into complete designs.

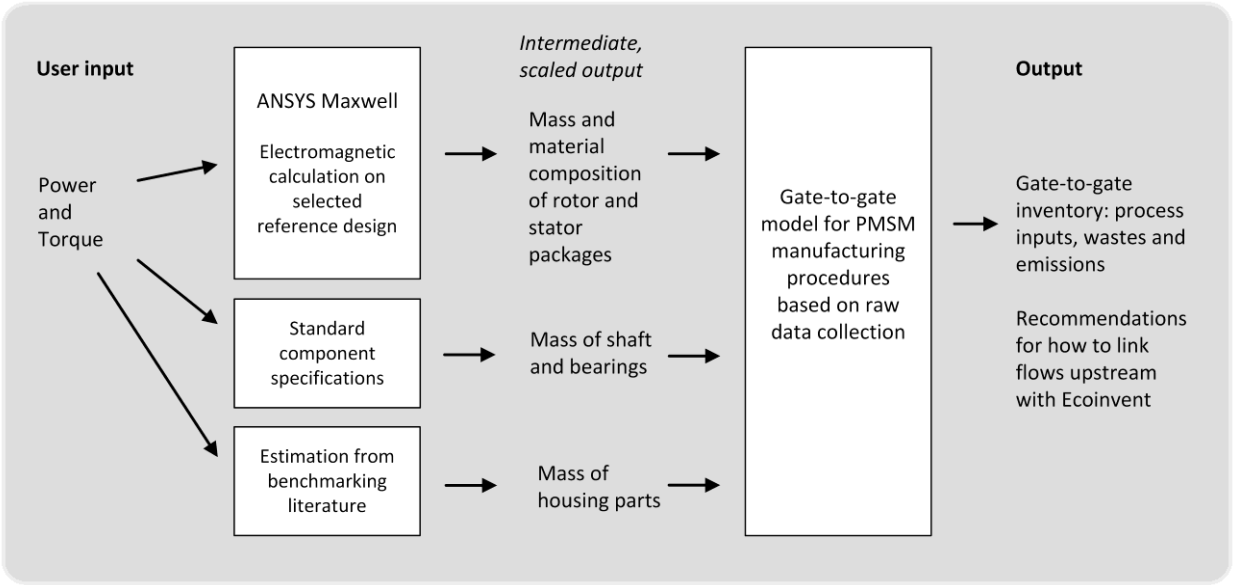

Figure 1: Structure of LCI model.

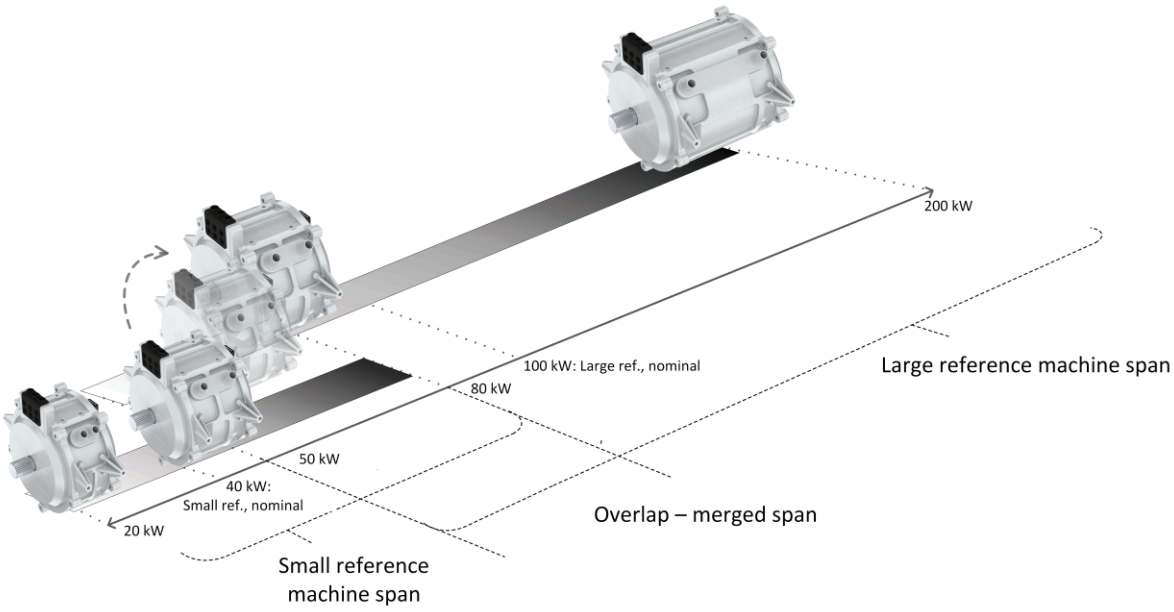

Figure 2: Schematic overview of the reference machine scaling over different spans and where the datasets have been merged to create on seamless model.

First, the two reference machines were modelled with different diameters and nominal lengths, matching a power of 40 kW and 100 kW respectively. Next, a span for torque and power was calculated for each of the two machines by scaling their active length up to the double nominal length and down to half of it; 20-80 kW and 48-191 Nm for the small machine and 50-200 kW and 119-477 Nm for the large machine. This resulted in two separate sets of electrical machine data, linked from torque, and power at a specific supply voltage, to the mass of each active constituent. Following, in order to establish one seamless model for the entire torque and power span, these two datasets had to be combined. This was done merging the two datasets within the overlapping span of 50-80 kW and 119-191 Nm by shifting over stepwise from the small to the large machine, i.e. corresponding to 100% of the small reference machine at 50 kW and 100% of the large reference machine at 80 kW. As a consequence, a real average (50% of each) between the two occurs at 65 kW and 155 Nm. Figure 2 shows the principles for the scaling including the merged span.

Next, PMSM manufacturing processes were studied in several steps. Data was collected for the production procedures of another electrical machine type, an induction machine, at ELMO Malmköpings Mekaniska Werkstad AB in Flen, Sweden (Walter, 2015, 2016) and adjusted to become representative for the selected PMSM machine design by gathering and complementing with data from other productions sites, expert interviews, technical literature and machine specifications. Also, Surahammars Bruk AB (Lindenmo, 2012, 2015) provided new original data for electrical steel production. For the fabrication of magnets, recently published data from NETL (2014b) and Sprecher et al. (2014a), (2014b) about NdFeB-magnets was found to be both detailed and a good starting point. However, it had to be corrected for some errors found and reworked with information from patents and technical literature, again to be representative for the automotive traction application of the LCI model. Additionally, to make the model complete, data was collected from literature to establish unit processes for the die casting of aluminum, purification of iron (necessary for magnet fabrication) and coating of magnet wire (enameling). Data for the reduction of rare earth oxides to rare earth metals, in the magnet fabrication production chain, was taken as found in the NETL (2014b) unit process library.

2.2 Assessment system boundaries

The LCI model provides mass and manufacturing data for one PMSM as delivered at the factory gate. The functional unit is one electrical machine intended for vehicle propulsion with specific power and torque requirements. It is a gate-to-gate LCI, with input as delivered from various stages of material processing, as available in Ecoinvent version 3 (Weidema et al., 2013). No use or end-of-life treatment has been included and

it is possible to combine the inventory with input data for virgin raw materials just as well as recycled materials. An overview of the technical system boundaries are shown in Figure 3.

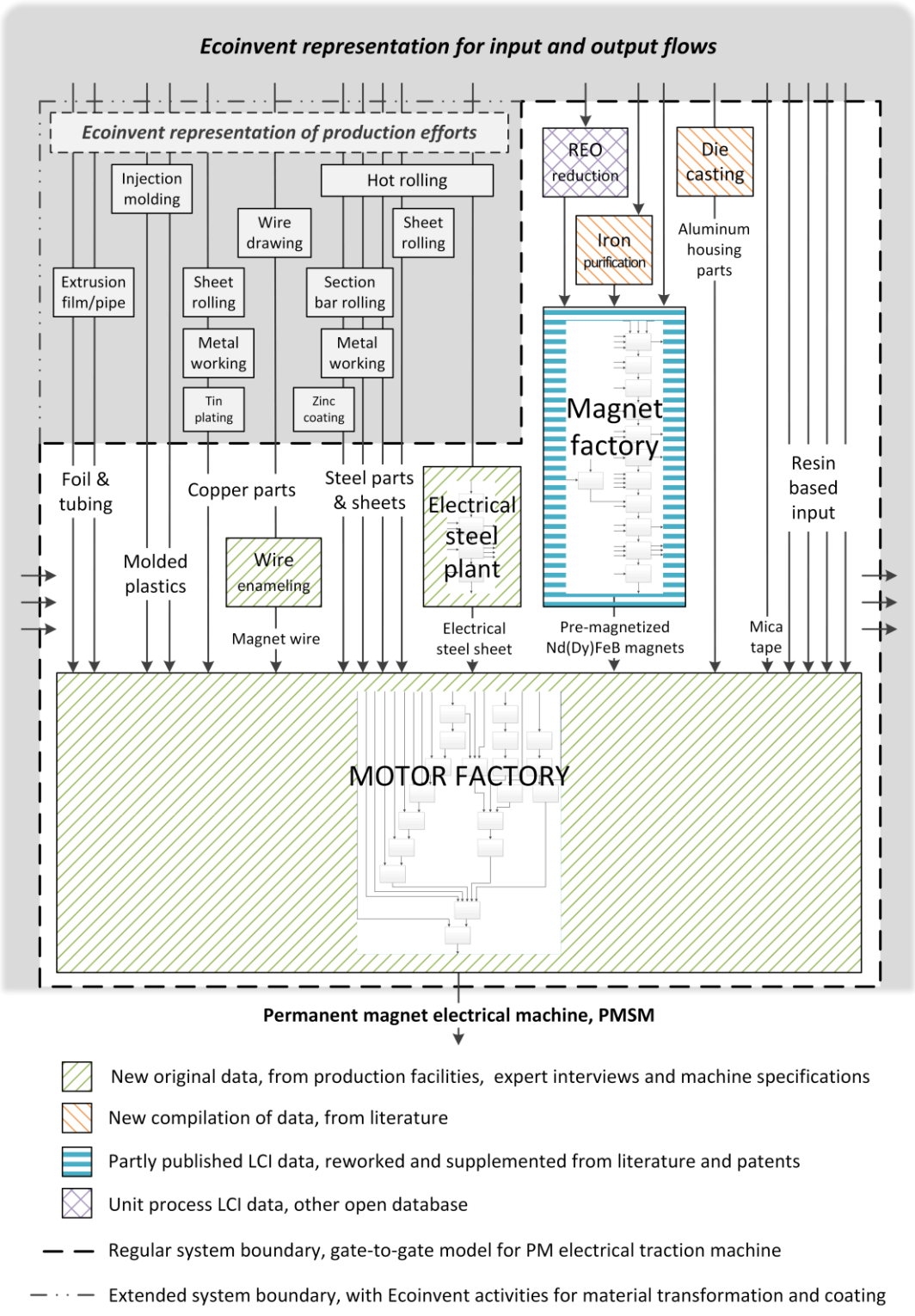

Figure 3: Overview of the technical system boundaries for the collected production data, including different main information sources, and how the LCI model relates to the Ecoinvent 3 database (Weidema et al., 2013).

As regards geographical system boundaries, the intention was to keep the model as flexible as possible for the user and representative on a global level. No specific countries, regions or sites have been defined for the various production steps. For example, all input electricity has been marked as "optional" for the user in terms of the production source or market mix. Nevertheless, for the machine design it can be noted that most of the benchmarking literature describes disassembly of Japanese brands (Burress et al., 2008, Burress et al., 2009, Burress et al., 2011). This is also true for the properties of the magnets and recent patents on how they are manufactured (Nagasaki and Shimao, 2015). For the manufacturing, two main data sources were Swedish production plants (Lindenmo, 2012, 2015, Walter, 2015, 2016), but machine and subparts specifications as well as expert interviews typically represent European, North American or Chinese conditions more broadly (Hendershot, 2015, Larrenduche, 2015, Magnusson, 2016, Willard, 2015, Xue, 2015). The technical scope and variability is also further discussed in the next section, i.e. Section 2.4.

As a consequence of the very broad geographical system boundary definition of the model, no transportation of gods was included. Instead, the user of the model is expected to add subpart transportation if it is relevant for the study in which the LCI model is used. In terms of time, both design and manufacturing data has been judged as representative for the current level of technology. All measured data from industry was collected within the last five years. Most textbooks, research articles and technical reports are from the same time period, or at least published within the last 10 years. However, in some cases, literature sources are older, due to the lack of new data.

2.3 Representation of flows in Ecoinvent

As mentioned in Section 2.1, and also shown in Figure 3, all raw material input to the PM electrical machine has been traced through upstream manufacturing processes up to a point where existing datasets for the production of materials are available in Ecoinvent version 3 (Weidema et al., 2013). "Linked flows" has been identified throughout this report, and provided in the model file, for an Ecoinvent representation of all inputs, wastes and emissions, unless the user is called on to make a more attentive selection. The linked flow is then noted as optional, as already exemplified for the use of electricity in production, see Section 2.2 above. Hence, all throughout chapters 3 and 5, there are descriptions of flows being "listed" or "coupled" to Ecoinvent, and this refers to the linked flow representation over at the system boundary, see Figure 3. For flows listed in figures and tables, Ecoinvent 3 has been abbreviated to E3 all throughout Chapter 5. Another abbreviation in the same set of tables is IF, denoting "internal flow" (i.e. a flow not crossing the system boundary).

Furthermore, also shown in Figure 3, there is an extended system boundary which encircles a set of Ecoinvent (Weidema et al., 2013) activities for material transformation and coating. These activities are also included in the LCI model file, but listed separately from the inventory for the charted gate-to-gate model with the regular system boundaries. The reason for this setup is the formulation of material transformation activities in Ecoinvent. The production efforts are analogous to services which reshapes one kilogram of input raw material or semi-finished product into one kilogram of output product (Hischier, 2007, Steiner and Frischknecht, 2007, Classen et al., 2009). In general, in the representation of metal forming, conversion of plastics and average machine working of metals, the amount of materials removed and scrapped are included as a flows in and out of the activities along with other auxiliaries and emissions, but not the materials and products being reshaped. Accordingly, the reference flow of the process refers to the activity and not the output product, also when the reference flow unit is expressed as a mass, see for example the description of "hot rolling" in Classen et al. (2009). Nevertheless, as described in sections 5.2.2, 5.2.5, 5.3.2 and 5.3.3, a number of these activities in Ecoinvent have been identified and included in the LCI model to properly account for the making of several subparts from their material constituents. In order to clarify the inclusion of these "service flows" crossing the ordinary system boundary and avoid confusion for the user, the setup with a separate activity list and the extended system boundary was selected. Moreover, users of the LCI model should be aware that the detailed definitions of these production efforts are not consistent within Ecoinvent version 3 (Weidema et al., 2013), and for more details about the differences between, for example, the formulation of metal forming activities and those for the conversion of plastics, we refer to the original sources (Hischier, 2007, Steiner and Frischknecht, 2007, Classen et al., 2009).

Finally, the coating processes for galvanization and tin plating are formulated in a similar way as the material transformation processes in Ecoinvent (Weidema et al., 2013). They also only relate to the actual process and do not include the material being treated, i.e. the reference flow is a layer of coating of a certain thickness, expressed per surface area, and not a coated product. Hence, they were included in the list of activities outside the regular system boundary, but inside the extended system boundary.

2.4 User options, technical scope and uncertainty

The inventory model file provides some options for the user to offer increased flexibility whether or not to include some subparts. First, the user must select if the calculations are to be based on the maximum power only, or on both power and torque. If only power is selected, the nominal DC voltage and the motor base speed are set to representative conditions for passenger vehicles at 400 V and 4000 rpm. No torque value must be entered, since it is instead derived from the power and the speed. For any other base speed, e.g. in the case of other vehicle types, the user must provide both maximum power and maximum torque. The motivation for this setup of the model input and the parameter entry is that the authors have estimated that maximum power, followed by the maximum torque, are the most easily accessible electrical machine parameters when gathering data for a life cycle assessment of a powertrain or comparison between different machine sizes.

On the other hand, information about different performance parameters of the battery may be much harder to acquire. For this reason, it important to point out that the use of a definition for maximum power based on a constant DC voltage pushes the value towards the upper level of what is reachable, from a system point of view. In other words, it provides the rating of the motor as evaluated stand-alone. In a vehicle, the battery voltage strongly impact the possibility of the motor to reach its rated maximum power (for more details on the fundamental electrical machine parameters, see Section 3.2.). In fact, some vehicle manufacturers select to state the maximum power rating for such limited operation (see Section 4.3.1), i.e. a rated upper power value which is always attainable instead of the actual maximum.

The motor torque relates more closely to the machine size than the motor power (again, see Section 3.2.). Hence, almost all subparts' and materials' masses in the model are calculated from the torque value, directly or indirectly, by a physical relation to the size, or weight, of one of the active parts generated from the ANSYS Maxwell (ANSYS, 2015) calculation. The exception is the housing, which was established and scaled directly in relation to power instead of torque. The reason is that a key role of the housing is to provide proper cooling to handle heat losses, which relates primarily to power, and only indirectly on torque.

Furthermore, as shown in Figure 4, the inventory can be calculated without some of the passive parts: the housing, the shaft and the bearings. For the housing this means that one or both endbells can be deselected, or the entire housing, including the cylindrical body. There are several reasons for these model options. Like the active parts of the motor, these parts are scaled in the model, but the scaling is not based on the ANSYS Maxwell (ANSYS, 2015) calculations for electromagnetic properties. Furthermore, both the housing and shaft may be shared or integrated with other components in a powertrain. Next, there are large variations in design

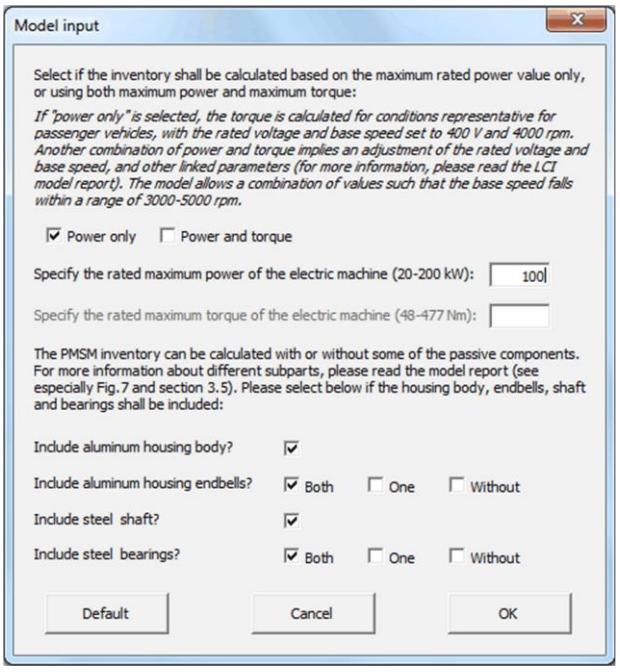

Figure 4: The LCI model input pop-up window, showing the alternatives for deselection of some passive parts.

of the motor housing depending on packing and cooling solutions. Data for the bearings and shaft may sometimes be acquired separately and endbells are not always used when the motor is mounted in series with some other unit, for example a gear box. Finally, there is large variability in terms of design options for the housing and the shaft and their contributions to uncertainty in the model are larger than those of other subparts. In turn, the bearing dimensions are linked to the shaft design. A way for the model user to decrease uncertainty can be to gather more specific data for the housing and the shaft, if desired.

However, these options come with some restrictions to avoid unintentional or unrealistic combinations. The inclusion of both or one endbells implies that at least the same number of bearings are included in the calculation, as well as the shaft and the housing body. Similarly, without the shaft, it is not possible to include the bearings.

In contrast to the user options in the model input entry, the LCI model also includes specific design selections, and manufacturing processes, which represent only a few out of a variety of common options for specific subparts or steps in the production. In such cases, the authors have based their decisions on expert interviews, overviewing literature and their own engineering judgement to achieve a reasonable combination for the data collection scope and the generality of the design. For example, there are many alternatives in the selection of stator winding insulation materials, as well as alternative procedures on how they are installed during manufacturing. One particular epoxy resin was selected in combination with a specific installation method called trickling, based on a combination of expert interviews and what literature reports on trends in manufacturing procedures. Variability in design is further discussed in Section 3.4.

Similarly, there can be many different techniques to manufacture the same electrical machine part. Many aspects are taken into consideration when selecting a specific method, for example: cost-efficiency, productivity and cycle time; geometry and strength of the part; surface finishing and material properties; and environmental hazards (Tong, 2014). An illustration of this is that for large production volumes of housing parts, some type of casting is the most suitable manufacturing method. But for lower volumes of only a few hundred samples, or in the case of prototypes, various types of machining from a solid block are selected, i.e. cutting, drilling, milling and turning (Jörgen Johansson, 2015). Likewise, in large scale production of core laminations, punching is most cost-efficient. However, the tools for punching are expensive, so again for small series or prototypes, it could be preferable to use laser cutting. In this inventory work, as a general approach, data representing high volume manufacturing processes were selected, to the largest extent possible.

Finally, coupled to the different decisions made for different data sources, uncertainty was quantified by the authors based on qualitative assessment of data quality according to the Ecoinvent pedigree matrix as described by (Weidema et al., 2013). The results of this assessment are presented in Appendix A.

3 Technical overview of electrical machine design

3.1 Basic principles and prerequisites

Electrical machines convert electrical energy to mechanical, and vice versa, by means of magnetic energy. The main purpose of an electric traction motor in a vehicle is to deliver mechanical power, or more specifically, a desired torque to the wheels when the speed level varies extensively. Electrical machines should preferably have high torque to mass or volume ratio, high efficiency, high controllability, low cost, and low noise and vibration levels. Recyclability, and minimized use of hazardous or scarce material, are other important design parameters. As a general rule of thumb it can be stated that the torque is proportional to the volume of the electrical machine, while the power also depends on the motor speed.

As the electrical machine is only one part of an electric drive system, e.g. see the schematic overview in Figure 5, there may also be additional external factors influencing the design options, e.g. limiting geometries, the maximum DC voltage level from the feeding battery (often around 400 V for passenger cars), or the maximum allowed AC current in the machine due to thermal constraints (often 400-600 A rms).

There are plenty of ways to classify electrical machines depending on their main characteristics, for example, the type of electric power feeding it (DC or AC), the type of motion it produces, the way to generate the magnetic field in the different parts and its orientation and the power rating (Tong, 2014). Hence, while there are several different kinds of AC electrical machines, for example induction machines (IMs) and permanent magnets synchronous machines (PMSMs), it is an interior permanent magnet (IPM) synchronous machine (IPMSM) that is described in this report, and accounted for in the LCI model. The IPMSM is subset of the PMSM, and it is the machine type which is most common in electrified vehicles. In IPMSMs, magnets are inserted in the rotor core close to its outer surface.

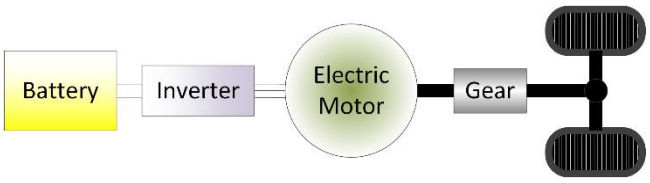

Figure 5: Schematic overview of an electric drive system

3.2 Fundamental electrical machine parameters

The design and scaling of the reference machines are based on two fundamental motor parameters, torque and power. Both relates to the electromagnetic force generated by the motor. Torque (T) is the measure of the rotation caused by this force around the motor's central axis, at the surface of the rotor where the distance to the axis is equal to the rotor radius. More specifically, it is the mathematical product of the force and the rotor radius. Hence, the unit of torque is Newton meter (Nm). In turn, power (P) is the rate of work made by the torque, i.e. per time unit. It is measured in Watts (W). Power and torque of a rotating electrical machine relates via the angular velocity (ω), measured in radians per second (rad/s). The relationship can be written as:

$$P = T \times \omega$$

However, as already mentioned, in the case of vehicles, the parameter speed (S), measured in rotations per minute (rpm), is used instead of angular velocity. Then, since

$$S = \frac{2\pi}{60} \times \omega$$

the expression for P can be rewritten to:

$$P = T \times \frac{30}{\pi} \times S$$

A conventional industrial electric motor, for example a pump, operates for a long time (more than 10 minutes) at its maximum power and torque. This is called continuous operation and the operating point is determined by the thermal maximum of the machine. In contrast, in a passenger vehicle it is common that a lot of power is required during accelerations, which lasts only for about 5-15 seconds. The remainder of the time much less power is needed. Electrical machines have long thermal time constants, so in vehicles it is possible to utilize the fact that the electromagnetic ability of an electrical machine is much higher than the thermal ability. The peak torque is typically two to three times higher than the continuous torque. Hence, if automotive and industrial electrical machines are compared, it is very important to note that the ratings of vehicle traction motors are always given according to the peak value, since the typical automotive sales and customer information reports the amount of power which can supplied during an acceleration event.

Modern electrical machines for vehicles have a very high efficiency. Peak efficiencies reach 96-97 % and average efficiencies goes up to 90 %, depending on the drive cycle (Grunditz and Thiringer, 2016a). Already at take-off an electrical machine can produce maximum torque, which is constant at low speed (see Figure 6), and as the speed increases so does the maximum attainable power. At a certain speed level called *base speed*, the power is limited (ideally constant) as seen in Figure 6, due to the voltage and power limits of the battery. Hence, the nominal rated voltage of the system (and for which the motor is designed) is fundamental for the relationship between power and torque.

Above the base speed, the maximum available torque decreases inversely proportional to the increasing speed level. This is referred to as flux weakening operation and it is commonly used in traction machines in order to support driving at high speed and to provide a mechanical output on the wheels which is similar to that of an internal combustion engine with a gearbox, i.e. with a loss of torque and slower response to acceleration requests at high speed compared to low speed. Using this method, the utilization of the motor is stretched up to the maximum speed value, which can be 2-4 times the base speed (Grunditz and Thiringer, 2016b), without requiring an increased machine size.

All electrical energy fed to an electrical machine is not converted into useful mechanical energy. Some is lost, for example in conduction resistance, core losses due to magnetic phenomena and mechanical friction. Almost all losses are turned into heat energy which requires cooling and pull down the performance of the motor. The motor efficiency is defined as the ratio of the power output to the power input.

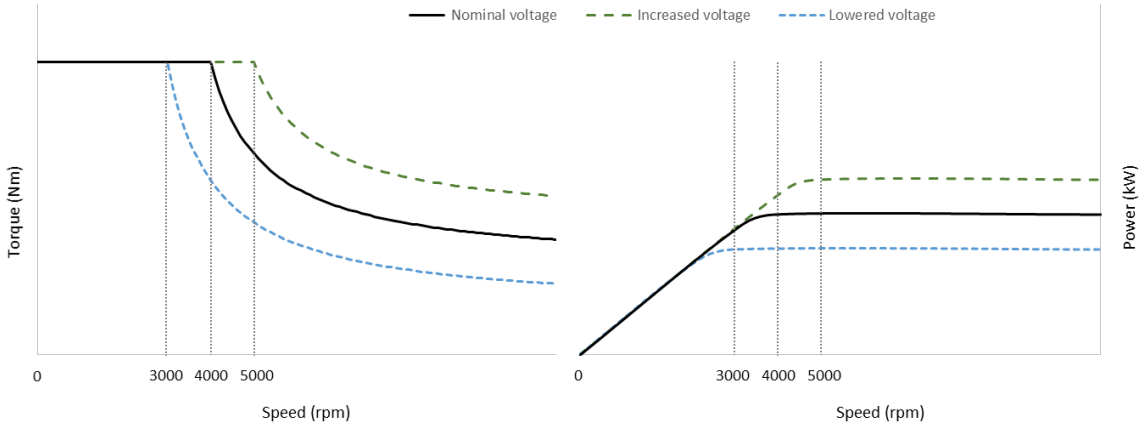

Figure 6: The typical relationship between torque, power and speed of an electrical machine, including how the maximum power, maximum torque and base speed also depends on the rated voltage, exemplified for the model validity span of 3000-5000 rpm.

Another important note is that electrical machines normally can be operated both ways in terms of how the energy flows. In the motoring mode, as described so far, electrical energy is converted to mechanical energy to propel the vehicle. In the generating mode, the machine acts as a break and recuperate mechanical energy into electrical energy which can be stored in a battery. This is an important feature of electrical machines and, when used for traction in a vehicle, it provides an additional capability to electrical powertrains compared to internal combustion engines, which are unable to recover energy during driving.

Electrical machines that are designed to exclusively operate in the generating mode, as in wind turbines, are thus called generators.

3.3 PMSMs in comparison to induction machines

This report presents the design and LCI of an IPM electrical machine. The reason is that electric vehicle traction machines very often are of PMSM type (Chan, 2007, Miller, 2013b). However, one of the most well-known electric vehicle models today, the Tesla Model S, use induction machines (IMs). In the following, we briefly discuss the differences between the two electrical machine types.

Generally, IMs are cheaper, but less energy efficient and larger compared to PMSMs producing the same torque. The difference between the two types is the rotor construction and the torque production mechanism. IMs contain no magnets, instead their rotors have aluminum or copper bars in which currents are induced and create the magnetic field necessary for the torque production.

PMSMs are often selected whenever high efficiency and/or a small motor volume are prioritized, as in hybrid vehicles or when a battery electric version is developed within an existing brand model series. However, if an electrified vehicle is developed from scratch, such as the Tesla, IMs may be the most suitable choice.

A simple variant of a PMSM is to place the magnets on the surface of the rotor, a so called surface mounted machine. In some cases such motors are used in electric powertrains. However, it is possible to get more torque out of the same machine and magnet volume, by placing the magnets inside the rotor, as in the IPMSM. They are also referred to as having buried magnets, and are more common (Burress et al., 2011, Sato et al., 2011).

3.4 Engineering approach and variability in design

There is a considerable variability in electric motor design for vehicles, also for apparently similar products such as electric busses or electric cars. The task of designing an electrical machine for an electric powertrain demands considerations in several different knowledge areas, for example electromagnetics, mechanics, thermal science, material science, vibrations and acoustics (Tong, 2014). Overall requirements on the vehicle or the powertrain are often the starting point. Design parameters and criteria for the different subparts are balanced and considered from a system perspective. If the engineering process is focusing on functional requirements of the motor as a whole then the process is commonly top-down oriented and iterative with design trade-offs made between the different parts. However, in order to achieve short design time, the subparts of a motor are sometimes designed more or less independently, and then assembled into one unit in a bottom-up component approach (Tong, 2014). The motor as a whole might then perform less well, or otherwise be oversized in one or several aspects. There are also numerous reasonable design routes to fulfill similar requirements. The output torque and power of an electrical machine is linearly proportional to the outer length the stator core, and quadratically proportional to its outer diameter. Still, any specific application may have geometric constraints, e.g. the available packaging space for the machine. It is often not possible for a vehicle manufacturer to get its ideal motor at a low price. Typically, a good price can be obtained by using a design that the machine supplier has sold to some other customer, possibly with moderate modifications. An important reason for this is that the tools for making the steel sheets are very expensive and therefore suppliers typically only offer machines with certain fixed diameters. However, the length can more easily be adjusted in order to deliver the desired power level (Hendershot and Miller, 2010).

3.5 The function of different subparts

For cylindrical electrical machines, which are normally used in vehicles, the mechanical output is transmitted through a rotating *shaft* which can drive an external load. The moving part of the machine attached to the shaft is therefore called *rotor* in any type of electrical machine. Another, stationary part is called *stator*, and the two parts are separated by a small air gap. (Other, less common types of machines may have several

moving parts or have a linearly moving rotor.) The rotor can be placed either inside or outside the stator; so called inner or outer rotor machines. Mechanically the stator and rotor are joined via *bearings* mounted on the shaft. Figure 7 shows a sketch of a PMSM, which has been exploded to demonstrate its main subparts.

The role of the stator is to create the magnetic field which will force the rotor to move. Input electric power at the stator is converted to a magnetic field. The magnetic flux crosses the air gap between the stator and rotor, and creates a force in the rotor which causes the rotor to rotate. The reason is that the rotor generates a magnetic field of its own or carries permanent *magnets* which interacts with the field generated by the stator. As discussed in section 3.2, the motor torque is a measure of the equivalent net force on the rotor surface that causes the rotation (Torque = Force × Rotor radius). The force production mechanism differs a bit between different machine types.

The magnetic field is created by AC current carrying windings, forming coils in the stator. In vehicles, so called three phase machines are often used. Then three groups of windings are placed in the stator, and controlled, such that a radially directed magnetic field is created, that continuously rotates 360 degrees inside the machine as well as in the air gap. For PMSMs, the magnetic field from the permanent magnets in the rotor, strive to align with the rotating magnetic field produced by the stator. The result is the force acting on the rotor, which can be controlled by varying the strength of the stator induced field, i.e. the current magnitude.

The electric current can be supplied from any voltage source, like a grid power supply or from a battery. In a typical electric vehicle powertrain, the current comes from a battery but via an inverter. The inverter controls the electrical machine operation by switching large transistors on and off. Equally important, at the same time it converts the DC voltage of the battery to a controllable, three phase AC voltage and current that feeds the electric motor. For a fast, reliable and stable machine control, the rotor position and speed is usually measured by a *resolver*, which is similar to a very small electrical machine with windings and an iron core.

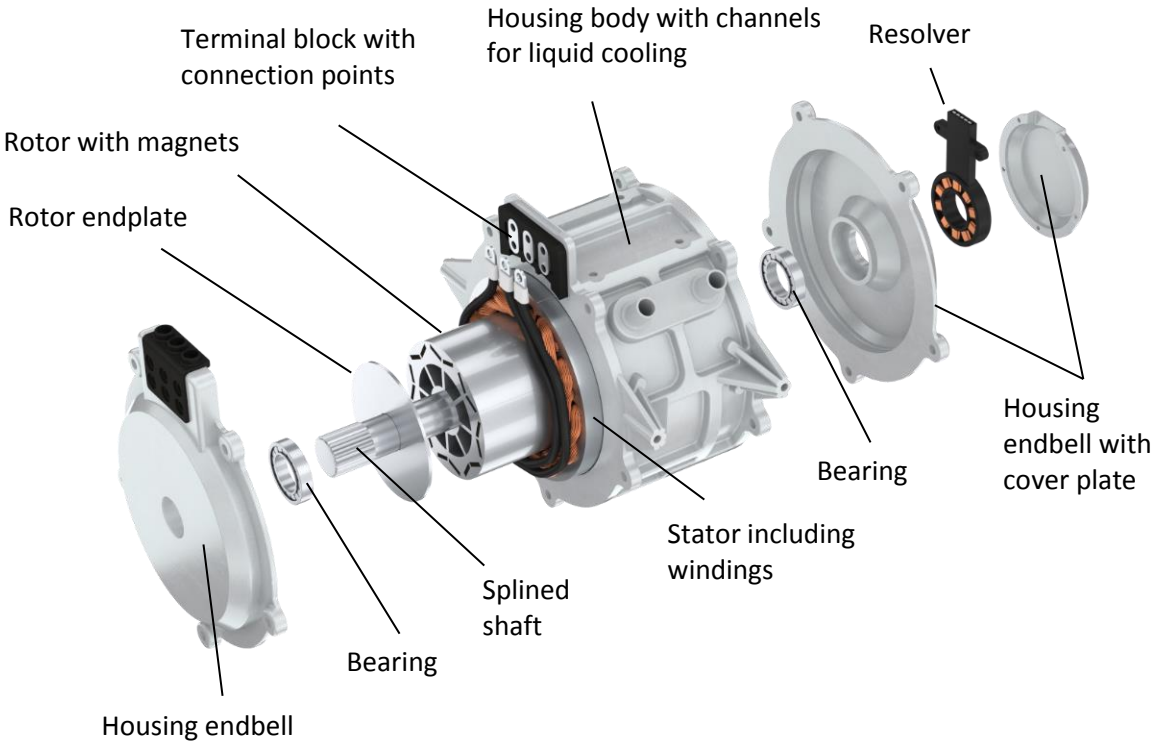

Figure 7: Exploded sketch of the selected PMSM design.

The main active machine parts, the rotor and the stator cores, generally consist of electrical steel in order to concentrate the magnetic flux, and thus to minimize flux leakage to the surrounding air, which would not contribute to the torque production. Furthermore, to minimize induced currents in the steel parts, both cores are made up of stacked thin steel discs, called laminations, each about 0.3 mm thick and electrically insulated. Laminations are pressed together to form a stack constituting the active length of the stator and rotor, e.g. about 100-200 mm for a rear axis electrical machine of a passenger car.

The shaft is put inside the rotor. It is often made of carbon steel, or sometimes, when corrosion must be avoided, of stainless steel (Tong, 2014). The machine is covered by a cylindric frame, or protective compartment, called housing, which in general, for vehicle applications, is made of aluminum (Tong, 2014). The cylindric bases of the housing structure, are referred to as endbells or endplates. They are mounted together with the bearings and included in the housing depending on how much integration there is with the surrounding powertrain components. Due to inevitable machine losses that cause heating (which increase with increasing power), electrical machines need to be cooled through the housing body. An efficient cooling makes it possible to run a higher power in the machine compared to what would have been the case with less efficient cooling. Liquid cooling is usually used for vehicle machines, unlike general industrial machines, where air cooling is often preferred.

Also, since the running speed of automotive traction machines usually is much higher than the vehicle's wheel speed, there is a need for a transmission ratio between the electrical machine shaft and vehicle's drive shaft. This is solved by coupling the electrical machine to the drive shaft via a gear box.

4 Design of the reference machines

4.1 Stator package

4.1.1 Electrical steel composition

The most common type of material for stator and rotor cores is electrical steel, which in turn can be divided into several subcategories. Important considerations in the selection of materials include trade-offs between electromagnetic, thermal, and mechanical properties besides material cost and fabrication processes. Silicon steel is a major subgroup with beneficial characteristics in terms of high resistivity and low losses (Tong, 2014). Additional alloying with aluminum and the use of very thin laminations also keep losses low. Different grades of electrical steel sheets range from 0.1-1 mm in thickness (Surahammars Bruk, 2014b).

The material requirements for stator and rotor laminations, i.e. the stacked thin steel discs, can be slightly different. The electromagnetic properties are generally most important in the stator. The rotor, on the other hand, must be able to handle larger mechanical forces. However, in practice, the same base material is generally selected for both stator and rotor laminations as it makes it possible to punch them simultaneously from the same sheet (Tong, 2014). The lamination patterns vary depending the desired magnetic prerequisites combined with the preferences for manufacturing.

Electrical steel sheets are often coated on both sides to improve the surface insulation resistance, and thereby minimize losses from the eddy currents which occur between laminations (Tong, 2014). A range of different thin layer coatings are available, both organic and inorganic. The coating can also be a part of the lamination bonding, for example organic epoxy resins which are heat activated to provide strong adhesion (Surahammars Bruk, 2015b). Thicknesses typically ranges from 1-6 µm on each side (Surahammars Bruk, 2014b).

Example model	Grade thickness
Nissan Leaf (2011)	300 µm
Toyota Prius (2004)	330 µm
Toyota Prius (2010)	305 µm
Lexus LS 600h	280 µm
Toyota Camry	310 µm

Table 1: Examples of lamination thicknesses in different motors of electrified vehicles (Ozpineci, 2014).

Data collection

Primary inventory data for electrical steel sheet properties was collected from Surahammars Bruk AB. The share of silicon and aluminum in their alloys vary between different grades, but on average they contain 2% silicon and 0.4% aluminum (Lindenmo, 2015). A non-oriented 300 µm thick grade (NO30) was selected for the laminations used in the reference machines (Surahammars Bruk, 2015a). This grade have been specifically designed for higher speed machines used in electric vehicles (Surahammars Bruk, 2014a). As shown in Table 1, this thickness is used in some of the most well-known electrified passenger vehicles of today. Also, for the selected steel lamination thickness, a standard coating on both sides consisting of 3 µm phenolic resin was found representative (Beckley, 2002, Surahammars Bruk, 2014b).

4.1.2 Stator core design

The stator core consist of laminations stacked into a cylinder. The laminations have sprocket patterns in them where the wound wire for current conduction is placed, so called *slots*. The parts of the core between the slots has the purpose to control the magnetic flux paths and are called *teeth*. Also, the tooth tip, or rim, helps keeping the winding in place, see Figure 8. The number of slots, and consequently also the winding arrangement, matches the magnet placement in the rotor to form the number of "poles" that the machine has

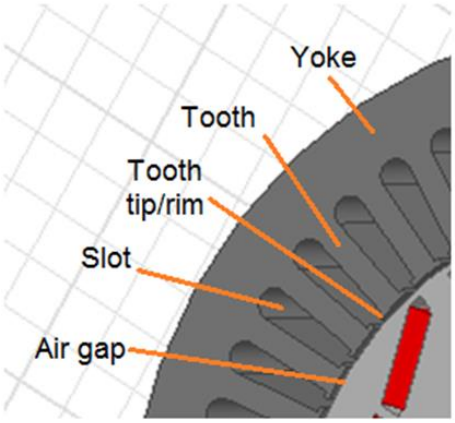

Figure 8: Close up of a stator core segment (and a small part of the rotor), with labeled parts.

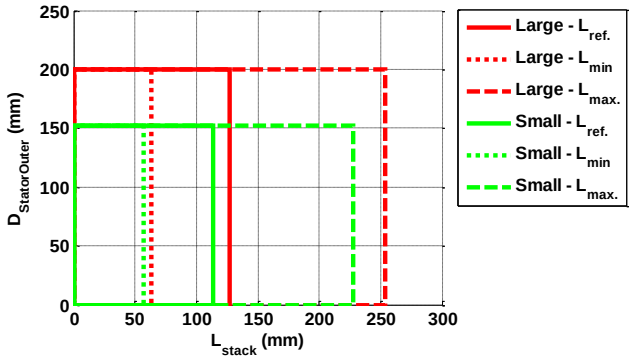

Figure 9: Minimum, maximum and nominal dimensions of the stator cores, for both the small and large reference machines.

Reference machine	Mass	Volume
Small	6.1 kg	0.81 dm^3
Large	12 kg	1.6 dm^3

Table 2: Stator core mass and volume for the small and large reference machine.

(Tong, 2014). The design phase generally incorporates tuning of numerous parameters, e.g. yoke and tooth thickness, and slot depth, see Figure 8, to ensure mechanical and thermal endurance, as well as electromagnetic performance.

Data collection

For both reference machines, a conventional stator design with 48 slots was used. This is the same as in all the car model examples given in Table 1 (Ozpineci, 2014). The stator's geometrical design in the reference machines was based on the Toyota Prius 2004 stator (ANSYS, 2011). Some minor adjustments have been made, such as a thinner yoke.

The selection of the reference machines' diameters and lengths were aimed to approximately reproduce how automotive electrical machine suppliers provide different series with different outer radiuses (Lenz, 2011). An outer diameter of 200 mm was chosen for the large reference machine, and 152 mm for the small. Inner diameters were set to 135 mm and 103 mm, respectively. Next, the nominal lengths of the stator cores were found through iterative calculations using ANSYS Maxwell (ANSYS, 2015) to be 127 mm for the large reference machine and 114 mm for the small. Both motors were then scaled down to half, and up to double, in length, again through calculations using ANSYS Maxwell (ANSYS, 2015), in order to establish a relationship between the torque, and power, with the core mass for various torque levels, such that the complete desired torque and power ranges were covered. As mentioned in Section 4.1.1, the material properties for the

lamination core, such as magnetic and iron loss characteristics, and the mass density of 7600 kg/m^3, were collected from Surahammars Bruk (2015a).

4.1.3 Magnet wire

The current conducting wire placed in the stator slots is often referred to as "magnet wire", as its purpose is to convert electrical energy into magnetic energy (Hitachi Metals, 2015a). However, the wire has no magnetic properties. A regular wire consists of a base metal, typically copper which is isolated by one or multiple layers of insulation materials (Tong, 2014). Apart from copper, aluminum can also be used, with the advantage of much lower cost, however with higher losses. Wires can be divided into two broad groups: enameled wires and covered conductor wires. The first type is coated with a hard glossy surface cover, made from polyester resins, polyamide resins or alkyd resins (Hitachi Chemical, 2015, Von Roll, 2012, Hitachi Metals, 2015a). The other type has at least one layer of plastic cover typically made from fibrous polyester, fiberglass yarn or polyamide film (Tong, 2014).

Common magnet wire diameters span from around a half to several millimeters. For high frequency applications the conductor may be made from several thinner wires, so called strands, which are only a few tens of µm up to almost a millimeter in diameter. Each strand is generally enameled but the conductor as a whole may also have additional insulation. Stranded wires are sometimes used for electric vehicle tractions motors (Von Roll, 2012), often without any additional insulation. The advantages of using stranded wire is that it can more easily be inserted into the slots and that resistance losses at higher frequencies are kept low.

Data collection

Enameled magnet wire was selected for the motor design. In the selection between regular or stranded magnet wires, the model calculations have not required this option to be specified, and the inventory result can considered equally representative in both cases. Instead, for the ANSYS Maxwell (ANSYS, 2015) calculations, it was the total copper fill factor (see next section, 4.1.4) in the slot cross sections that was the important factor.

For the enamel layer, it was observed from catalogued values for magnet wire that the thickness of the coating decrease with decreasing bare wire diameter, but also that the relative thickness of the coating layer slightly increases in relation to the same diameter. For example, depending on the coating grade, wires with a bare diameter smaller than 0.5 mm become 5-15% thicker and those bigger than 0.5 mm become 2-10% thicker, with enamel insulation, according to Von Roll (2012). Hence, as a simple but reasonable approximation for the magnet wire in general, both regular and stranded, it was assumed that they increase by 10% in diameter due to the coating. Next, based on the geometry of a cylindrical wire and the defined relationship between mass, volume and density, it was possible to derive that:

$$\text{Enamel coating mass} = 0.21 \times \frac{\text{Coating density}}{\text{Copper density}} \times \text{Copper mass}$$

The density of copper used in the calculations was set to 8940 kg/m^3 (Luvata, 2015). The coating was modeled as a cured unsaturated polyester resin with a density of 1930 kg/m^3 (Polynt Composites, 2015). Further details about application of the liquid resin on the enamel wire and the link to Ecoinvent version 3 database are presented in Section 5.3.1. The mathematical relation between the copper and coating mass can be simplified to:

$$\text{Enamel coating mass} = 0.045 \times \text{Copper mass}$$

4.1.4 Winding configuration

The copper conductors in the stator are wound in several turns through the core slots to form *coils*; 3-12 turns are typical. Either one or two coils, referred to as the number of layers, are inserted into each slot. Two layers give a smoother magnetic wave. Only the parts of the copper conductors placed within the stator core contributes to the torque production, i.e. belong to the active part of the machine. The parts outside the stator core, the end-turns, are passive and it is desirable to minimize their length. Also, in order to form complete

circuits the coils must be connected to a terminal block, or some other type of connector, in one end, and to a neutral point in the other end. Hence, conduction cables run along the end-windings on one side of the stator and through the housing.

The winding arrangement can be either concentrated or distributed. In a concentrated winding each coil is wound with multiple conductor turns around a single tooth. This leads to a compact design with short end-windings and less copper when comparing with a distributed type of similar torque performance (Tong, 2014, Choe et al., 2012, Barré and Napame, 2016, Kwon et al., 2006). In the distributed winding type, coils make turns in non-adjacent slots, overlapping other coils in a section of the stator. This is the most common type of winding for PMSMs, mainly because it yields a higher power density and higher efficiency compared to the concentrated type (Choe et al., 2012, Barré and Napame, 2016). Additionally, the distributed type creates less vibration and noise and it is simpler to cool (Tong, 2014, Choe et al., 2012), but much more difficult to automate for high volume production production (Kwon et al., 2006).

Due to the need for various insulation the share of copper typically fill 45 % of the slot area (Dutta et al., 2013). This is defined as the "fill factor" or "slot fill ratio" and represents a value for the space occupied by magnet wires compared to the total slot area. Generally, distributed windings provide a better fill factor than a concentrated windings (Tong, 2014, Kwon et al., 2006). It should preferably be as high as possible to maximize the power density and minimize losses due to resistance. Instead of using wire for the stator winding, it is also possible to use copper bars that are inserted into the stator and welded to form coils. It gives a higher fill factor than wire and it is used in some vehicle machines (Tong, 2014).

Data collection

The reference machines simulated in ANSYS Maxwell (ANSYS, 2015) were set-up with a two-layer distributed winding configuration and eight poles (to match the rotor, see Section 4.2.1). The coils were grouped into four parallel branches. Each conductor, in both layers of the winding, make seven complete turns per coil in the large reference machine, and ten in the small (at nominal length). The number of turns per layer then vary with the stack length, in order to stay with the same maximum current density and base speed. Hence, the highest number of turns will be used in the shortest stack length, and the lowest in the longest stack length. Roughly, the number of turns in a coil is doubled when the stack is scaled down to half of the reference length and, conversely, the number of turns is halved when the length is doubled. Still, the fill factor of each slot in all machines was set to 45%. It implies that that thinner conductors are used in short machines with many turns, and thicker conductors in long machines with fewer turns, compared to the proportions at nominal length. Commonly, when motors are custom scaled in length for an application, the conductor size is varied by adding or removing strands of a fixed size, rather than shifting wire to a different size.

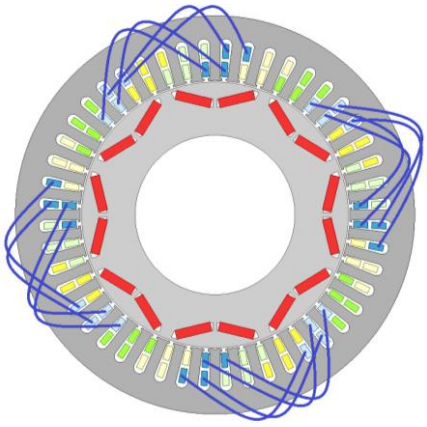

Figure 10: A schematic drawing of the distributed winding configuration. Blue, yellow and green coils (different shades for the two directions of the same coil) show how the three phases are distributed in the layers and branches of the winding. The blue arcs show how the coils (of only one phase) run in the end-winding. Each arc represents several turns.

Reference machine	Active section	End-windings	Phase conductors	Total mass
Small	1.3 kg	1.1 kg	0.03 kg	2.4 kg
Large	2.5 kg	2.2 kg	0.1 kg	4.8 kg

Table 3: The copper mass in wound wire and phase conductors in the small and large reference machines, in total and split between active and passive sections.

Moreover, the chosen distributed winding arrangement has a separation of 120 electrical degrees to form a smooth flux. The simulations were executed using a conductivity[3] of copper equivalent to an assumed normal winding operating temperature of 120°C.

It was assumed that the end-turns extend 2.5 cm from stator core on each side. A formula for estimating the average conductor length for half a turn, divided into one active and one passive section, has been provided by Lindström (1999), based on the inner stator diameter and the number of poles. Lindström's (1999) formula was used to calculate the share of active versus passive conductor per turn, as well as the total weight of the different sections. All phases are equally distributed around the stator and each branch occupies a quadrant of the stator cross section, see Figure 10. There are four coils per phase and branch, involving half of a slot (as there are two layers) per coil in each direction through the stator. For the small and large reference machines, 43% and 47%, respectively, of the coil lengths are passive in the end-windings, based on Lindström's (1999) formula.

Additionally, the copper used in the phase conductors running from the terminal block down to and along the circumference of the stator to the windings of each branch, have been considered. The parallel wires of each phase are distributed to the four branches around the stator. All return wires are then interconnected to form a neutral. In order not to underestimate the lengths, the outer stator diameter was used for the calculation (i.e. the outer circumference of the stator). The total phase conductor length was estimated to equal about two complete laps along the stator's circumference in both machines, as well as an added 5 cm and 3.8 cm for the large and small reference machines, respectively, accounting for the distance from the terminal block down to the end-winding. Then, the conductor cross section area (i.e. the sum of areas in the case of stranded magnet wire) was estimated using the total copper area per slot and layer, in combination with the number of turns in each layer (including change of the number of turns with different stack length). By combining these estimations, the copper mass for the phase conductors could be calculated. Results for the reference machines at their nominal lengths are presented in Table 3. As can be seen, the phase conductor mass was found to be small compared to that of the end-windings, and the passive amount of copper varies marginally compared to the variation of mass in the active sections when the reference machines are scaled in length.

4.1.5 Insulation and impregnation

The winding coils must be firmly mounted and insulated to be protected from short circuiting, to each other and to the stator core. Thus, in addition to the wire enamel coating, the slots are provided with an isolation layer at the boundary to the core, called slot liner. Also, when two layers are used it is common to place a slot separator between coils in the slot, especially if they are of different phases (Pyrhönen et al., 2008). When all coils are in place, the stator package is partially or fully encapsulated to protect it from vibration, moist and dirt. Full encapsulation means that the entire stator package is soaked in some impregnation material which is then cured, for example an epoxy compound or a silicone elastomer (Tong, 2014). Partial encapsulation can refer to that the voids of the slots, and possibly also the end-windings, are filled with impregnation, with more deliberate application. Additional to the vibration protection, this provides good thermal conduction from the winding to the core, which is important for proper cooling (Dorrell et al., 2011).

The slot liners and separators are made of paper, plastic foil, powder coating, or molded thermoplastic materials (Tong, 2014). Thicknesses vary from 0.1 mm to around half a millimeter, depending on the material and operation requirements. Slot liners are placed in the slots before the coil winding, and extend a few millimeters outside the stator core.

Another form of insulation, phase to phase insulation, protects the winding at the end-turns between adjacent phases. The enamel layer is often sufficient to meet the demand for turn to turn and coil to coil

[3] 41 821 756 S/m

insulation, for low- or moderate voltage stators (Tong, 2014). Full impregnation, for example through varnish dipping, may be satisfactory for the phase to phase insulation. However, for higher stator voltages, or for partial impregnation, supplementary insulation becomes necessary. Different types of insulating tapes or sheets can be wrapped around the coil ends to enhance the dielectric strength between the phases and protect against high voltage peaks which may occur, for example in inverter driven traction machines (Von Roll, 2007). Tapes made with glass cloth or plastics, sometimes covered by mica, a type of silicate mineral, are used for this purpose (Von Roll, 2007, Kauppinen, 2014).

Next, the phase conductors must also be electrically isolated. Ready-made, insulated cables may be used or, if the bare magnet wires are used to connect with the terminal block, they can be threaded with tubes for protection. Sometimes such tubing is crimped with heat. Extruded crosslinked polymers are common insulation materials for power cable applications, since they can provide the desired combination of electrical and mechanical properties with high temperature operation (Hampton et al., 2007). For example, crosslinked polyethylene or silicone rubber is used (Leoni, 2014).

Finally, in order to tighten the packing of the end-windings, including the various types of insulation, they are commonly tied-up using lacing cords or bands, referred to as lacing or banding. Cords or bands can be made in many different materials: cotton, linen, nylon, polyester or fiberglass (Essex Brownwell, 1998).

Data collection

For the slot liners and separators, a 0.3 mm thick PET (polyethylene terephthalate) foil, with the brand name MYLAR, was selected (Dupont, 2004, Carbex, 2015b). This type of rigid polyester foil is typically applied as electrical insulation in electrical machines and transformers. A tabulated density of 417 g/m^2 (Carbex, 2015b) was combined with the ANSYS Maxwell results for the slot circumference and the width a the slot midpoint for the 48 slots, to calculate the total mass of slot liners and separators necessary for the two reference machines in relation to the stator core length. All slot liners and separators were assumed to extend 5 mm outside the stator stack on each side, i.e. adding a total of 1 cm compared to the stator core length. Table 4 shows the resulting values.

Reference machine	Mass	Volume	Fill ratio
Small	8.4 g / cm	6.0 cm^3 / cm	25%
Large	11 g / cm	7.6 cm^3 / cm	16%

Table 4: Mass, volume and fill ratio of the MYLAR slot liners and separators, in relation to their lengths (active length plus 1 cm), established for the cross-section geometries of the small and large reference machines.

Next, to estimate the amount of phase-to-phase insulation and impregnation outside the stator slots, in the end-windings, a simple geometrical analysis was conducted for the selected configuration and combined the proportions of active and passive conductor length provided by Lindström (1999). Moreover, about one fourth of each slot cross section corresponds to magnet wire of one coil (two coils per slot and around 50% of the fill factor including the enamel). For a phase bundle of four coils it matches one complete slot. However, as shown in Figure 11, circular conductors cannot be packed together without voids, even with the tightest possible packing. Even so, such tight bundles are not achievable. Hence, the bundle cross section was approximated to be 25% larger than that of the wires only (i.e. with 20% void in the cross section), and the circumference 12% larger based on the square root relation to the area.

For phase-to-phase insulation of the winding end-turns, data for a thin mica covered glass cloth electric isolation tape named SAFIREX PGC was gathered from (Saveway Isolierstoffe, 2015). The surface weight is 170 g/m^2, comprising 70 % mica, 19% glass fiber cloth and 11% silicone bond (Saveway Isolierstoffe, 2008, 2015). Mica is a group of silicate minerals which can be found in and extracted from various rocks, gravels and sands. Flaked mica is mainly recovered in the beneficiation procedures to make industrial sands (U.S. Geological Survey, 2014). Silica sand is the main product from such processing (Kellenberger et al., 2007). Hence, the mica content was proxied as silica sand for the link to the Ecoinvent 3 database (Weidema et al., 2013). The cloth was listed as “glass fibre” and the bond as a “silicone product”.

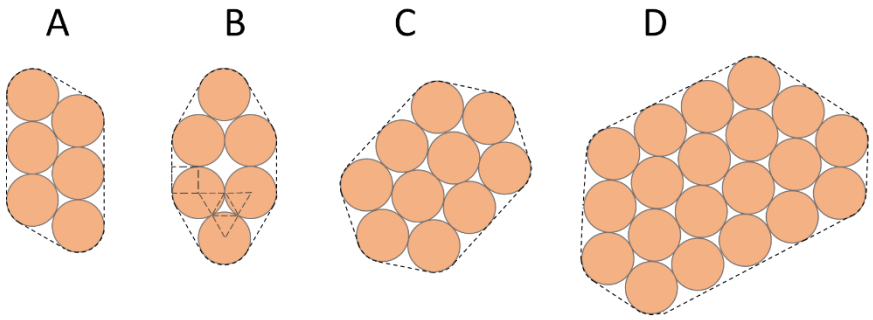

Figure 11: Examples of how magnet wires may end up when tightly packed in a bundle, to minimize voids. As indicated in alternative B, voids were identified and approximated based on the area difference between squares and circles (larger voids) and equilateral triangles and segments (smaller voids). Results came to 15% void for alternative A, 17% for B, 13% for C and 12% for D.

For the quantity of tape used, there is a large variability. Using the circumference for a phase bundle with four coils from the geometric approximation, the tape was expected to vary in overlap with 10-50% if wrapped once around a bundle (Saveway Isolierstoffe, 2015). But, tapes may be wrapped several times around a bundle. On the other hand, tapes or sheets do not have to completely cover the end-windings as the purpose is to insulate between the phases and not to enclose them. Neither do not all three phases have to be wrapped with insulation. Under such diverging circumstances, it was found reasonable to use a fairly high estimate, and to approximate the phase insulation use based on the amount required to encircle the slot circumference with 50% overlap for all of the passive coil lengths in the three phases and four branches. The results for the two motors are shown in Table 5.

Reference machine	Mass	Area
Small	26 g	15 dm^2
Large	37 g	22 dm^2

Table 5: Mass and area of the mica phase insulation material.

The design also includes an impregnation of the windings, calculated in two parts. One for the amount of epoxy based compound to fill the voids of the stator slots and one to encapsulate the wire bundles of the end-windings. Data was gathered for a prefilled and solvent-free, one component based epoxy resin suitable for several different processing methods and impregnation of stators for traction motors, called Damisol 3500 HTC (Larrenduche, 2015) The compound contains about 25% silica based filler material and has a density of 1310 kg/m^3 (Larrenduche, 2015, Von Roll, 2015), noted as silica sand for the inventory link to the Ecoinvent 3 database (Weidema et al., 2013). The remaining 75% was listed as liquid epoxy resin, but there are also some losses of the chemical base during the impregnation curing process, see Section 5.4.4.

The total amount of impregnation compound for the stator slots, specified relative to the stack length, was determined by deducting the combined slot fill ratio for the copper wire, increased by 10% to include the enamel coating, and the fill ratio of the slot liners and separators, from the total slot cross section. Table 6 presents the volume per length unit and the mass. The length used was that of the slot liners, including the 5 mm extension on each side of the stator core.

Reference machine	Mass	Volume	Fill ratio
Small	9.2 g / cm	7.0 cm^3 / cm	25%
Large	22 g / cm	17 cm^3 / cm	35%

Table 6: Mass, volume and fill ratio of epoxy impregnation resin in the stator slots in relation to the slot liner length (active length plus 1 cm), established for the cross-section geometries of the small and large reference machines.

The impregnation of the end-windings was based on the geometrical analysis for the phase bundles presented above. Assuming an application method without excessive encapsulation of the entire stator package, see Section 5.4.4, it was assumed that only the voids of the phase wire bundles are filled with the Damisol 3500 HTC epoxy resin. Results are presented in Table 7.

Reference machine	Mass	Volume
Small	45 g	34 cm^3
Large	90 g	69 cm^3

Table 7: Mass of volume of epoxy impregnation resin in the stator end-windings for the small and large reference machines.

For completeness, data for silicone isolation of the phase conductors and a nylon lacing cord was gathered. Both silicone ("silicone product") and nylon (nylon 6) can be found in Ecoinvent 3 (Weidema et al., 2013). The mass of the cover or tubing for the phase conduction cables was established by combining tube dimension data from Carbex (2015a) with a material density of 1250 kg/m^3 stated by (Leoni, 2014), and adapting it to the size of the conductor wires, as described in Section 4.1.4. For simplicity, the tubing dimensions were set constant for the two reference machines respectively, based on the thickest phase conductor width. Results were 13 grams for the small reference machine and 28 grams for the large.

Data for nylon lacing cord was gathered from (Breyden, 2015) and combined a rough estimate for the amount of cord based on the dimensions of the end-windings. As regards the length, it was assumed that the number of knots made by a lacing machine is governed by the number of slots in the stator core. Since the number of slots and roughly also the thicknesses of the end-windings, are the same for the two reference machines, this length was found to dominate over the distance between the knots, which is longer for the larger machine. Hence, the length of the cord was estimated to 9 meters for both reference machines, with a small weight contribution of 6 grams.

4.2 Rotor package

4.2.1 Rotor core design

The task of the rotor is to produce a torque which can be transmitted to the wheels. By providing a magnetic field which interact with the magnetic field of the stator windings, it converts magnetic power to mechanical power. In the case of a PMSM, the rotor field is generated by permanent magnets. The rotor core is made up of stacked electrical steel laminations, analogue to the design of the stator core, see sections 4.1.1 and 4.1.2.

The magnet field paths generated by the permanent magnets and the stator currents typically flow in the outer part of the rotor, whereas the inner parts do not contribute to the electromagnetics of the machine. Hence, the magnets are placed in the outer segment. Consequently, the amount of laminated steel in the inner parts of the rotor can be reduced by punching holes, decreasing both weight and inertia[4] of the machine, and enabling quicker acceleration.

In an IPM machine (the type modelled here), the magnets are placed inside the rotor core, in pockets. Another common alternative is to attach the magnets on the surface, referred to as surface mounted. IPM rotors are well suited for high speed applications, such as vehicle machines, due to their mechanical robustness since the magnets are well protected against centrifugal forces (Gieras, 2010, Krishnan, 2010). Another benefit of IPMSMs over surface mounted PMSMs, is that the magnets can be rectangular instead of arced, which are more difficult to manufacture and, consequently, more expensive (Hendershot and Miller, 2010). In IPMSM the magnetic reluctance[5] varies around the rotor, which causes a second torque producing component called reluctance torque. By placing the magnets in a V-shape, this effect is enhanced so that the total produced torque per pole increases (Hendershot and Miller, 2010).

[4] The mass resistance to changes in rotational speed.

[5] The flux resistance.

Lastly, a permanent magnet rotor package often also comprises some type of mechanical stopper, in combination with an adhesive, to hinder the magnets from moving in the axial direction, to protect them from corrosion and to cover the rotor voids at the core ends (Tong, 2014). Such a design is referred to as a closed end rotor. In order to also use the plates to limit flux leakage, non-magnetic stainless steel material are preferably used for the mechanical stoppers in IPM machines (Kolehmainen and Ikäheimo, 2008, Dawsey et al., 2009, Tessarolo et al., 2014).

Data collection

Based on observations of existing PMSM designs, for example by Toyota, the rotors of the two reference machines were designed as IPM machines, with magnets placed in a V-shape for each of the 8 poles (Ozpineci, 2014). The large reference machine has been modeled with an outer rotor diameter of 134 mm, and the small with one of 101 mm. The inner boundary of the magnetically active area of the rotor core was established at 80 mm diameter and around 61 mm, respectively, for the two motors. Inside this boundary, the laminated steel design is governed by mechanical considerations such as the connection to the shaft, minimizing mass and handling rotational forces. As a simple, but reasonable estimation it was assumed that this area consists of 25% laminated steel and 75% void for both references rotors, and throughout the scaling. This matches with the scaling of the shaft, as described in Section 4.2.3, and design variations for different shafts. Also, it is in agreement with observations made from literature on the amount of void granted for and around the shaft in the rotor core (Burress and Campbell, 2013, Ozpineci, 2014). The results for the total steel core are shown in Table 8. Again, referring to Section 4.1.1, the properties of the laminations were collected from Surahammars Bruk (2015a). As with the stator core, both reference lengths were decided through iteration, and both were scaled down to half, and up to double the length using ANSYS Maxwell (ANSYS, 2015).

Reference machine	Mass	Volume
Small	4.4 kg	0.58 dm^3
Large	8.4 kg	1.1 dm^3

Table 8: Rotor core mass and volume for the small and large reference machines, excluding rotor endplates.

Examples of rotor endplate thicknesses were studied in pictures from literature (Kolehmainen, 2007, Kolehmainen and Ikäheimo, 2008). The endplates were assumed to increase in width with the maximum machine torque. The shaft also increase in diameter with higher torque, see Section 4.2.3, reducing the mass in the endplate as the hole for the shaft increases. Hence, these two factors were found to roughly balance each other and two constant mass endplates of stainless steel were included in the reference machines, one on each side of rotor core. The volume and mass of the rotor endplates are shown in Table 9, calculated with a density of 8030 kg/m^3 for a type of 18/8 grade of stainless steel (AK Steel, 2007), linking to the data for chromium steel 18/8 in Ecoinvent 3 (Weidema et al., 2013). These may be solid, with widths as stated in Table 9, or be thicker and only cover the active part of the rotor core.

Reference machine	Mass	Thickness per plate
Small	250 g	2-2.2 mm
Large	580 g	2.7-3 mm

Table 9: Total mass of the rotor endplates for the small and large reference machines and corresponding thickness spans if the plates are solid.

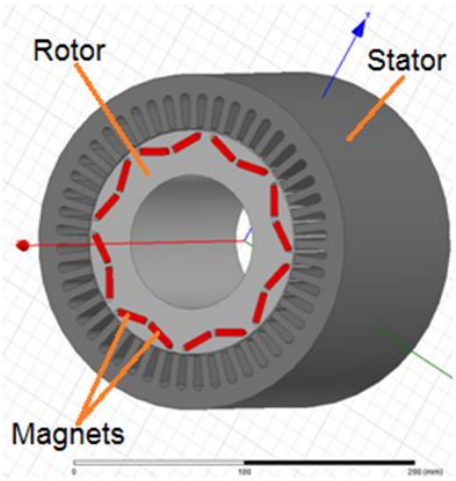

Figure 12: The stator and rotor cores, including magnets. The rotor only includes the magnetically active parts, i.e. the structure connecting to the shaft is missing.

4.2.2 Permanent magnet composition

Some compounds, referred to as ferromagnetic materials, can be permanently magnetized. Among the most powerful are rare earth metal magnets containing samarium or neodymium (Tong, 2014). Important properties of a magnet are remanence[6], i.e. the magnetic strength, coercivity[7], i.e. the resistance to demagnetization, and the energy product[8], central for the amount of magnetic energy which can be stored in them magnet. At room temperature, neodymium-iron-boron (NdFeB) magnets have the highest energy products of all permanent magnets (Lucas et al., 2015, Vaimann et al., 2013). They also have high remanent magnetization, and good mechanical properties for processing of complex shapes (Lucas et al., 2015, Tong, 2014). This has led NdFeB magnets to become widely used, and the most common type of permanent magnet for electrical traction machines (Lucas et al., 2015, Vaimann et al., 2013).

However, the properties of the magnets are temperature dependent and in automotive applications occasional operating peak conditions can reach above 150°C (Lucas et al., 2015). Ordinary NdFeB magnets are not well suited for such high temperatures, because the coercivity drops as the temperature goes up, and they also corrode unless coated (Yan et al., 2010, Vaimann et al., 2013, Tong, 2014). Samarium-cobalt magnets are an alternative and well suited for high performance applications as they can withstand both corrosion and high temperatures much better, up to 350°C, but they are more expensive (Lucas et al., 2015, Tong, 2014).

The main problem related to the temperature dependency of the magnet properties is the risk for demagnetization. This may happen if the loading currents of the opposing magnetic field of the stator becomes too high, typically during faulty operation of the machine or the inverter unit, for example during a short circuit (Vaimann et al., 2013). One way to address the less good thermal performance of NdFeB magnets is to divide them into segments and thereby reduce thermal losses and avoid subsequent heat escalation. Segmentation also reduce magnet losses, but especially for V-shaped IPM rotors this of less importance, where magnet losses account for only about 0.5% of the total electromagnetic losses (Dutta et al., 2013).

The thermal stability of NdFeB magnets can also be increased to become suitable for vehicle motor applications by adding another rare-earth element to replace some of the neodymium, dysprosium (Brown et al., 2002, Yan et al., 2010, Vaimann et al., 2013). However, at the same time as dysprosium increases the ability to withstand demagnetization at high temperature, it lowers the overall remanence of the NdFeB magnet (Brown et al., 2002, Vaimann et al., 2013). Also, rare earth metals are costly materials in general, and especially dysprosium is expensive, due to a limited supply (Dorrell et al., 2011, Gutfleisch et al., 2011). Hence, recent development efforts have focused on minimizing the addition of dysprosium and still accomplish the desired benefits. It has been found that the effect of substituting neodymium differs within the microstructure of the

[6] The degree of permanent magnetization, residing without any external magnetic field being applied.
[7] The ability to withstand an external magnetic field without becoming demagnetized.
[8] The maximum magnetic energy density which can achieved in the magnet.

magnet and that it is beneficial to apply dysprosium mainly at the boundaries between grains of the magnet material, in order increase the coercivity without too much loss of remanence (Yan et al., 2010, Hitachi, 2014, Nakada et al., 2014, Vaimann et al., 2013). This type of NdFeB magnets can have a magnetic flux ability of up to 1.4 Tesla (Hitachi, 2014), which enables highly efficient PMSM machines. A typical NdFeB magnet composition consist of up to 10% dysprosium, 22-32% neodymium, 67-70% iron and 1% boron (Yan et al., 2010, Gutfleisch et al., 2011, Fyhr et al., 2012).

Furthermore, the coating of NdFeB magnets can be conducted with various methods and substances, such as nickel, gold, chromium or epoxy resin (Tong, 2014). Electroplating with nickel is most common, resulting in a thin layer around 5-25 µm thick. For automotive electrical machine applications, epoxy resin is another common surface treatment, typically in layer of 10-30 µm (Magcraft, 2007, Hitachi Metals, 2014b). Epoxy and other types of casting resins are also used for fixating the magnets in the rotor cavities where the gap between the core and the coated magnet are at least of 0.1 mm (Tremel et al., 2013). There are also cavities at the end of each magnet to provide magnetic flux barriers. Filling these voids is important in order to improve heat dissipation and avoid mechanical friction losses, and wear, between the magnets and the rotor core.

Data collection

A low dysprosium NdFeB magnet grade from Hitachi's NEOMAX-series (NMX-37F) was used for the magnet data (Hitachi, 2014, Hitachi Metals, 2014a, b, 2015b). It contains about 4% dysprosium and has been rated to withstand operation at 140°C (Hitachi Metals, 2014a). This magnet can be expected to handle all operating points of the modelled electrical machine and the magnetic properties are well in line with published data on magnets used in automotive machines (Burress et al., 2011). The calculations made in ANSYS Maxwell were conducted for an operating temperature of 70°C. The electromagnetic properties used can be seen in Table 10 (Hitachi Metals, 2014a).

The NEMOAX-series magnets have densities in the range of 7500-7700 kg/m^3 (Hitachi Metals, 2015b), and based on a comparison with the pure element densities for the modelled composition, 7500 kg/m^3 was found representative for the 37F grade. There are two magnets per pole, to achieve the V-shape, and consequently 16 magnets in total. The mass proportions of the uncoated magnet are shown in Table 11. It was established by combining the base body NdFeB alloy configuration provided by Sprecher et al. (2014b) with the addition of 4% dysprosium taken from Hitachi (2014), and to become in accordance with typical Nd(Dy)FeB compositions (Yan et al., 2010, Gutfleisch et al., 2011, Fyhr et al., 2012). For more details on the alloying and addition of dysprosium, please see Section 5.1.3. Also, it was assumed that the magnets are segmented, but without any specification of the segment arrangement, because its contribution to the reduction of losses inside the magnets was neglected in the performance calculations, in line with Dutta et al. (2013). Also, it was assumed that the magnet is coated with nickel in a layer of 10-15 µm, resulting in a nickel mass corresponding to 1% of the total magnet mass[9]. The mass for coated magnets in the two reference machines in Table 12.

A methacrylate ester resin (Henkel, 2010, 2015) was selected for the adhesive used to fixate the magnets based on a description of the procedure given by Hendershot (2015). The amount of adhesive was calculated for a layer of 100 µm around the circumference of all magnets, and in triangular cavities at both magnet ends, along the active length of the rotor. A resin density of 1100 kg/m^3 (Henkel, 2010) was used. Result are shown in Table 13, and indicate that only a few grams are needed, i.e. significantly less than the amount of epoxy in the stator. For the link to Ecoinvent 3 (Weidema et al., 2013), the adhesive was proxied as "methyl methacrylate".

The magnets material matching to upstream data for the will be further discussed in Section 5.1, along with the details of the magnet production procedures.

Relative permeability	Coercivity at 70°C	Electric conductivity at 70°C
1.04	902 kA / m	750 kS / m

Table 10: Electromagnetic properties of the Nd(Dy)FeB magnet (Hitachi Metals, 2014b).

[9] The density of nickel is 8900 kg/m^3 (Lagneborg and Waltersson, 2004)

Element in alloy	Mass share
Neodymium	26%
Dysprosium	4%
Iron	69%
Boron	1%

Table 11: Modelled mass proportions of the Nd(Dy)FeB magnet (Hitachi, 2014, Sprecher et al., 2014b), excluding the nickel coating.

Reference machine	Mass	Volume
Small	0.65 kg	87 cm^3
Large	1.3 kg	168 cm^3

Table 12: Magnet mass and volume for the small and large reference machines, including the nickel coating.

Reference machine	Mass	Volume
Small	2.7 g / cm	2.5 cm^3 / cm
Large	4.4 g / cm	4.0 cm^3 / cm

Table 13: Magnet fixation resin mass and volume in relation to the rotor core lengths for the small and large reference machines.

4.2.3 The motor shaft

The role of the shaft is to transmit the torque produced by the motor to the external load, via the mechanical drivetrain. Shafts must be able to handle various types of mechanical stress and strain during operation. For this reason, the aim of its design is to reach highest possible stiffness and rigidity in combination with lowest possible deflection. Both the selection of shaft material and the motor dimensions are important, especially the diameter of the shaft and the distance between the two bearings. The more torque the shaft shall be able to transmit the thicker it must be. The coupling between the electrical machine and the subsequent mechanical drivetrain can be accomplished through many different forms of coupling devices such as flanges, splines, belts, or chains (Burress et al., 2011, Tong, 2014). The shaft can be either solid or hollow, again depending on the specific design. Considering shaft materials in general, carbon steel is the most common selection. However, in corrosive environments stainless steels are also used, for example in food and medical device industry machines.

The shaft also includes some type of connection, intended to secure coupled axles and to transmit the generated motor torque to external equipment. Splined or key connections are two common types (Tong, 2014). For a key connection there is often a keyseat drilled into the shaft where the key is fitted. Splines can be viewed as many parallel keys or a large cogwheel machined directly onto the shaft. Torsion and bending loads are uniformly distributed over many teeth, making splines a very robust solution. The number of spline teeth per shaft varies greatly depending on the design, with examples from four up to 40 mentioned in literature (Barsoum and Khan, 2012, Tong, 2014). The tooth depth is coupled to the total number of teeth, in order to achieve proper strength, with the required depth decreasing as the number of teeth is increased (Barsoum and Khan, 2012, DIN, 2006). For example, for a shaft with a 20 mm diameter with 20 teeth a depth of 1 mm can be expected, whereas for a 40 mm shaft with only 4 teeth, the depth is more likely set around 1 cm. The average diameter in the splined section is referred to as the pitch diameter (DIN, 2006).

Data collection

The shaft is one of the passive parts in the motor, as discussed in Section 2.4, whose mass did not result directly from the ANSYS Maxwell (ANSYS, 2015) calculations of its electromagnetic properties. Instead the shaft was scaled in diameter to match the maximum motor torque and in length with the active length of the core parts. The mass was then calculated from the volume with for a low-alloy medium carbon steel with

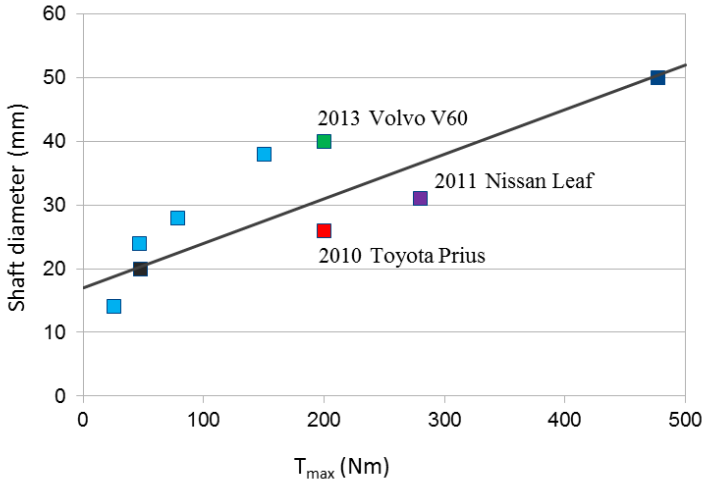

Figure 13: Shaft diameter as a function of maximum torque selected in the model (grey line and grey endpoints), in comparison to Baumüller's industrial machines, DSP1-045-100 (blue),2011 Nissan Leaf (purple), 2010 Toyota Prius (red) and 2013 Volvo V60 (green) (Burress et al., 2011, Sato et al., 2011, Schwartz, 2014, Baumüller, 2014).

a density of 7870 kg/m^3 (AK Steel, 2014), classified as low-alloyed steel for the link to Ecoinvent 3 (Weidema et al., 2013).

The length of the shaft logically depends both on the length of the motor and how the coupling to mechanical drivetrain is constructed. For both reference machines it was assumed that it extends about 4.5 cm from the machine housing, with a splined section for the coupling. For the detailed calculation, a length of 120 mm plus the active length of the motor was used, including 35 mm for the splined section.

It can be expected that the shaft includes notches, rims and sections with varying diameters, for instance to secure the rotor core. However, for simplicity the shaft was modelled with an average uniform and solid shaft diameter, including the pitch diameter for the splined section. The diameter was based on comparison with solid shafts in industrial machines from Baumüller (2014) and automotive machines from Toyota, Nissan and Volvo (Burress et al., 2011, Miller, 2013a, Sato et al., 2011, Schwartz, 2014). Both the Nissan Leaf and Volvo V60 shafts were measured in drawings for an estimated average diameter point, to account for the variations over the shaft length. Figure 13 shows the scaling of the shaft diameter as a function of the maximum motor torque in the LCI model. The endpoints of the torque span, 48 Nm and 477 Nm, corresponds to 20 mm and 50 mm shaft diameter, respectively.

4.3 Integration, protection and monitoring

4.3.1 Housing

In order to protect and contain the stator and rotor packages, a housing is needed. For large industrial machines this frame is often made of cast iron (Tong, 2014). For smaller applications, e.g. in automotive powertrains, aluminum is a common material (Sato et al., 2011, Tong, 2014, Johan Johansson, 2015). The housing generally consists of a cylindrical or rectangular casing, the housing body, with various internal and external structures for cooling, strength and mounting, and two endbells at the sides of the casing. The shape of the housing largely depends on the stator form as it is mounted on the outside of the stator core, extending far enough on both sides to cover the end-windings and connection cables. The design also depends on the conditions for mounting the entire machine in the vehicle. Each endbell is shaped to encircle and hold a bearing on each side of the active part of the motor.

Cooling of electrical machines is realized through the design of the housing. Air cooling is common for industrial machines. Fans are used and different types of fins dissipate heat to the air flow. Passive air cooling, i.e. without fans, include various forms of surface treatment to increase radiation and convection. However, for automotive applications, liquid cooling is most common (Sato et al., 2011, Nakada et al., 2014), with channels designed inside the housing body. A liquid is pumped through the channels via connecting hoses to and from the motor. Typically, the liquid is a 50/50 mixture of water and ethylene glycol or propylene glycol

(Tong, 2014). Effective cooling, or the lack of it, has a direct influence on the capability, reliability, and lifetime of electrical machines. Especially, proper cooling is required to combine high performance with small size and low power consumption (Tong, 2014). In general, large machines have less losses, and thus higher efficiency that smaller sized motors. Simpler, and comparably smaller housings could then be expected, i.e. that the housings' share of the mass configuration would decrease, since less cooling is necessary. However, large motors require more structural design for other reasons, for example to handle larger mechanical loads and vibrations, as a counterbalancing effect.

Data collection

The housing body and endbells belong to the passive parts in the motor. As already mentioned in Section 2.4, all active and most passive motor parts with variable size (e.g. shaft, bearings and insulation materials), scales directly with the maximum torque value in the LCI model, or with the active motor geometry, indirectly linked to the torque vale. However, the housing parts were set to scale directly with the maximum power value since an important function of the housing is to dissipate heat losses, which relates principally to power.

The housing of the reference machines, including the endbells, was modelled as encircling the active stator core, end-windings and connection cables with a cylindrical shape, which is not integrated with any other powertrain part, similar to the version of the Nissan Leaf electrical machine analyzed by Sato et al. (2011). Data for the masses of the housings, motor volumes and measured maximum power was collected for disassembled models of the Toyota Camry, Lexus LS 600h, Toyota Prius and the Nissan Leaf from Burress et al. (2011), Miller (2013a) and Shimizu et al. (2013). The volumes occupied by the stator and rotor packages inside the housings were then calculated based on the measured values for the stator diameter and core length from the same sources, plus an estimation for how far end-windings and connection cabling extend outside the stator core. Based on the authors' own experience as well as observations made in photographs and drawings in literature (Sato et al., 2011, Burress et al., 2011, Burress and Campbell, 2013, Burress, 2013), it was established that this additional length typically is 5.5-6 cm in the axial direction of the machine. Hence, the housing volumes could be calculated for each vehicle model and related to the motor power, in the form of a ratio. Also, the actual mass of the housing could be related to what the housing would weigh if the entire volume consisted of aluminum (with a density of 2700 kg/m^3 (Lagneborg and Waltersson, 2004)), in the form of a "solid share". Results are shown in Table 14.

As can be observed, the encased volume is similar for all four motors, while the volumes of the housings diverge. But the alignment in the volume to power ratio indicate that the volume has a fairly linear correlation with power. This can be expected, since a motor with high power produces high heat losses that the housing and the cooling system must be dimensioned to handle during operation. Furthermore, the ratio for the Nissan Leaf motor is the highest of the four vehicles. An explanation is the use of a different definition of maximum power in its specification. For example, the 2010 Toyota Prius electrical machine has been measured to 60 kW peak power, and powertrain is able to deliver this for 18 seconds before the motor is overheated (Burress et al., 2011). In the Nissan Leaf, the electrical machine can operate continuously at 80 kW, and tests indicate that

Example model (Year)	Measured motor volume	Estimated encased volume	Resulting housing volume	Measured housing mass	Solid share
Nissan Leaf (2011)	16.7 dm^3	6.5 dm^3	10.2 dm^3	19 kg	69%
Toyota Prius (2010)	12.5 dm^3	6 dm^3	6.5 dm^3	14.1 kg	81%
Lexus LS 600h (2008)	16.7 dm^3	6 dm^3	10.7 dm^3	14 kg	48%
Toyota Camry (2007)	14.8 dm^3	6.5 dm^3	8.3 dm^3	14.7 kg	65%

Example model (Year)	Rated max. power	Housing volume to power ratio	Sources
Nissan Leaf (2011)	80 kW	0.13 dm^3/kW	Miller (2013a), Sato et al. (2011), Shimizu et al. (2013)
Toyota Prius (2010)	60 kW	0.11 dm^3/kW	Burress et al. (2011)
Lexus LS 600h (2008)	110 kW	0.10 dm^3/kW	Burress et al. (2011)
Toyota Camry (2007)	70 kW	0.12 dm^3/kW	Burress et al. (2011)

Table 14: Measured and calculated data on the aluminum housings, including endbells, for the Nissan Leaf, Toyota Prius, Lexus LS 600h and the Toyota Camry. Model year in parenthesis.

much higher power levels are possible (Burress and Campbell, 2013, Miller, 2013b). Instead, for Nissan Leaf, the inverter and battery limit the power performance, rather than the machine itself. In another powertrain, using the same definition for maximum power as Toyota, the volume to power ratio for the Nissan Leaf electrical machine would be lower.

Still, masses differ also in relation to the maximum power, implied by the difference in "solid share" of Table 14. Acknowledging that there are many case specific explanations for this, it can still be argued that the minimum casting thickness of various details in the housing is important, especially for smaller housings. Observations in the literature indicate casting thicknesses of around 6-7 mm for the Toyota Prius (Burress et al., 2011) and the Nissan Leaf (Burress, 2013). On the other hand, according to Johan Johansson (2015), thinner castings, more slender designs and thereby reduced weight, but still with sufficient strength, is achievable with a standard lowest thickness of 3 mm, and a solid mass share down to 40%. Based on this discussion, it was found that a volume to power ratio of 0.1 dm^3/kW_{max} with a solid share of 50-60% aluminum, results in in an approximate mass to power relationship of 130-160 g/kW_{max} for the complete housing. However, the observations also indicated that if the model would be directly based on a mass to power relationship in this span, it would overestimate the mass for high power value and underestimate the mass for low power, within the span of 20-200 kW. Hence, as an adaption, the total mass for 20 kW was assumed to be 4 kg and the power to mass factor is 130 g/kW_{max} for the scaling up to 200 kW.

Furthermore, as shown in Figure 14, and already mentioned several times previously, the housing consists of three separate parts, one cylindrical body and two endbells. Thus, in the next step, the share of each housing part out of the total had to be established. Each endbell is supposed to encase a bearing but they differ in the modelled design as one also integrates the resolver with an additional smaller cover plate, and the other includes an adaption for the terminal block. For simplicity, these differentiating functions and shapes were assumed to be balanced in weight, and result in an equal mass of the two endbells. The individual mass shares of the parts were then estimated based on the housing inner surface area shares for the two ends and the cylinder encircling to stator at the nominal lengths of the reference machines, with an addition of 55 mm to cover for the encased end-windings and phase conductors outside the core.

It was found that each endbell constitute around 15% of the total housing mass for the small reference machine at nominal length, and around 17% for the large machine. Furthermore, these results were combined with the mass to power relationship and the maximum nominal power of each reference machine. The results are presented in Table 15. Finally, the established data was combined to express the masses of the different housing parts as functions of the specified maximum power, as presented in Table 16 and Figure 15. More particularly, the endbells' masses were held constant for each reference machine and only scaled linearly in the merged overlapping section of the maximum power span (see Section 2.1 and how the two reference machine datasets have been combined). The mass of the housing body was then adjusted to match the total weight of the housing predicted by the established mass to power relationship, also shown in Figure 15.

Figure 14: The housing consisting of a cylindrical body and two endbells.

Reference machine	Housing mass		
	Total	Cylindrical body	One endbell
Small	6.6 kg	4.6 kg	1.0 kg
Large	14.4 kg	9.4 kg	2.5 kg

Table 15: Estimated masses for the aluminum housing parts, for each reference machine at its nominal length and power.

Housing part	Mass at 20 kW	Power to mass constant		
		20-50 kW	50-80 kW	80-200 kW
Housing body	2.0 kg	130 g/kW	30 g/kW	130 g/kW
Endbell, per piece	1.0 kg	0 g/kW	50 g/kW	0 g/kW
Total mass	4.0 kg	130 g/kW	130 g/kW	130 g/kW

Table 16: The complete set of parameters specified in the housing mass estimation.

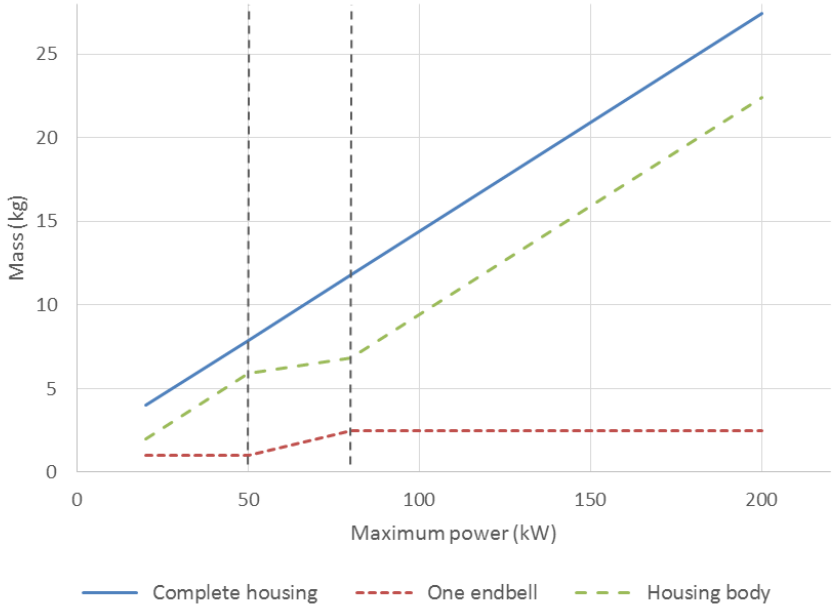

Figure 15: Estimation of the housing parts' masses, and the mass of the complete housing, as a function of the specified maximum power from 20-200 kW, based on the power to mass constants and starting masses presented in Table 16. Endbell masses are constant under 50 kW (1.0 kg) and above 80 kW (2.5 kg), in line with Table 15.

Lastly, it should be noted that the housing mass was established based on a few observations only, although there are many design options to meet the same functionality. No theoretical analysis has been made based on the main parameters which decide the housing dimensions, such as thermal and mechanical properties. Nevertheless, the housing gives an important contribution to the total motor mass. Together with the stator and rotor core masses it is the biggest contributor to the overall mass. In contrast to the housing, the masses of the stator and rotor have been established from model calculations based on fundamental electromagnetic properties. Therefore, the data model has been constructed in such a way that a user may deselect the inclusion of housing parts. More specific such data, with a higher mass precision, may then be collected independently and combined with the inventory data for the rest of the motor.

4.3.2 Bearings

The bearings couples the housing to the shaft and carries the rotor package in its correct position inside the stator. They are supposed to support and properly locate the rotor in radial direction and maintain a uniform air gap between the rotor and stator (Tong, 2014). Many different types of bearings can be used, but ball and roller bearings are most common. Bearings rings and the rolling elements are primarily made in steel grades with 0.2-1% carbon and 1-1.5% chromium, or slightly higher in combination with molybdenum or nickel (NSK, 2013). The bearing cage is generally also made of steel, but sometimes brass or plastics (NSK, 2013).

Data collection

Similar to the shaft and housing, the bearings are passive parts in the motor, as discussed in Section 2.4, and they are not scaled directly with the electromagnetic properties of the motor. The size of the bearings depend on the size of the shaft and the mechanical load they must carry. Accordingly, in analogy with the shaft, the bearings scale linearly with the maximum motor torque, between two bearing sizes, representing the end points of the torque span.

Data for single-row all-steel shielded ball bearings with sufficient requirements for loads and speeds were gathered from (NSK, 2013). Matching the scaling of the shaft, a steel mass of about 40 grams was registered for a bearing with a 20 mm inner diameter (6904 ZZ) and 140 grams for one with a 50 mm inner diameter (6910 ZZ). This yields a total span of 80-280 grams of bearing steel in the model. Both bearing sizes were found to be about 1 cm wide in the axial direction. In line with the description above, the steel was classified as low-alloyed steel for the link to Ecoinvent 3 (Weidema et al., 2013). The bearings are assumed to be delivered with lubrication. However, both the mass of the grease, and environmental impact from the production of it, were considered negligible.

4.3.3 Resolver

In order to correctly control an electrical machine, it is important to know the angular position of the rotor. The most common type of sensor used for this is the position resolver. Due to rapid development and minimization of these devices, they have become common in hybrid and electric vehicles (Kisner et al., 2012). A resolver is constructed as a small electrical machine; a stator with coils and a rotor. Some resolver types use permanent magnets on the rotor and others have coils which are excited through brush contacts. The most modern resolvers are based on variable reluctance (VR) between the stator and rotor (Kisner et al., 2012). The rotor consist of electrical steel laminations only, with asymmetrical shape (Tamagawa, 2014). It is connected to the shaft on one side of the electrical machine, and follows the rotations of the machine rotor. The stator of the resolver has both exciting coils and output coils. The variable radius of the rotor provides altered reluctance with different angular positions, generating a varying voltage signal in the output coils. The analog signal is converted to a digital signal in an IC circuit, and used by the inverter unit to control the electrical machine.

Data collection

Data for a VR-type resolver (TS2224N1014E199) was collected from Tamagawa (2014). Similar resolvers are used in the Hyundai Sonata, Toyota Prius and Nissan Leaf (Kisner et al., 2012). It is a small resolver with a mass of only 76 grams, which is mounted at the end of the shaft. It was assumed not to scale in size with altered power and torque, in the LCI model. The resolver-to-digital-IC-converter was assumed to be placed in the inverter unit. The stator windings are isolated from the stator core by a molded plastic case also comprising a connector. This type of plastic insulation is commonly made in PBT (polybutylene terephthalate) (Namiki and Sakamoto, 2005), but it was proxied as another similar thermoplastic in Ecoinvent 3 (Weidema et al., 2013), PET (polyethylene terephthalate, granulate, bottle grade). A material configuration was derived by analyzing of the resolver geometrical drawings (Tamagawa, 2014) and combining the derived subpart volumes with densities for electrical steel (Surahammars Bruk, 2015a) and PBT (1300 kg/m^3) (Dupont, 2005). The remaining mass was identified as magnet wire. The mass shares were found to be 34% magnet wire, 10% PBT plastics, 32% electrical steel in the rotor core, and 24% in the stator core. The mass of the adhesive used to stack the laminations, was identified as negligible.

4.3.4 Terminal block, bolts, nuts and paint

In order to assemble the electrical machine into one functioning component and connect it to the high voltage cables coming from inverter, it must have bolts and nuts which secures the endbells to the cylindrical housing body, and a terminal block. In the terminal block, cables or bus bars coming from the inverter can be fastened and connected to pins mounted on the conduction wires of the different phases in the windings. It contains both threaded steel sections and some type of isolating plastics. Cables or bus bars are fastened to the terminal block using bolts. Other bolts are used to mount the block itself onto the housing. Endbells can be fastened using bolt–nut fasteners or screw-threaded fasteners.

Also, vehicles operate under corrosive conditions, which can deteriorate the electrical machine performance and shorten its lifetime. Consequently, although aluminum have inherent corrosion resistance, it is common that motor manufacturers paint the housing as a final step after the assembly with some thermally conductive coating, for example acrylic varnish, enamel, alkyd or epoxy-based paints (Tong, 2014). A typical thickness is around 0.5 mm. Similarly, the steel bolts and nuts are generally coated with zinc to avoid corrosion, either through electroplating for layers below 20 µm or by hot-dip galvanization for layers around 50 µm or thicker (Walraven, 2011).

Data collection

Bolts, nuts and the terminal block were assumed not to scale with torque or power in the inventory model, i.e. they are the same in both reference machines. Each housing endbell has been fastened to the housing body using five galvanized M6 hexagonally headed and threaded bolts (DIN 933) with a length of 20 mm, mounted in corresponding hexagonal nuts (DIN 934) together with two flat washers (DIN 125) based on data from Fuller (2013). Also, the same type of bolt was selected for mounting the terminal block to the housing body, and for fastening conducting pins and bus bars to the terminal block. The steel was identified as low alloy carbon steel, listed as low-alloyed steel in Ecoinvent 3 (Weidema et al., 2013). In summary, bolts, nuts and washers came to a total of 140 grams of steel with a total surface area of 2.2 dm^2 which has been galvanized with a layer of zinc[10] ranging up to 50 µm in thickness, for a total of about 8 grams.

The structure and size of the terminal block was estimated based on observations made in Shimizu et al. (2013) in combination with the assumption made for the aluminum housing design. The block mainly consists of a plastic frame attached to the housing with three galvanized steel plates forming the connection points for each phase of the machine with the inverter, either with cables or bus bars. As in the case with the resolver, it was assumed that the plastic insulation was constructed in PBT (Namiki and Sakamoto, 2005), but it was proxied as PET for the pairing with data in Ecoinvent 3 (Weidema et al., 2013). The density of the PBT was set to 1300 kg/m^3 (Dupont, 2005) and density of the low-alloy medium carbon steel to 7870 kg/m^3 (AK Steel, 2014). The mass and the surface area for galvanization of the steel plates was found to be 40 grams and 0.3 dm^2 respectively for the small reference machine, and 100 grams and 0.6 dm^2 for the large.

Summarizing for the total galvanized steel surface area, the small reference machine was calculated to 2.5 dm^2 and the large reference machine to 2.8 dm^2. This area data was used to proxy the galvanization process based on an existing Ecoinvent zinc coating procedure for a layer thickness varying from 20-45 µm, which was judged to be sufficiently in agreement with the design data, see Section 5.2.2.

The phase conductors from winding are ended with tin plated copper lugs, securing the wires to the block. The design and mass per piece were collected from NSi (2010). The area for tin plating was estimated to 0.3 dm^2 and 0.4 dm^2 for the small and large reference machine, respectively. For a 2 µm thin layer of tin (Kellenberger et al., 2007) this results in a negligible contribution to the mass of the lugs. The resulting amount of steel, zinc, copper and PBT plastics for the reference machines are presented in Table 17.

Reference machine	Low-alloyed steel	PBT	Copper	Zinc
Small	180 g	60 g	24 g	9 g
Large	240 g	130 g	51 g	10 g

Table 17: Summary of estimated masses per material in the terminal block, copper lugs, washers, nuts and bolts.

[10] The density of zinc is 7130 kg/m^3 (Lagneborg, R. and Waltersson, E. 2004).

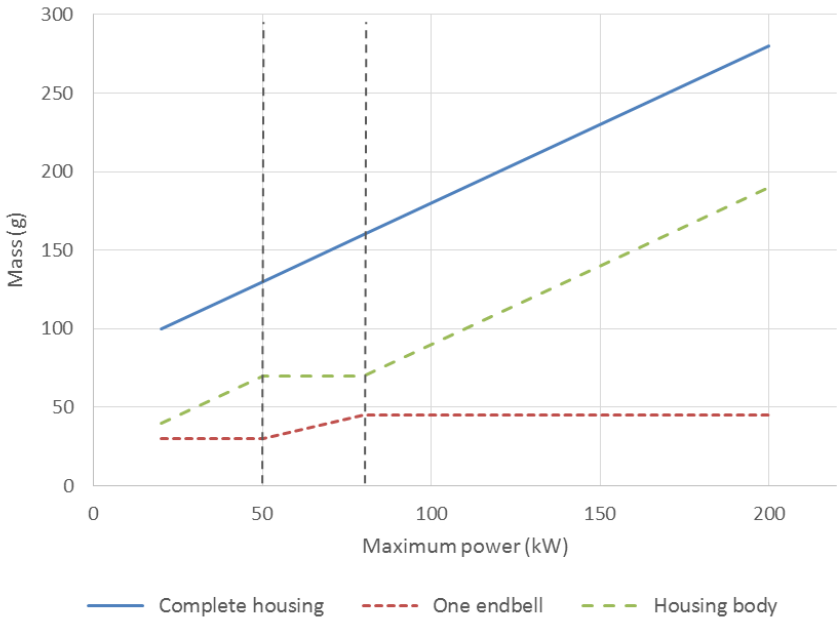

Figure 16: Estimation of the paint masses on the different housing parts as a function of the specified maximum power from 20-200 kW, based on the power to mass constants and starting masses presented in Table 19. Endbell paint masses are constant under 50 kW (30 g) and above 80 kW (90 g), in line with Table 18.

A clear varnish was selected for the final coating of the aluminum housing. Data was gathered from Von Roll (2013) for an alkyd resin based coating intended for electrical machine housings. The varnish mass was estimated for a 0.5 mm thick layer, when dried. It was combined with a rough estimate of the housing surface area, based on the housing design discussed in Section 4.3.1. Table 18 shows the results for the different parts of the housing, at nominal lengths of the reference machines. Table 19 presents the parameters estimated in order to formulate the varnish mass as a function of the maximum motor power. Figure 16 shows the resulting graphs. For further details about the amount of paint applied in liquid state, see Section 5.4.8.

Reference machine	Varnish mass		
	Total	Housing body	One endbell
Small	0.12 kg	60 g	30 g
Large	0.18 kg	90 g	45 g

Table 18: Estimated mass of the varnish on the aluminum housing parts, for the reference machines at their nominal length and power.

Painted housing part	Paint mass at 20 kW	Power to mass constant		
		20-50 kW	50-80 kW	80-200 kW
Housing body	40 g	1 g/kW	0 g/kW	1 g/kW
Endbell, per piece	30 g	0 g/kW	0.5 g/kW	0 g/kW
Total mass	100 g	1 g/kW	1 g/kW	1 g/kW

Table 19: The complete set of parameters specified in the housing paint mass estimation.

4.4 The assembled unit

4.4.1 Summary of design parameters

A summary of parameters important for the design of the two reference machines have been compiled into Table 20.

Reference machine	**Small**			**Large**		
Scaled length	Shortest	Nominal	Longest	Shortest	Nominal	Longest
General						
Maximum torque	48 Nm	96 Nm	191 Nm	119 Nm	239 Nm	477 Nm
Maximum power[1]	20 kW	40 kW	80 kW	50 kW	100 kW	200 kW
Core stack lengths	57 mm	114 mm	228 mm	63 mm	127 mm	253 mm
Current density	20 A /mm^2					
Maximum current[1]	53 A	105 A	210 A	166 A	260 A	607 A
Number of poles	8					
Air gap	0.57 mm			0.75 mm		
Parallel circuits per phase	4					
Stator						
Outer diameter	152 mm			200 mm		
Inner diameter	103 mm			135 mm		
Core mass	3.1 kg	6.1 kg	12.2 kg	5.9 kg	11.8 kg	23.6 kg
Number of slots	48					
Slot fill ratio	45%					
Slot depth	16 mm			17 mm		
Slot opening	1.5 mm			2 mm		
Slot area	58 mm^2			101 mm^2		
Slot circumference	38 mm			48 mm		
Turns per coil	20	10	5	14	7	3
Rotor						
Outer diameter	101.5 mm			133.5 mm		
Inner diameter, active core	61 mm			80 mm		
Core mass, active core	1.9 kg	3.8 kg	7.5 kg	3.6 kg	7.2 kg	14.4 kg
Core mass, total	2.2 kg	4.4 kg	8.7 kg	4.2 kg	8.4 kg	16.8 kg
Magnet length	57 mm	114 mm	228 mm	63 mm	127 mm	253 mm
Magnet width	13.7 mm			18 mm		
Magnet thickness	3.46 mm			4.55 mm		
Magnet volume, per slot	2.7 cm^3	5.4 cm^3	10.8 cm^3	5.2 cm^3	10.4 cm^3	20.7 cm^3
Total magnet mass[2]	0.32 kg	0.65 kg	1.29 kg	0.62 kg	1.25 kg	2.49 kg

Note 1: Values valid at 400 V and 4000 rpm.
Note 2: Mass of nickel coating not included, adding about 1% of mass for the finished magnet.

Table 20: Summary of important parameters in the ANSYS Maxwell modelling setup (ANSYS, 2015).

4.4.2 Machine efficiency and performance

Some of the main electromagnetic electrical machine characteristics discussed in Section 3.2 have been evaluated for the reference machines. ANSYS Maxwell (ANSYS, 2015) was run through several finite element simulations to determine the maximum torque and power of the reference machines. Initially at the respective

nominal stack lengths machine, and then also at both half and double the lengths. Given the lack of a standard definition for the calculation procedure of the maximum torque and power ratings, these were decided using a maximum supply AC RMS current of 20 A/mm^2 for each slot, as a median based on observations of real motor values presented in benchmarking literature (Ozpineci, 2011). The resulting maximum RMS phase current for the large reference machine is 260 A, and 105 A for the small at their nominal lengths. Furthermore, it was assumed that the maximum torque can be sustained during normal operation, since no thermal analysis has been made. Next, the maximum power of the reference machines were determined at a speed of 4000 rpm for the maximum torque level. The number of winding turns were adjusted such that a maximum DC voltage level of 430 V can be maintained, irrespective of the stack length. Practically, it is likely that somewhat higher peak power levels can be reached at higher speed levels, depending on more precise design selections, the capability of external components and the control method. The nominal DC system voltage has been declared to be 400 V, i.e. defined with slightly less precision and with a margin compared to the definite maximum, in line with the difference between typical nominal and peak battery voltage ratings for vehicles, according to (Grunditz and Thiringer, 2016b).

On the other hand, under these simplified conditions the ANSYS Maxwell simulation was able to provide the relationship between both torque and power with speed, and also the electromagnetic losses at the different working points. Hence, Figure 17 and Figure 18 present the resulting combined efficiency maps and torque-speed diagrams for the reference machines at the nominal lengths. Mechanical losses, for example friction losses in the motor bearings, or in any external mechanical coupling, such as a gearbox, are not included.

An additional note is that the reference machines have a high magnetic flux constant, which results in good torque performance at low speed and current, as well as high power values. But, it also has implications for how the motor is handled if the inverter fails and is turned off for some reason, referred to as tripping. During such a fault case, the rectified voltage going from the still rotating machine back into the dc-link of the vehicle will be high, around 700 V. For safety reasons, this must be avoided and the rotor must be brought to a stop, either by decoupling the motor or stopping the vehicle. However, in the case of single electric propulsion motor, which was a design criteria for reference machines, the vehicle cannot continue to drive anyway, since the motor control is not functioning. But, in some other cases, e.g. if the vehicle has two electric propulsion

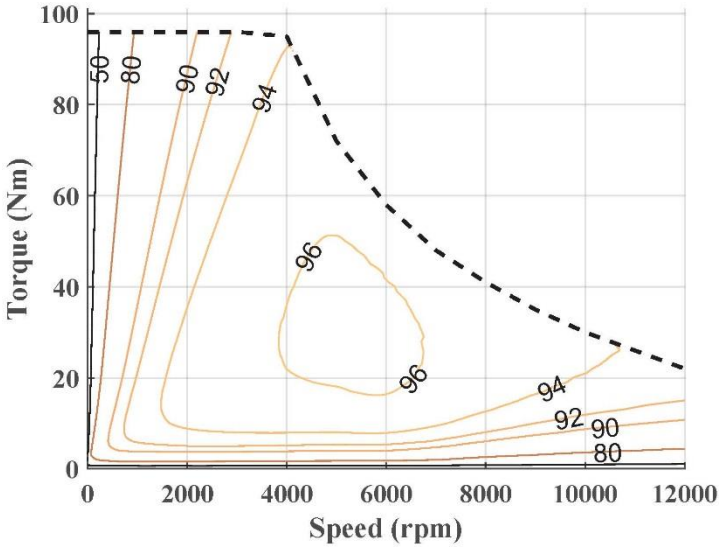

Figure 17: The electromagnetic efficiency map of the small reference machine at nominal length within the torque-speed diagram.

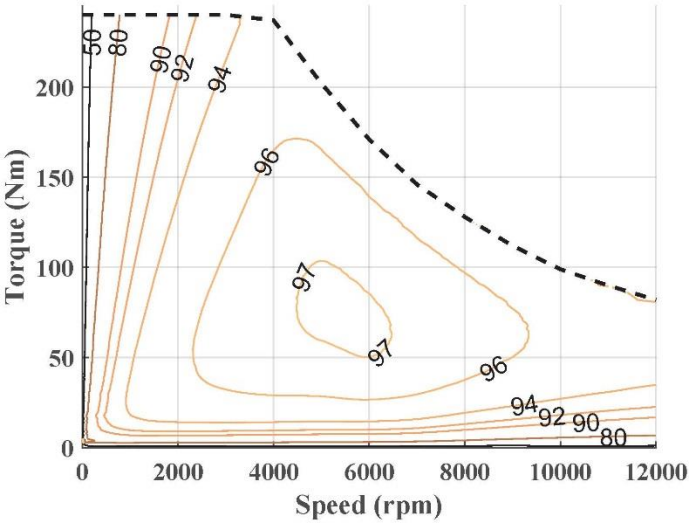

Figure 18: The electromagnetic efficiency map of the large reference machine at nominal length within the torque-speed diagram.

motors, or in a hybrid vehicle, where the combustion engine can be used, a different motor design with a lower magnetic flux constant could make it possible for the vehicle to operate also after an inverter tripping has occurred, since the voltage generated in such a situation is lower and will not lead to any uncontrolled rectified current flowing into the battery, or a high voltage if the battery contactors open. One way to decrease the magnetic flux constant is to use fewer turns in the stator coils. Nevertheless, for the reference machines, the choice was made to prioritize a high power density.

5 Assessment of production procedures

5.1 Magnet production chain

5.1.1 Coupling rare earth oxides to upstream data

Data for the Nd(Dy)FeB magnet production chain has been included in the inventory model, as indicated in Figure 3 in Chapter 2 of this report. However, unlike all other raw material input to the LCI model (as will be presented subsequently, in sections 5.2 and 5.3), no explicit recommendations for linked flows in the Ecoinvent 3 database have been provided for the rare earth oxides (REOs), which were taken as the starting point for the magnet production chain (further described in sections 5.1.2 and 5.1.3). The reason is that REOs can be expected to be an important contributor to the environmental load of the electrical machine while the Ecoinvent 3 dataset for REOs is lacking in detail and include a ready-made allocation. Instead, it is recommended that the model user evaluates different upstream data options for REOs each time the model is used. In the rest of this section, we provide some background information and a brief discussion to support the user in this work.

Several steps are required to produce the raw materials necessary for fabrication in of a permanent magnet of the type described in Section 4.2.2, and this chain of activities involves both extraction and processing of many compounds from the same ore, especially for the rare-earth metal content. Hence, important methodological aspects in life cycle assessment, for instance the allocation of environmental burden between the products from each multi-output activity, must be considered. Such methodological decisions have been kept outside the inventory model system boundaries, and must be made by the user. This is the reason that the system boundary for the fabrication of the magnets was drawn where REOs, i.e. neodymium oxide (Nd_2O_3) and dysprosium oxide (Dy_2O_3), enter the production chain.

Additionally, most assessments made on the environmental load from the extraction of rare earth elements can be expected to depend on economic allocation from volatile prices. The environmental load of the rare earth content in the electric motor can be expected to of be specific interest for a PMSM. Hence, users of the model are urged to take extra consideration in linking the rare earth oxides to upstream inventory data.

Rare earth element resources are often expressed as REOs, since they often occur as oxidic compounds, due to a strong affinity for oxygen (US EPA, 2012). Still, depending on the ore content and the separation processes, the outcome from purification may also be rare earth phosphates or fluorides, besides oxides (Lucas et al., 2015). Among the rare earth metals, neodymium is classified as a light element and dysprosium as a heavy element. Neodymium is the third most abundant of the rare earths in present known ores after cerium and lanthanum (Althaus et al., 2007, Koltun and Tharumarajah, 2014). The occurrence of dysprosium in same ores is less than a hundred times lower, on average. For all REOs, the purification stages are dominating the environmental burden (Koltun and Tharumarajah, 2014, Nuss and Eckelman, 2014). Both the occurrence and recovery rates are low and large amounts of energy, chemicals, and water is needed. Toxic waste is also common (Koltun and Tharumarajah, 2014). Heavy elements require additional beneficiation processing compared to lighter ones, including even greater energy use, for example in the case of dysprosium oxide (Koltun and Tharumarajah, 2014). Since rare earth elements do occur in conjunction in the natural deposits, they are mined together. Thus, the beneficiation and separation steps of different REOs from the same ore concentrate, typically are multi-output processes. Commonly, the allocation procedure to split the burden of environmental load from earlier steps in the production is conducted using economic allocation based on the price on each compound. For a more thorough discussion on both mass based and economic allocation of the burden of different REOs in production from different mineral concentrates as well as the energy and water consumption of different routes, the authors refer to Koltun and Tharumarajah (2014).

The Ecoinvent 3 database (Weidema et al., 2013) contains a multi-output unit activity named “rare earth oxides production from bastnäsite concentrate” where one of the reference products is “neodymium oxide”. This data may of course be used to link with upstream data. However, it is important to be aware that the allocation of burdens was based on rare earth bulk prices from 2006 (Althaus et al., 2007). Furthermore, the Ecoinvent 3 database contains no specific dataset for dysprosium oxide, which has been roughly one order of magnitude more costly than neodymium oxide over the last ten years (Lucas et al., 2015). As an alternative, Sprecher et al. (2014a), (2014b) have provided an inventory for the fabrication of some REOs from ore which build on version 2 of the Ecoinvent database, but with additional details. Alternatively, the life cycle inventory unit process library of NETL (2015) can be used to model several different routes from mining of rare earth crude ore to metals.

5.1.2 From rare earth oxides to rare earth metals

REOs can be reduced to pure metals using different methods. Fused-salt electrolysis is the most common industrial process for the light REOs, such as neodymium oxide (Koltun and Tharumarajah, 2014, Sprecher et al., 2014a). Main advantages are that it can be run at ambient pressure and in continuous operation, which is suitable for large scale operation (Lucas et al., 2015). Metallothermic processing is more common for medium and heavy REOs. It is a slow batch process suitable for producing smaller quantities of metal. Some rare earth metals can only be produced using metallothermic reduction, for example samarium (Lucas et al., 2015). However, neodymium oxide can be reduced using either method. In comparison, fused-salt electrolysis is more energy demanding than metallothermic processing (NETL, 2014a, c), but for industrial processing of larger metal quantities it is the more straightforward and cost-efficient option (Lucas et al., 2015).

Fused-salt electrolysis typically uses a fluoride electrolyte (Lucas et al., 2015). Neodymium oxide is fed to and dissolved in the electrolyte. The anode is made of graphite and the cathode often of tungsten or molybdenum. The graphite at the anode is consumed and molten metal is electrodeposited at the cathode, and drops off into a small crucible made of graphite, wherefrom it is collected. If the designated product is a NdFeB magnet, a pure iron cathode may be used instead yielding a high purity neodymium-iron alloy directly from the fused salt electrolysis (Lucas et al., 2015).

In metallothermic reduction the rare earth compound reacts with a metal reductant, often calcium, in a liquid bath. The constituents are heated above their melting temperatures by induction heating of a vessel, inside a vacuum chamber (Lucas et al., 2015). For oxide reduction, a molten salt solution of calcium chloride and sodium can be used as invented by Sharma (1986). The calcium chloride and sodium reacts to produce the calcium which reduces the rare earth oxide to its metal form.

Data collection

Data for the reduction of neodymium oxide to metals were collected from NETL (2015) unit process library. It was assumed that fused-salt electrolysis is used to reduce the neodymium oxide, in line with the discussion about different processes for light and heavy rare earth metals. No data was collected for the reduction of dysprosium oxide since dysprosium enters the magnet fabrication in its oxide form, see Section 5.1.3.

Additional to the production process itself, the data for the electrolytic process includes actions for emission abatement of neodymium oxide dust and hydrogen fluoride emissions (NETL, 2014c). Table 21 presents the process inputs and Table 22 presents emissions and waste, for the fused salt electrolysis. Matching input data, waste and emission flows are available in Ecoinvent version 3 (Weidema et al., 2013). For the graphite anodes, "anode, graphite, for lithium-ion battery" can be selected, and the electrolysis sludge can very roughly be proxied as "sludge, NaCl electrolysis". For the dust, it has crudely been expected to be particulates > 2.5 um and < 10 um, since this size of neodymium dust typically occurs in and is surveyed in measurements of industrial aerosol distributions (Lahd Geagea et al., 2008).

For simplicity, the dataset describes the reduction of neodymium oxide to a pure neodymium metal ingot and not to a neodymium-iron alloy, although an alloy is the most likely form when the metal enters the magnet fabrication. Instead, since it does not alter the overall results, all iron addition was modelled in the subsequent process step, see Section 5.1.3.

Process input	Amount per kg	Source	Linked flow
Neodymium oxide	1.3 kg	NETL (2014c)	Optional, see Section 5.1.1.
Electricity	10.6 kWh	NETL (2014c)	Electricity, optional
Lithium fluoride	10 g	NETL (2014c)	E3, lithium fluoride
Lime[1]	45 g	NETL (2014c)	E3, quicklime, milled, packed
Graphite anodes	0.3 kg	NETL (2014c)	E3, anode, graphite, for lithium-ion battery

Note 1: Assumed to be quicklime (CaO).

Table 21: Process input for the production of 1 kg neodymium metal through fused-salt electrolysis.

Emissions to air	Amount per kg	Source	Linked elementary flow
Carbon dioxide	1.1 kg	NETL (2014c)	E3, carbon dioxide
Hydrogen fluoride	7 g	NETL (2014c)	E3, hydrogen fluoride
Dust[1] (Nd_2O_3)	5 g	NETL (2014c)	E3, particulates, > 2.5 µm, < 10 µm
Solid waste	**Amount per kg**	**Source**	**Linked flow**
Sludge[2], dry content	96 g	Summarized, from NETL (2014c)	E3, sludge, NaCl electrolysis

Note 1: Assumed to be PM10, i.e. particulates > 2.5 um, and < 10um, based on the use of Nd PM10 isotopes to measure anthropogenic emissions of aerosols in Lahd Geagea et al. (2008).
Note 2: Consist of 47% calcium fluoride (CaF_2), 6% calcium sulfate ($CaSO_4$) and 47% neodymium oxide (Nd_2O_3) based on NETL (2014c).

Table 22: Emissions and waste from the production of 1 kg neodymium through metal fused-salt electrolysis.

5.1.3 Fabrication of magnets

The process for producing sintered Nd(Dy)FeB magnets starts with the making of a mother alloy of neodymium, iron and boron through strip casting (Sprecher et al., 2014a). Notably, unlike many other iron containing products, elemental iron of high purity is used, for example electrolytic iron (Croat, 1992, McCallum and Branagan, 1996, Zakotnik and Tudor, 2015). Boron is conventionally also added to the alloying process in its elemental form (Croat, 1992), or as ferro boron (McCallum and Branagan, 1996, Zakotnik and Tudor, 2015). Other metals than the base constituents are sometimes also added, replacing some of the iron, for example cobalt, aluminum, copper, gallium or niobium (McCallum and Branagan, 1996, Li et al., 2011). Small amounts of carbon may also be added to replace boron (Liu and Stadelmaier, 1986, McCallum and Branagan, 1996). As a result, it was shown possible to use boron carbide as the source of boron in the magnet alloy (Chen et al., 2006).

The complete magnet fabrication procedure, from alloying to the coated and magnetized magnet, is depicted in Figure 19. In the strip casting process, metal ingots or powders are melted together in a furnace with a controlled argon atmosphere. The molten blend is rapidly water cooled and separated into flakes. Subsequently, the material is pulverized in two steps, first by means of hydrogen precipitation and then jet milling. In precipitation, hydrogen gas is supplied to form hydride in the grain boundaries of the alloy. As a consequence, the alloy expands and the flakes crack into a fine particle powder (Sprecher et al., 2014a). In jet milling, this powder is further milled in a grinding chamber with compressed gas. The resulting powder has a mean particle size around 5 µm (Brown et al., 2002). In the next step, particles are magnetically aligned by applying a strong magnetic field of about 3 tesla and then compressed into a partially dense state in a mold (Brown et al., 2002, Lucas et al., 2015). Common procedures are die setting, where pressure is applied from the sides, or isostatic pressing, where pressure is applied from all around using an oil (Sprecher et al., 2014a). Following, the compacted cake is vacuum sintered above 1000°C. The particles are bonded into a solid structure and the magnet base body shrinks as the density is roughly doubled (Fang, 2010).

The final shape of magnets is then obtained by grinding, slicing, and drilling the base body into the desired geometry. Subsequently, the magnet is cleaned, to prepare for the dysprosium addition and the final coating. First, an alkaline bath is used to degrease the surface, and then the surface is deoxidized by electrocleaning in an acid (Schlesinger and Paunovic, 2010).

The most novel method for applying a minimum amount of dysprosium to the base body for the improvement of NdFeB magnets' coercivity and heat resistance, is referred to as grain boundary diffusion (Lucas et al., 2015, Vaimann et al., 2013). The main principle is to apply a dysprosium carrying substance as a powder coating on the base body of the magnet and put it through subsequent heat treatments, so that the dysprosium diffuses into the neodymium rich phase between the grains of the magnet body, but not into the grains. For this reason, the temperature is preferable kept close to, but below the sintering temperature. This is also important in order not to deform the magnet body structurally or alter the already achieved magnetic alignment (Nagasaki and Shimao, 2015). Several methods have been proposed on how to apply the powder on the magnet to make grain boundary diffusion suitable for industrial processing. One way is to cover the surface with an adhesive and then stir or vibrate the magnet body in the powder (Sagawa, 2013) and another method is to dip the magnet into a suspension liquid containing the powder (Sagawa, 2014). However, both these methods suffer from difficulties in controlling the coating coverage. A third method, which overcomes this problem, is to electrodeposit the powder on the magnet body (Nagasaki and Shimao, 2015). In this case,

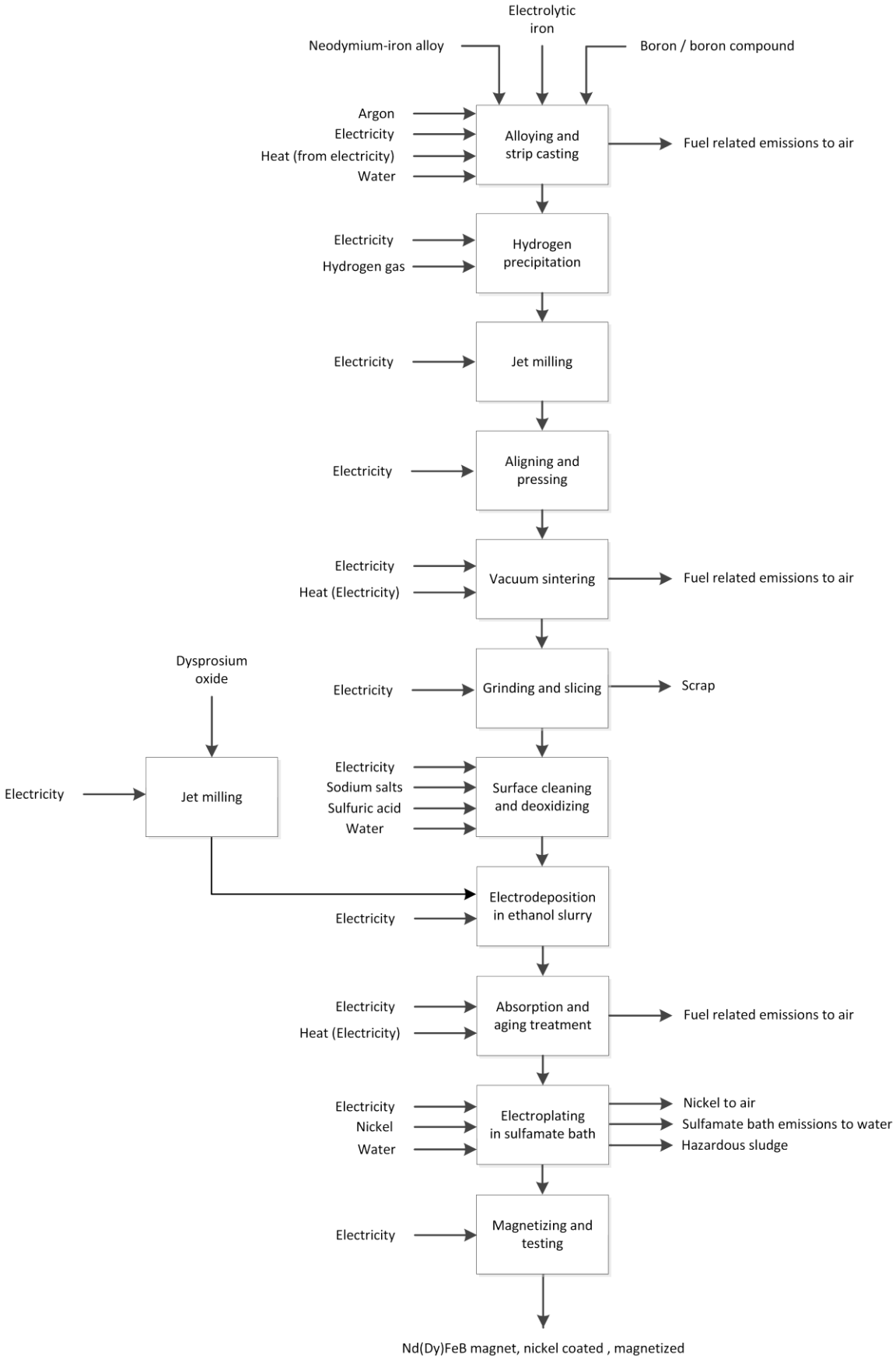

Figure 19: The process flow for the making of a nickel coated neodymium-iron-boron magnet with dysprosium added by means of the grain boundary diffusion method.

dysprosium oxide is milled to a particle size below 10 µm and then mixed with a solvent to form a bath. Stainless steel is used as inert anode material and the magnet body acts as the cathode for the dysprosium deposits. After dysprosium has been deposited, the magnet is heated twice, first in an absorption treatment and then in an aging treatment.

The final coating is applied by electroplating the magnet body in a nickel sulfamate bath. Pure nickel is dissolved at the anode and plated on the magnet, acting as the cathode. Several rinsing steps lead to water emissions from drag-out losses, but there can also be some evaporation of nickel to air (Moing et al., 2009). Finally, all magnets must be magnetized, either before they are sent-off to the motor factory (premagnetization), or after they have been mounted into the rotor (postmagnetization). The benefit of premagnetization is that the magnet easily can be magnetized to 100% saturation (Tong, 2014). On the other hand, the magnet becomes difficult to handle, for example by automated equipment for the mounting into the rotor. Therefore, postmagnetization can be preferred, but then a 100% saturation level is difficult to acquire since there are several magnets close to each other in the rotor. Also, large rotors may be difficult to fit into the magnetization equipment. The magnetization process itself is very quick. A strong magnetic pulse of 6 tesla (4-8 T) is applied during less than a millisecond (Sprecher et al., 2014a, Lucas et al., 2015).

In modern procedures, it reasonable to assume that the heating processes in magnet fabrication are conducted in electric furnaces, based on indirect resistance or induction (McCallum and Branagan, 1996, Fang, 2010). Vacuum processing is often used for sintering of metals as it avoids adding impurities from a surrounding atmosphere. Instead, the vacuum aids evaporation of impurities from the sintered body. A risk is that the constituents being sintered also can evaporate at high temperatures, when the pressure reaches the vapor pressure of each specific material. However, sintering parameters are typically regulated to avoid evaporation as it leads to furnace contamination (Fang, 2010). Hence, emissions from both alloying and sintering of NdFeB magnet bodies can be assumed to derive from the process providing the heat, either the burning of a fuel or the production of the electricity consumed, rather than the process itself.

Data collection

The data for the magnet manufacturing was compiled from several sources. First, it was observed that data for high purity elemental iron is not available in the Ecoinvent 3 database (Weidema et al., 2013). Instead, information was gathered for the making of electrolytic iron, which uses 2 kWh of electricity to produce one kilogram of iron in an ferrous chloride electrolyte bath (Oeters and Ottrow, 2012). Similar chloride baths used for iron plating consist of a mixture of 52% ferrous chloride and 48% calcium chloride, or 46% ferrous chloride and 54% potassium chloride, dissolved in water (Schlesinger and Paunovic, 2010). Cathode efficiencies range from 80-99%. In this case the efficiency was set to 90%. Iron is consumed at the anode and can be recovered at the cathode as brittle pieces. Preferably, low carbon iron is used as anode material, but ordinary steel grades can also be used although there is a risk for contamination of the chloride bath from impurities (Schlesinger and Paunovic, 2010). Unalloyed steel was assumed here. Over time, the electrolyte bath can be expected to require refill and exchange due to drag-out losses during rinsing, losses to sludge formation and contamination. However, these effects are assumed to be both small and slow, and hence, not included, for simplicity. The formation of the sludge itself was included, taken as dry matter of ferrous chloride based on the iron loss at the cathode. The process inputs for the production of electrolytic iron is shown in Table 23 and the solid waste is shown in Table 24.

Process input	Amount per kg	Source	Linked flow
Unalloyed steel	1.1 kg	Schlesinger and Paunovic (2010)	E3, steel, unalloyed
Electricity	2 kWh	Oeters and Ottrow (2012)	Electricity, optional

Table 23: Process input for the production of 1 kg electrolytic iron.

Solid waste	Amount per kg	Source	Linked flow
Sludge[1], dry content	0.25 kg	Calculated from cathode efficiency	Hazardous waste, optional

Note 1: Assumed to be ferrous chloride.

Table 24: Solid waste from the production of 1 kg electrolytic iron.

Second, data for the making of the mother alloy and the NdFeB base body was gathered from a NETL (2014b) unit process and from Sprecher et al. (2014a), (2014b), but with some important modifications. In order to end in the selected magnet composition (see Section 4.2.2), the base body composition should contain about 27% neodymium, 72% iron and 1% boron before the addition of dysprosium through grain boundary diffusion and the nickel coating, i.e. the same as the composition described by NETL (2014b) and Sprecher et al. (2014a), (2014b). Indeed, the NETL (2014b) dataset is in turn based on Sprecher et al. (2014a), (2014b), but a difference between them is that the data for energy use during vacuum sintering has been divided into auxiliary electricity and heating energy in NETL (2014b) in an approximation from iron ore sintering data available in the Ecoinvent database (Classen et al., 2009, Weidema et al., 2013).

Here, all heating processes were modelled as electric and therefore stated in kWh. Differing from NETL (2014b), specific use of auxiliary electricity was added to the alloying and strip casting process, to account for casting machine operation, based on data for strip casting in steel making (Worrell et al., 2010). Also, vacuum induction furnace losses during alloying were accounted for, and the efficiency was set to 85% based on (Miller, 2009). Furthermore, the electric energy use for vacuum sintering was taken directly from Sprecher et al. (2014b), because NETL (2014b) calculate an average sintering energy by combining the data for vacuum sintering with that of iron ore sintering, and this was not found representative.

In fact, there are major differences between the sintering of iron ore into iron oxide sinter and vacuum sintering of a metal alloy consisting of an essentially pure element mixture. Iron ore is burnt together with coke breeze ignited by natural gas burners (Classen et al., 2009). A check with the group of reports (IPPC, 2001) which was the primary source of the iron oxide sinter production for the Ecoinvent dataset, shows that all emissions relate to the ore feed content and the burning of the coke, with some additional dust created during handling and crushing. Even so, Sprecher et al. (2014a), (2014b), and consequently also NETL (2014b), have based their emissions to air on iron ore sintering. None of these emissions were included in this inventory, as they are not considered representative. Instead, vacuum sintering emissions can be expected to mainly derive from energy conversion steps coupled to the heating of the sintering oven, in the burning of a fuel or during upstream electricity production. Additionally, water may be used for cooling in vacuum furnaces (Fang, 2010), but no reference was found for its use directly in the sintering process. Hence, no water has been included for sintering in this dataset.

Argon use was estimated for the alloying and strip casting step and thereafter neglected. Example settings for normalized[11] argon flow rates during steel alloying and casting were compared with the predicted alloy yield (Li, 2016). This data indicated that even if the flow rates during magnet alloying are significantly higher, or the casting rates much lower, the argon use is only a fraction of a gram per kilogram of alloy.

Other important assumptions used in this compilation are that grinding and slicing losses rate to 30%, and that 50% of these losses are recycled back to the material input directly at the plant (Sprecher et al., 2014b). This closed recycling loop was accounted for in the inventory, differing from NETL (2014b). Remaining scrap was assumed to be collected as iron scrap, to account for material quality degradation and to balance the optimistic assumption of a closed recycling loop at the plant. Furthermore, it was assumed that the concluding magnetization adds a negligible contribution to the overall electricity consumption.

NETL (2014b) assumes a 150 µm thick nickel coating layer on the magnet, based on Moing et al. (2009), corresponding to about 10% of the magnet mass (Sprecher et al., 2014a). But here, in line with the discussion in Section 4.2.2, the coating thickness was set to 15 µm and nickel to 1% of the total magnet mass. Therefore, electroplating data was gathered directly from Moing et al. (2009), but again, with some modifications. Inputs for the cleaning are based on surface area, but all the sodium salts (sodium carbonate, trisodium phosphate, sodium gluconate and caustic soda) have been proxied as caustic soda, which is the largest constituent, for simplicity. For the nickel sulfamate bath efficiency the best case of 95% was selected, as this is more in line with other references than the worst case (Schlesinger and Paunovic, 2010). The bath consists of nickel sulfamate, nickel chloride and boric acid (Moing et al., 2009). To account for the thinner coating layer, the amount of electricity used was decreased proportionally with the mass, fully in line with Faraday's law for electrolysis (Schlesinger and Paunovic, 2010). The anode provides the nickel being consumed and the magnet body acts as the cathode. Similar to the electrolytic iron bath, only waste and relevant emissions to water of the nickel sulfamate bath was included in the inventory, and not the consumption of the bath itself. Moing et al. (2009) assumes water emissions of nickel based on the French regulations for electroplating, which is 2 mg nickel per liter of waste water, in the form of nickel sulfamate. The remaining lost nickel can be expected to

[11] The actual flow rate, for a certain pressure and temperature, is recalculated to a normalized flow rate. The conditions for a "normal" flow rate (in liters per minute) often refers to room temperature and 1 atmosphere in pressure.

be caught in internal waste treatment processes and was assumed to be fixed as a sludge, consisting of nickel sulfamate and nickel chloride (Moing et al., 2009).

Finally, a process description and data for the grain boundary diffusion of dysprosium into the base magnet body was gathered from Nagasaki and Shimao (2015) and Suppan et al. (2015). It was combined with a theoretical description of electrodepositing described in Schlesinger and Paunovic (2010). The energy used for jet milling of the dysprosium oxide to proper particle size was taken from Sprecher et al. (2014b). In this case it is not the anode being consumed, but a slurry mix with 50% of the fine dysprosium oxide powder and 50% ethanol. It was assumed that new powder is mixed into the slurry for each batch and that losses of ethanol due to drag-out are negligible, i.e. the consumption of ethanol is not considered. Faraday's law for electrolysis (Schlesinger and Paunovic, 2010) was used to calculate the amount of electricity used to deposit dysprosium to a total amount of 4% of the magnet mass, prior to the nickel coating. It states that:

$$\text{Deposited mass} = \frac{\text{Molar mass}^{12}}{\text{Oxidation state} \times \text{Faraday's constant}} \times \text{Bath efficiency} \times \text{Current} \times \text{Time}$$

By introducing the DC voltage used, it can be rewritten to:

$$\text{Electric energy} = \frac{\text{Oxidation state} \times \text{Faraday's constant} \times \text{Voltage}}{\text{Molar mass} \times \text{Bath efficiency}} \times \text{Deposited mass}$$

A typical DC voltage is 10V (Nagasaki and Shimao, 2015). The molar mass of dysprosium is 162.5 g/mole (Haynes, 2015). Bath efficiencies of 75-80% for similar dysprosium depositing has been described by (Suppan et al., 2015). 75% was assumed here. Faraday's constant expressed in ampere hours is 26.8 A h/mole (Schlesinger and Paunovic, 2010). The oxidation state of the metal ion is the same as the number of electrons taking part in the reaction per atom of the element. Dysprosium(III)oxide reacts in oxidation state three (+3). Hence, the direct current electric energy consumed per amount of deposited dysprosium mass was calculated to 6.6 kWh/kg. Assuming 90% efficiency for the AC to DC conversion this was recalculated to 0.3 kWh/kg magnet of ordinary grid electricity. Finally, the absorption and aging treatments involve two temperature increases up to a level not far off the sintering temperature and, in total, at least double the time of the sintering. Hence, these two procedures were approximated by doubling the electricity and heat used for the sintering process of the base body magnet and adjusted to include the additional dysprosium. Table 25 and Table 26 present summaries of process inputs, wastes and emissions for the magnet fabrication.

Process input	Amount per kg	Source for calculations:	Linked flow
Electrolytic iron	830 g	NETL (2014b)	IF, see Table 23
Neodymium	310 g		IF, see Section 5.1.2
Boron carbide	15 g		E3, boron carbide
Nickel	11 g	Moing et al. (2009)	E3, nickel, 99.5%
Dysprosium oxide	46 g	Multiple sources, see text.	Optional, see Section 5.1.1
Electricity, heating	8.4 kWh		Electricity, optional
Electricity, other	5.6 kWh		Electricity, optional
Hydrogen	0.6 kg	NETL (2014b), Sprecher et al. (2014b)	E3, hydrogen, liquid
Caustic soda	1 g	Moing et al. (2009)	E3, sodium hydroxide, without water
Sulfuric acid	1.4 g		E3, sulfuric acid
Water	6 kg	NETL (2014b), Moing et al. (2009)	E3, tap water

Table 25: Process input for the production of 1 kg of Nd(Dy)FeB nickel coated magnet.

[12] For pure elements, the relative atomic mass is often tabulated. It relates to the molar mass through the molar mass constant *Mu*, which is 1 g/mole in SI units.

Emissions to air	Amount per kg	Source for calculations:	Linked elementary flow
Nickel	4.2 mg	Moing et al. (2009)	E3, nickel, unspecified
Emissions to water	**Amount per kg**	**Source for calculations:**	**Linked elementary flow**
Nickel, in sulfamate[1]	5.1 mg	Moing et al. (2009)	E3, nickel, ion[2]
Solid waste	**Amount per kg**	**Source for calculations:**	**Linked flow**
Neodymium-iron-boron scrap	200 g	Sprecher et al. (2014b)	Iron scrap, unsorted
Sludge[3], dry content	2.2 g	Moing et al. (2009)	Hazardous waste, optional

Note 1: Consist of 23% nickel.
Note 2: Relevant flow for the nickel share. It is assumed that the salt is fully dissolved.
Note 3: Consist of 97% nickel sulfamate and 3% nickel chloride, and contain, in total, 24% nickel.

Table 26: Emissions and waste the production of 1 kg of Nd(Dy)FeB nickel coated magnet.

5.2 Manufacture of steel, copper and aluminum subparts

5.2.1 Alloying silicon steel

The starting point for the making of electrical steel is high quality hot rolled coils of silicon steel, made from an alloy of carbon steel with silicon and aluminum. Alloying of crude steel into silicon steel is conducted during the processing of liquid steel, before casting (Ghosh, 2000). The unalloyed steel is mixed with ferrosilicon and aluminum in a ladle furnace (Ghosh, 2000, Lagneborg and Waltersson, 2004). Ferrosilicon is already a common deoxidation agent in all types of steelmaking, but in silicon steel alloys larger amounts are mixed in to reach the desired residual silicon level after solidification. The most common grade of ferrosilicon contains 75% silicon and release heat when mixed with liquid steel (AMG Vanadium, 2015). Aluminum may be added to the liquid steel in the form of solid cast grade ingots or, in more modern practices, as aluminum wire (Ghosh, 2000). After casting, the silicon steel is further processed by means of hot rolling into coils, described in next section, 5.2.2, before it is delivered to the electrical steel plant (Section 5.2.3).

Data collection

The alloying of silicon steel takes place outside the system boundary of the inventory. It was accounted for by combining proper amounts of unalloyed steel, ferrosilicon and aluminum in flows which enter into the extended system, for general processing of steel parts (see Section 5.2.2). However, computationally, owing to the Ecoinvent data linkage, it was regarded as full account of the silicon steel alloying process. It was assumed that ferrosilicon and aluminum are added to the unalloyed steel during the liquid phase of the steel making, in the alloying ladle. Containing 75% silicon and 25% iron, ferrosilicon must be blended in to about 2.7% of the alloy mixture in order for the steel to receive the desired composition, as specified in Section 4.1.1. The data representing ferrosilicon in the Ecoinvent 3 database (Weidema et al., 2013) covers the mixing of iron and silicon in a furnace, and it was assumed that no further treatment is needed to recover smaller lumps or granulates used in the subsequent steel alloying step. No discount was made for any small content of silicon in the crude steel mixture or deriving from its standard use for deoxidation. More importantly, the addition of 75% grade ferrosilicon is a major source of heat in the melt (AMG Vanadium, 2015). It was assumed that this exothermic reaction covers the melting of both the ferrosilicon itself and the aluminum ingots. Furthermore, the alloying additions was assumed not to alter any of the data for the casting process, included in the making of unalloyed steel. Table 27 summarizes the input of unalloyed steel, ferrosilicon and aluminum together with the representation of the data in Ecoinvent 3 database (Weidema et al., 2013).

Process input	Amount per 1000 kg	Source	Linked flow
Unalloyed steel	979 kg	Lindenmo (2015)	E3, steel, unalloyed
Ferrosilicon	27 kg	Lindenmo (2015)	E3, ferrosilicon
Aluminum	4 kg	Lindenmo (2015)	E3, aluminium, cast alloy

Table 27: Process input for the alloying of 1 ton of silicon steel.

5.2.2 General processing of steel parts

Hot rolling is an intermediate steel making process where the ingots, blocks, and beams from raw steel making are treated to receive enhanced durability, shock resistance and tensile strength. The incoming alloy is heat treated and rolled into long or flat products. These go on to further treatment to become sheets, bars, rods or wire. The environmental burden of hot rolling is mainly emissions to air of nitrogen oxides, sulfur oxides and dust, along with the energy consumption and oil containing wastes. All steel parts included in this inventory have been subject to hot rolling.

After hot rolling the different steel alloys and parts are subject to different treatments. The silicon steel aimed for the rotor and stator cores goes to the electrical steel plant, which is further described in Section 5.2.3. The stainless steel sheets used in the rotor endplates are rolled to sheets in a similar process. The low alloyed steel bar which will become plates in the terminal block, the input rod to make the shaft at the motor factory, and bolts, nuts and washers, are also reheated, rolled and mechanically machined to proper dimensions. Round or hexagonal carbon steel rods are forged, threaded and cut, or cut and drilled to become bolts, nuts and washers which are cleaned and coated with zinc in a galvanizing procedure.

The low alloy steel that will become the bearings goes from hot rolling into different forms of processing: ball making from steel rods, rings from steel bars and bearing seals from steel strips (Löfgren et al., 2011). The different parts are then machined, hardened and assembled at the bearing factory.

Data collection

All making of steel parts going into the motor factory, excluding the electrical steel sheet processing, were modelled with metal working and forming activities existing in the Ecoinvent 3 database (Weidema et al., 2013), described by Steiner and Frischknecht (2007) and Classen et al. (2009). As explained in Section 2.3, production efforts of this type have been included within the so called extended system boundaries of the model. "Hot rolling" was applied on all types of steel alloys. A specific sheet rolling activity for stainless steel sheets is available in "sheet rolling, chromium steel". All low alloyed carbon steel parts were assumed to go through "section bar rolling, steel" followed by "metal working, average for steel product manufacturing" to account for the machining to correct lengths and dimensions. The bearings were assumed to go through the bar rolling procedure as a proxy for the intermediate rolling and cutting steps and then the metal working procedure to cover for the activities at the bearing factory. However, this can be regarded as a low estimate as hardening procedures are not included in this averaged Ecoinvent 3 machining procedure (Weidema et al., 2013).

The steel product forming activities selected, i.e. the different rolling procedures, are specified per the amount of metal being processed (Classen et al., 2009), but do not include the material itself. Implicitly, the assumption is that any scrap is recycled back to alloying plant from the rolling mill without net material losses. Hence, in the model of the process, one kilogram of input gives one kilogram of output. The same is true for the Ecoinvent activity for the machine processing of the low alloyed carbon steel parts, but instead it includes averaged data for the losses accounted for within the process (Steiner and Frischknecht, 2007). Figure 20 shows an overview of the recommended Ecoinvent 3 production efforts for steel parts which have been included within the extended system boundary of the LCI model and listed in the model file.

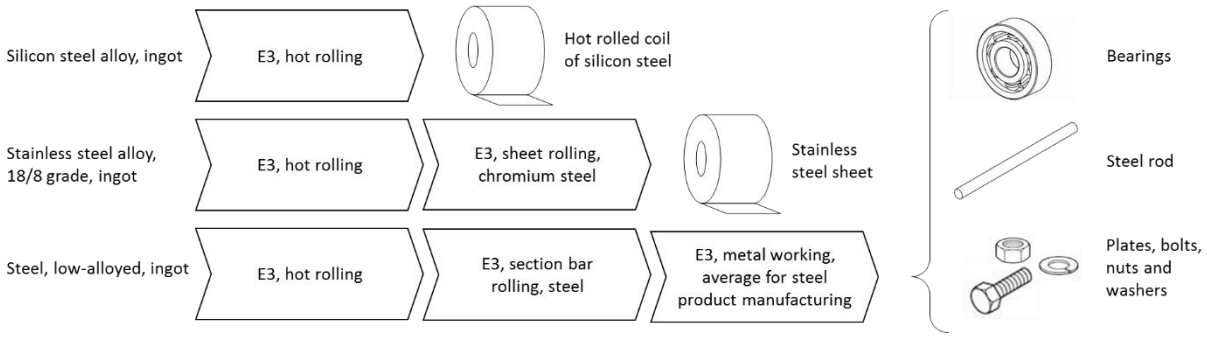

Figure 20: Production efforts for steel available in Ecoinvent 3 (Weidema et al., 2013), specified per kilogram of material being processed. The processes have been included within the extended system boundary of the LCI model, to account for general processing of steel parts.

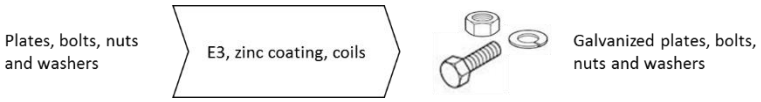

Figure 21: Galvanization procedure in Ecoinvent 3 (Weidema et al., 2013), specified per square meter of surface area being processed. The process has been included within the extended system boundary of the LCI model, to account for the zinc coating of several steel parts.

As a final point in this section, the terminal block plates along with nuts, bolts and washers are galvanized, in order to become finalized subparts ready for the motor factory. Like to the other manufacturing activities for steel parts, this was modelled within the extended system boundary as proxy based on the "zinc coating, coils"[13] activity of the Ecoinvent 3 database (Weidema et al., 2013), see Figure 21.

5.2.3 Electrical steel sheet production

At the electrical steel plant, the incoming silicon steel coils are pickled, cold rolled into the desired thickness and annealed to receive the desired "non-oriented" magnetic properties. Sheets are commonly also coated with some insulation material. The process flow is shown in Figure 22. Electricity is required for all building services such as ventilation and lighting and general machinery, but it is also the main input for the rolling. Annealing is executed in a furnace fired with propane which causes emissions of mainly carbon dioxide but also some nitrogen oxides and sulfur oxides. Pickling requires sulfuric acid in a bath. After passing the bath the sheets are rinsed with water. Lime is used to neutralize the rinsing water and, sometimes, remaining

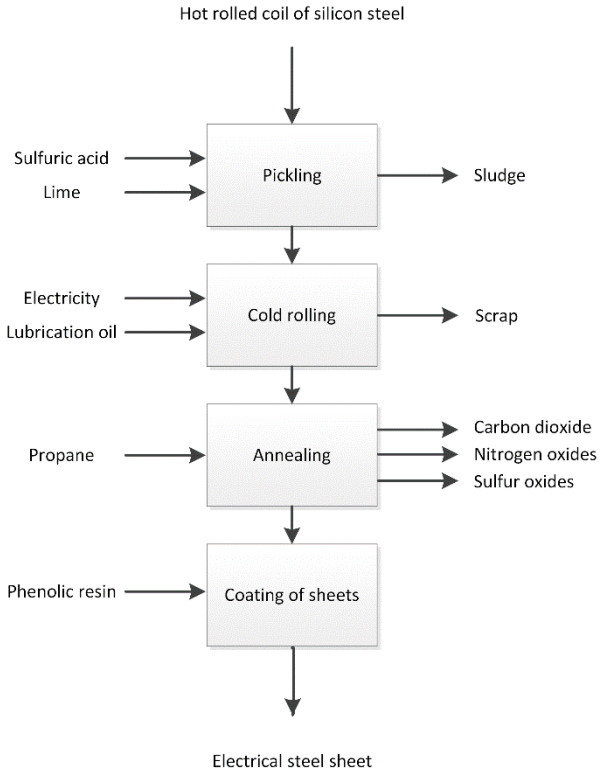

Figure 22: Electrical steel plant process flow.

[13] This activity was preferred over "zinc coating, pieces" due to a better alignment of the coating layer thickness (20-45 μm for selected activity compared to 130 μm) in relation to the "up to 50 μm" thickness of the design.

acid on the steel surface (The National Lime Association, 2015). Also, additional lime use can be required for neutralization of the pickling bath itself. The neutralization processes yield a waste sludge which must be disposed, usually to a landfill. However, the pickling bath may also be used further in other industrial processing, for example in making precipitation chemicals. The most common commercial lime product for neutralizing acid baths is quicklime[14] (Lewis and Boynton, 1999). Punching of the sheets into laminations, shifts the magnetic properties around the cutting edges. For this reason, laminations are sometimes re-annealed in the motor manufacturing process to become fully non-oriented again. However, when non-oriented annealed electric steel sheets are referred to as "fully processed", it denotes that the manufacturer guarantees the quality of the sheet also for further processing without re-annealing.

Data collection

Primary data for the treatment of the silicon steel into fully processed electrical steel sheets was gathered from Surahammars Bruk AB (Lindenmo, 2012, 2015), an electrical steel plant situated in Sweden. Data for the production of 1 ton of electrical steel sheets is presented in Table 28 and Table 29. About 88% of the incoming steel coils become electrical steel (Lindenmo, 2012). About 1% is lost to the pickling bath and 1% is rinsed off and lost with the water. The remaining losses, 10%, are collected as steel scrap which is sent to a recycling facility. It was assumed that the pickling bath is further processed to new products outside the technical system boundaries of the inventory in line with procedures at Surahammars Bruk AB (Lindenmo, 2015), and not neutralized to become sludge. No burden is placed on this by-product in the calculation of the inventory. On the other hand, the lime use and waste handling of sludge only includes the neutralization required for the steel sheet surface, mainly in the rinsing water. The inventory does not include the load of additional lime use necessary for to neutralize the complete pickling bath when refilling, and also not the subsequent waste handling of additional sludge. Phrased differently, in life cycle assessment methodology terms, the used pickling bath was regarded as a by-product from the electrical steel sheet production with no value, and all of the environmental load was allocated to the main product.

Process input	**Amount per 1000 kg**	**Source**	**Linked flow**
Silicon steel, hot rolled	1140 kg	Lindenmo (2012)	IF, see sections 5.2.1 and 5.2.2
Phenolic resin	1 kg	Calculated, see text.	E3, phenolic resin
Electricity	630 kWh	Lindenmo (2012)	Electricity, optional
Propane/LPG	12 kg	Lindenmo (2015)	E3, liquefied petroleum gas
Sulfuric acid	19 kg	Lindenmo (2015)	E3, sulfuric acid
Rolling/lubricating oil	0.4 kg	Lindenmo (2015)	E3, lubricating oil
Quicklime powder	0.8 kg	Lindenmo (2015)	E3, quicklime, milled, packed

Table 28: Process input for the production of 1 ton electrical steel sheets.

Emissions to air	**Amount per 1000 kg**	**Source**	**Linked elementary flow**
Carbon dioxide	36 kg	Calculated, using Haynes (2015)	E3, carbon dioxide, fossil
Nitrogen oxides	0.1 kg	Lindenmo (2015), based on permit	E3, nitrogen oxides
Sulfur oxides	60 mg	Lindenmo (2015), based on permit	E3, Sulphur dioxide
Solid waste	**Amount per 1000 kg**	**Source**	**Linked flow**
Steel scrap	114 kg	Lindenmo (2012)	Steel scrap for recycling
Sludge[1], dry content	3.3 kg	Calculated, using Haynes (2015)	Hazardous waste, optional

Note 1: Consist of 60% calcium sulfate ($CaSO_4$) and 40% ferrous hydroxide ($Fe(OH)_2$).

Table 29: Emissions and waste from the production of 1 ton of electrical steel sheets.

[14] Calcium oxide (CaO)

The amount of resin required for the coating of 1 ton of steel sheets was based on the grade and coating thicknesses presented in Section 4.1.1, combined an electrical steel of density of 7600 kg/m^3 (Surahammars Bruk, 2015a) and a phenolic resin density of 1100 kg/m^3 (Chang Chun Plastics, 2012). All process inputs and emissions have been matched with suitable datasets in version 3 of the Ecoinvent database (Weidema et al., 2013).

5.2.4 Die casting of aluminum parts

Casting is a common method to produce aluminum shapes such as cylindrical housings and endbells (Tong, 2014). Other competing methods can also be used, for example extruding aluminum or, in case of the endbells, forging or stamping. The benefit of casting is that geometrically complex shapes can be produced with high efficiency and at low cost, especially in large series production. Molten metal is poured or pressed into a die, and overflows the cavity, in order to make sure that the complete part is casted (Dalquist and Gutowski, 2004). The die can be of different types, e.g. permanent molds of steel, salt cores, wax, ceramics or various minerals, referred to as sands (Campbell, 2011). A steel mold is a reusable die which can last up to a million castings (Dalquist and Gutowski, 2004). In other methods, the die is dissolved or spent after the casting process, which is a benefit in terms of the easy release of the casted product. Hence, the volume of production is very important when selecting a suitable method for casting. As regards the terminology used, 'die casting' mostly refers to the use of a permanent mold. The method is often divided further into gravity fed, low pressure or high pressure die casting. Confusingly, the first two types are sometimes referred to as permanent mold casting, and then instead, is only the last one called 'die casting', especially in the US (Campbell, 2011).

The major steps in the die casting process are die preparation, metal preparation, casting and finishing. Around 30% of the input aluminum can be expected to derive from scrapped material (Dalquist and Gutowski, 2004). The metal melting is commonly conducted using natural gas heating whereas other processes use electricity (Heinemann, 2016). Direct emissions mainly derive from the burning of the natural gas, but oil based lubricants used in the die preparation and casting, also produce VOC emissions from the casting process, which are not caused by the energy consumption (Dalquist and Gutowski, 2004). Metal scrap and dross is generated in each step and to a large extent recovered and remelted within the casting facility. However, some metal fumes of aluminum are lost as emissions to air in both preparation and casting, and some of the dross, filings and other metal losses are lost as waste (Heinemann, 2016).

Data collection

Data for aluminum die casting is not available in Ecoinvent 3 database (Weidema et al., 2013). For this reason, it was compiled by combining data from Roberts (2003), Dalquist and Gutowski (2004) and (Heinemann, 2016) for casting in a permanent steel mold. The energy figures reflect the average use of electricity and heat at 19 different die casting foundries in Europe (Heinemann, 2016). The raw material for the steel mold has not been included, as a simplification, since it can be assumed to have a very small contribution per part in large scale production.

The process input for the die casting process is presented in Table 30 and emissions and waste in Table 31. All data have matching datasets in the Ecoinvent 3 database (Weidema et al., 2013). For the use of natural gas in this process, it is recommended to use the Ecoinvent 3 activity for "heat production, natural gas, at boiler atmospheric low-NOx non-modulating <100kW", which represent a small natural gas furnace for industrial purposes. For the aluminum input, the linked flow specify an alloy suitable for casting, which includes scrap aluminum as raw material. This is important to take into consideration along with, for example, modelling selections regarding recycling, to avoid an underestimation of the environmental load for the aluminum use.

Process input	Amount per kg	Source	Linked flow
Aluminum[1]	1.06 kg	Heinemann (2016)	E3, aluminium, cast alloy
Heat, from natural gas	10,8 MJ	Heinemann (2016)	E3, heat, central or small-scale, natural gas
Electricity	2.6 kWh	Heinemann (2016)	Electricity, optional
Lubricating oil	20 g	Approx. from Roberts (2003)	E3, lubricating oil

Note 1: In practice, this flow often consist of 75% scrap aluminum and 25% virgin aluminum (Heinemann, 2016). The recommended linked flow corresponds to about 80% scrap and 20% virgin aluminum (Weidema et al., 2013).

Table 30: Process input for die casting of 1 kg of aluminum.

Emissions to air[1]	Amount per kg	Source	Linked elementary flow
Aluminum	0.4 g	Heinemann (2016)	E3, aluminium, unspecified
VOC	1 g	Dalquist and Gutowski (2004)	E3, NMVOC
Solid waste	**Amount per kg**	**Source**	**Linked flow**
Waste aluminum[2]	60 g	Heinemann (2016)	E3, waste aluminium

Note 1: The emissions from the burning of natural gas has not been included and must be added separately.
Note 2: This waste can be assumed not to be recovered, but instead be removed in mixture with other fine scrap and dirt during cleaning.

Table 31: Emissions and waste from die casting of 1 kg of aluminum.

5.2.5 Production efforts for copper parts

The magnet wire used in the stator windings is an important part of the electric motor, as well as the copper lugs used to connect the windings with the terminal block and further to the current controlling inverter. It is fabricated from pure copper wire by applying an enamel coating. Further details about the coating procedure are presented in Section 5.3.1. Copper wire production starts with the making of a wire rod by rolling and cutting. The rod is then repeatedly pulled though drawing dies to reduce the cross section into the desired size (Classen et al., 2009).

Copper cable lugs are made by cutting and forging copper tubes, which in turn were made by rolling and drawing. Lugs are then coated with tin in a plating process.

Data collection

The processing of copper parts refers to existing activities in the Ecoinvent 3 database (Weidema et al., 2013), included within the extended system boundary of the model, as described in Section 2.3. "Wire drawing, copper" was selected for the making of the pure copper wire. Lugs were assumed to go through "sheet rolling, copper" covering initial rolling and drawing and then "metal working, average for copper product manufacturing" to cover for forging and cutting. The final coating of the lugs is covered for as a proxy by using "tin plating, pieces", established for the plating of chromium steel (Kellenberger et al., 2007). See Figure 23 and Figure 24.

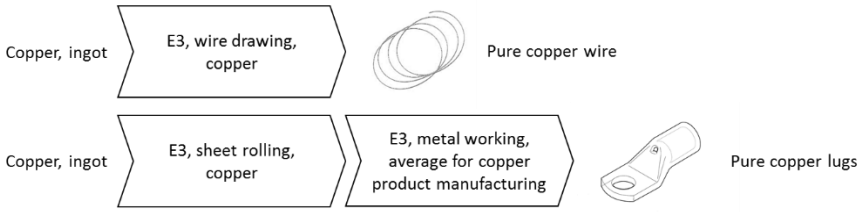

Figure 23: Production activities for copper available in Ecoinvent 3 (Weidema et al., 2013), specified per kilogram of material being processed. The processes have been included within the extended system boundary of the LCI model, to account for general processing of copper parts.

Figure 24: Plating procedure in Ecoinvent 3 (Weidema et al., 2013), specified per square meter of surface area being processed. The process has been included within the extended system boundary of the LCI model, to account for the tin plating of copper lugs.

Similar to the steel product forming activities presented in Section 5.2.2, the procedures are specified per the amount of copper being processed, but do not include the material itself, so that one kilogram of input gives one kilogram of output. Averaged data for losses was accounted for within the processes (Classen et al., 2009, Steiner and Frischknecht, 2007).

5.3 Preparation of parts with coatings, plastics, elastomers and resins

5.3.1 Enameling of the copper wire

The enamel coating layer of the magnet wire is applied to the copper surface after the wire drawing process, using a dedicated enameling machine. Liquid enamel is pumped from a tank into a nozzle where the wire is pulled through (Brenn et al., 2012). Next, the applied enamel film is dried and cured. The wire continues into an oven with circulating hot air. The liquid enamel solvents evaporate while chemical reactions inside the film leads to cross-linking of the enamel polymers.

The enamel machine oven is heated using electricity (Czaputa, 2012). However, almost half of the heat necessary to keep the process running is released from the curing reaction which is exothermic (Czaputa, 2012). Due to its high heat capacity, the copper wire absorbs a lot of thermal energy during the process, and the wire must be cooled outside the oven.

Data collection

Data for the enameling process was gathered from MAG (2016), for the amount of electricity used per kilogram of magnet wire produced, and Polynt Composites (2015), for the composition of the liquid enamel. It was assumed that there are no losses of wire during the enameling step, and the summary below, in Table 32 and Table 33, is based on the mass relationship established between the copper and enamel layer in Section 4.1.3.

Process input	Amount per kg	Source	Linked flow
Copper wire, uncoated	0.96 kg	Calculated, see Section 4.1.3.	IF, see Section 5.2.5.
Liquid enamel, polyester share	43 g	Polynt Composites (2015)	E3, polyester resin, unsaturated
Liquid enamel, xylene solvent share	23 g		E3, xylene
Electricity	0.5 kWh	MAG (2016)	Electricity, optional

Table 32: Process input for enameling 1 kg of magnet wire.

Emissions to air	Amount per kg	Source	Linked elementary flow
Xylene	23 g	Polynt Composites (2015)	E3, xylene

Table 33: Emissions to air from enameling 1 kg of magnet wire.

5.3.2 Subparts with molded plastics

Two subparts in the machine design contain PBT (polybutylene terephthalate) plastics, the resolver and the terminal block. In both cases, injection molding is a common but energy-intensive process method to fabricate the desired shape from plastic granulates. The important process steps are melting, injection, cooling and shaping (Hischier, 2007).

In the case of the resolver the molded form has been assumed to be pinched onto the small stator core and around the copper pins in the connector, and then equipped with hand wound magnet wire, produced as described in sections 5.2.5 and 5.3.1. The stator and rotor cores are punched from an electrical steel sheet, similar to the process described in Section 5.4.2, and laminations glued using an adhesive. For the terminal block, the molded part is combined with the galvanized steel parts when the block is mounted onto the aluminum housing, in the motor factory.

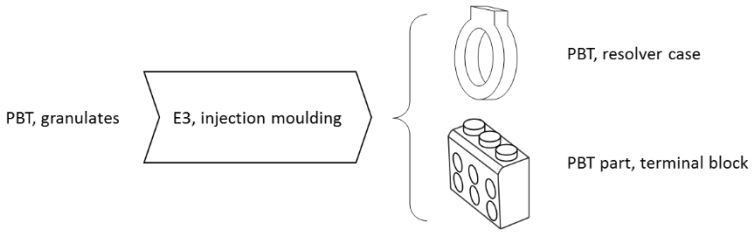

Figure 25: Production activity for plastics available in Ecoinvent 3 (Weidema et al., 2013), converting 0.994 kg of plastics per kilogram of input. The process has been included within the extended system boundary of the LCI model, to account for the fabrication of plastic parts.

Data collection

For the shaping of the PBT parts in the resolver and the terminal block the activity "injection moulding" in the Ecoinvent 3 database (Weidema et al., 2013) is a suitable process. In line with the description in Section 2.3, this process was included within extended system boundaries of the model. Similar to the other material conversion processes of this type, it has the functional unit of one kilogram, but it does not include the material being processes. Confusingly, due to losses, reshaping one kilogram with this production activity forms 0.994 kg of plastics (Hischier, 2007), see Figure 25.

The punching of the resolver stator and rotor laminations was assumed to cause about 50% losses, see Table 34 and Table 35. The electricity consumption for punching laminations and pressing the cores with adhesive was assumed to be negligible (based on a comparison with the motor laminations).

Process input	Amount per 100 g	Source	Linked flow
Electrical steel sheets	200 g	Estimated, based on geometry	IF, see Section 5.2.3

Table 34: Process input for punching of 100 g of resolver core laminations.

Solid waste	Amount per 100 g	Source	Linked flow
Steel scrap	100 kg	Estimated, based on geometry	Steel scrap for recycling

Table 35: Waste from punching of 100 g of resolver core laminations.

5.3.3 Extrusion of foils and cable tubes

Extrusion is another method for shaping plastics and elastomers (rubber-like materials), even more common than injection molding (Hischier, 2007). Plastic films and pipes of various thickness, hard and stiff, or soft and flexible, can be produced from granulates. This production method applies both to the slot liners and separators made of PET (polyethylene terephthalate) and the soft crosslinked silicone rubber insulation on the phase conductors. Generally, most of the energy use in the procedure derives from the heat necessary to plasticize the granulates. In the case of silicone, it is extruded cold, i.e. below 20ºC, but on the other hand it requires heat for the crosslinking process (Leoni, 2014), directly after the extrusion. This takes place in a special furnace where a crosslinking agent links the silicone molecules into a three-dimensional web.

Data collection

For the shaping of the MYLAR foil the reference product "extrusion, plastic film" in Ecoinvent 3 database (Weidema et al., 2013) was listed, and "extrusion, plastic pipes" for the crosslinked silicone phase conductor insulation. This activity was found relevant although the silicone is extruded at low temperature, as the subsequent crosslinking furnace process was assumed to balance up the lower heat use during the extrusion. For further details, read Section 2.3.

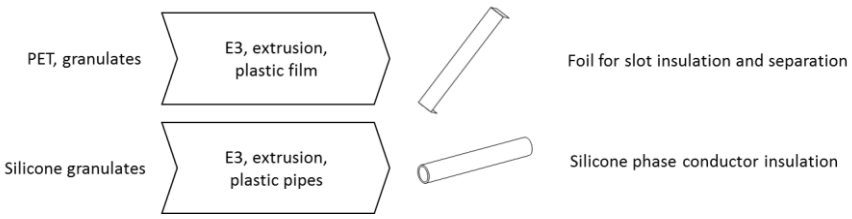

Figure 26: Production activity for plastic-like materials available in Ecoinvent 3 (Weidema et al., 2013), converting 0.976 kg kilogram of material into film, and 0.996 kg of material into pipes, per kilogram of input. The processes has been included within the extended system boundary of the LCI model, to account for the fabrication of foils and phase conductor insulation.

5.3.4 Other insulation and coating materials

Additionally to the subparts presented in sections 5.3.1and 5.3.3, the machine design contains synthetic products such as the stator impregnation resin, the magnet fixation adhesive, the nylon lacing cord and the housing varnish. For all these materials, it was assumed that no further processing is necessary other than what is included in the Ecoinvent3 dataset reference products (Weidema et al., 2013), identified throughout Chapter 4. This includes the stator impregnation resin, where the mixing of the base resin and the silica filler was assumed to be made by hand or using a negligible amount of electricity.

However, the mica tape used for the phase insulation of the stator windings requires several fabrication steps compared to the material composition presented in Section 4.1.5. First, glass fibers are spun and woven into a fabric. Flaked mica is made into sheets by means of grinding, mixing with water and a colloid agent, and pressing onto a mesh in vacuum, followed by drying and curing (Towne and Bombicino, 1975). The mica sheet and the glass fiber cloth are combined using conventional tape coating equipment (Momentive, 2016). The glass cloth goes through a bath where it is saturated with silicone adhesive before the mica sheet is applied. In the next step, the tape is dried for two minutes, typically at 90°C, and then cured for two to three minutes at 165°C (Momentive, 2016). Tapes are also cut and rolled to the desired width and length.

Still, for simplicity, and given the very low contribution to the overall machine mass from the mica covered tape, the processing of the mica tape beyond the material constituents has been neglected.

5.4 At the motor factory

5.4.1 Process overview

A process flow representative for a PMSM motor factory is shown in Figure 27 on the next page, based on a site visit made to ELMO Malmköpings Mekaniska Werkstad AB in Flen, Sweden (Walter, 2015), complemented with a description for the IPM rotor mounting at Motorsolver LCC in Crestwood, Kentucky, USA (Hendershot, 2015). Also, the procedures for splining and surface hardening of the shaft was included based on an expert interview with Låftman (2012), since they were pointed out as relevant for the manufacturing of automotive traction machines.

Please note that the tables throughout sections 5.4.2-5.4.8 only present processing data additional to the material input of the electrical machine itself, and how the input substance flows are modified in each process step. The full account of all input and output flows in all process steps shown in Figure 27, in a unit process format, is provided in the model file (Nordelöf, 2016, 2017) (see sheet “5. The motor factory”).

5.4.2 From steel sheets to core stacks

Electric motor manufacturing begins with the cutting of laminations from electrical steel sheets, process number 1 in Figure 27. There are mainly two alternative methods used for this step, either punching or laser cutting. In punching, a large stamping machine is used to punch out the laminations from the sheet. Stamping machines are fast and efficient but require the making of an expensive stamping tool, designed to provide the desired geometry of the laminations. However, for sufficiently large production volumes, this method becomes

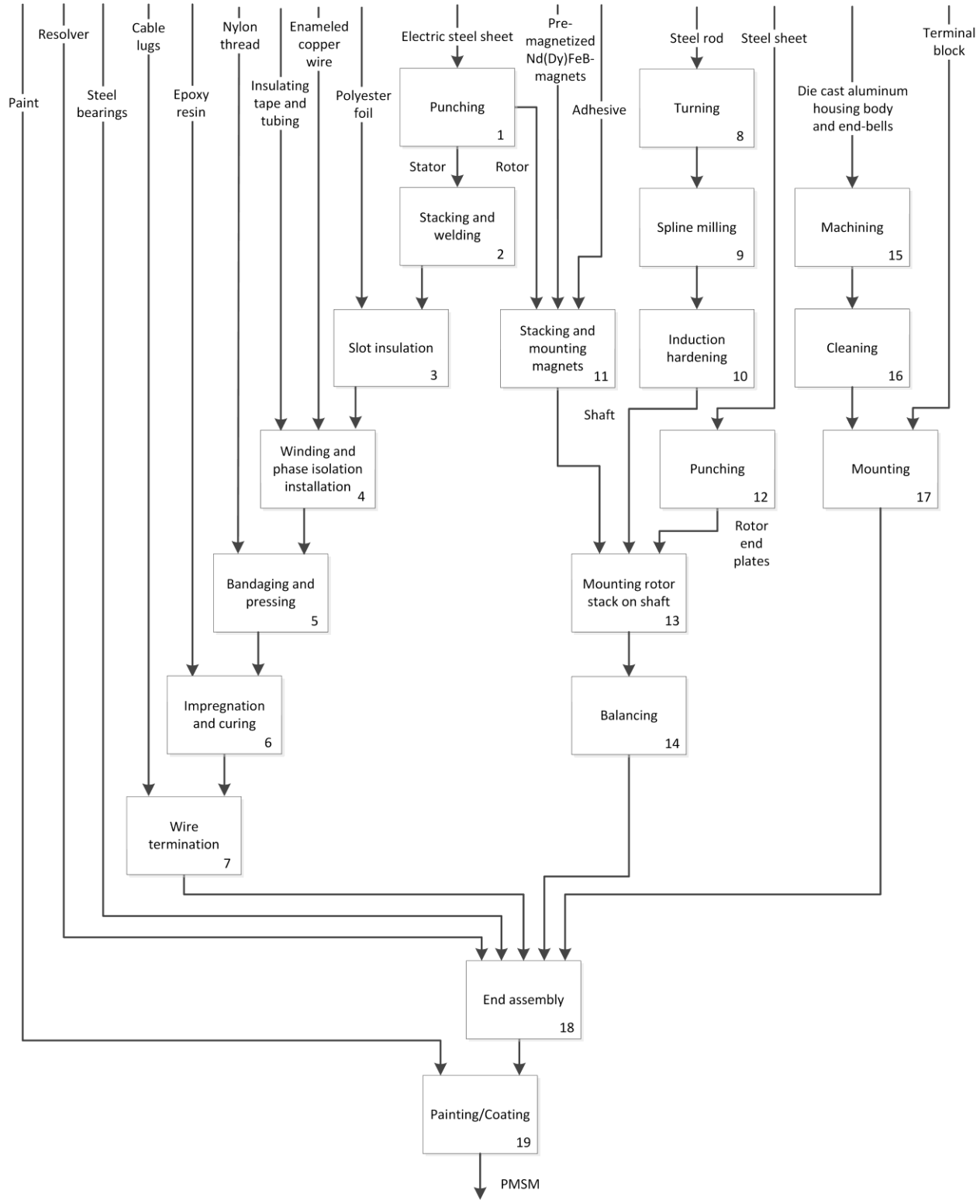

Figure 27: Motor factory process flow chart for a PMSM, divided into 19 processes.

inexpensive when counted per piece (Tong, 2014). Depending on the motor requirements and the pre-treatment of the steel sheet, punched laminations may need a heat treatment to re-stabilize its properties and release internal stress caused by the punch (see Section 5.2.3 and the definition of fully processed electrical steel).

Laser beam cutting is the other method. It has no need for any toolmaking and can cut out very complex shapes, but the productivity is lower and the energy use is higher compared to punching (Tong, 2014). Hence, it is better suited for low volume production, for example in making prototypes or very large machines. In both cases, laminations can be made either in one piece or in segments. If the mechanical requirements for the stator

and rotor cores are the same, and the geometry allows for it, the stator and rotor laminations can be cut from the same steel sheet, even simultaneously in the case of punching. This is beneficial as it reduces the large amount of steel scrap generated by the cutting process.

Next, the laminations are stacked by hand onto a fixture to form a core stack. The stacks are pressed and each lamination is fixed in its position by means of welding, applying an adhesive or some other locking method (Walter, 2015). Sleeves, bolts, rivets or an interlocking design can be used. For the rotor, knurls on the shaft is another option, when the rotor is mounted onto the axle shaft (Hendershot, 2015). The rotor stacking procedure takes place in process number 11 in the motor factory process flow shown in Figure 27. It will be further described in Section 5.4.6.

Welding provides a robust joining of the laminations. However, if welds are applied improperly they can contribute to electromagnetic losses in the core, for example in critical flux path locations (Tong, 2014). The stator stacking procedure was numbered as process 2 in the factory process flow in Figure 27, and found likely to be based on welding.

Data collection

Data for the punching of the core laminations, both for the stator and the rotor from the same electrical steel sheet, was gathered at the manufacturing facilities of Malmköpings Mekaniska Werkstad AB (Walter, 2015). The energy use of the stamping machine was estimated based on a maximum power rating of 20 kW and a 20% power load regulation (expert estimation) for a punching speed of 180 laminations per minute, when the sheet is 0.3 mm thick (Walter, 2015), for the small reference machine. The same energy use per kilogram then corresponds to a higher power load for the large reference machine, about 35%, required for the larger cutting shape. The amount of scrap was calculated based on the geometry of the laminations in combination with data from Walter (2015). The data compilation for the punching is presented in Table 36 and Table 37.

Next, as regards the stacking and welding of the stator, the data has also been gathered from Walter (2015), for an automatic welding machine which is able to weld four beads simultaneously with a measured welding speed of 2.3 mm per second. Argon gas use was based on the yearly consumption, recalculated from 50 liter bottles (Wilhelmsen, 2016), and the electricity consumption on the adjusted power load during the welding. Resulting data for this process is shown in Table 38, Table 39 and Table 40. Argon production data is available in the Ecoinvent 3 database (Weidema et al., 2013) expressed in liquid mass. For reference, the value in Table 38 roughly corresponds to a shielding gas flow of 4 liters per minute and weld bead.

Process input	Amount per kg	Source	Linked flow
Electrical steel sheets	1.9 kg	Walter (2015)	IF, see Section 5.2.3
Electricity	13 Wh	Walter (2015)	Electricity, optional

Table 36: Process input for punching of 1 kg of laminations, both for the stator and the rotor, from the same sheet (process number 1 in Figure 27).

Solid waste	Amount per kg	Source	Linked flow
Steel scrap	0.9 kg	Walter (2015)	Steel scrap for recycling

Table 37: Waste from punching of 1 kg of laminations, both for the stator and the rotor, from the same sheet (process number 1 in Figure 27).

Process input	Amount per cm	Source	Linked flow
Argon	2.2 g	Walter (2015)	E3, argon, liquid
Electricity	2 Wh	Walter (2015)	Electricity, optional

Table 38: Process input in energy and shielding gas for stacking and welding of 1 cm of stator core (process number 2 in Figure 27).

Process input	Amount per kg	Source	Linked flow
Stator laminations	1.01 kg	Walter (2015)	IF, see Table 36

Table 39: Process input in lamination mass for stacking and welding of 1 kg of stator core (process number 2 in Figure 27).

Solid waste	Amount per kg	Source	Linked flow
Steel scrap	10 g	Walter (2015)	Steel scrap for recycling

Table 40: Waste from stacking and welding of 1 kg of stator core (process number 2 in Figure 27).

5.4.3 Installing and securing the winding

The slot liner is delivered to the motor factory as a roll. The roll is placed in a machine which cuts, shapes and installs each slot liner directly into the stator in a few seconds. Pieces can also be cut and shaped for manual insertion, for example to make the slot separators. The installation of the slot liners are depicted as process number 3 of Figure 27.

Next, in process 4, the procedure for mounting the winding into the stator slots and installing phase insulation, consists of a number of sub steps which all can be conducted either by hand or using machines. First, the magnet wire is wound into coils. The coils are mounted onto a fixture matching the number of slots in the stator. The coils are then pulled through the stator into the slots, inside the slot liners. In the case of a two layer winding, the layer placed deepest in the slots is pulled through first. Slot separators are placed in the slots and isolation tape is applied on the end-turns of the installed layer, by hand. Next, the coil layer placed closest to the air gap is pulled through, and equipped with phase insulation, if it is considered necessary. Often phase conductors are also prepared at this stage, for example by pinching or soldering ready-made insulated cables to the coils, or by threading tubes over the magnet wire conductors extending from the coils.

Following, in order to secure the winding ends and make sure that they do not bulge further than necessary outside the stator core, end-turns are laced with a thread and then pressed in the axial direction, in process number 5. Lacing can be done by hand or using a machine which ties different end-turns to each other by stitching around the copper bundle at each slot. For the pressing, machine power is necessary. The pressing step is fast and takes around four to five seconds (Walter, 2015).

Data collection

Data for installing the winding including slot liners, phase insulation and phase conductors, and the pressing and lacing of the end-turns, was gathered from Malmköpings Mekaniska Werkstad AB (Walter, 2015), combined with machine data from Ningbo Nide (2014). Waste from the bending and cutting of slot liners and slot separators was assessed as negligible (Walter, 2015). For both magnet wire and phase insulation tape, 1% of the mass goes to scrap (Walter, 2015) (excluding the wire termination, see section 5.4.8). However, given the very small amount of phase insulation tape used in total (see Section 4.1.5), this waste stream has also been neglected. For the magnet wire, additional input is presented in Table 41 and copper scrap in Table 42. The amounts at nominal length of the large and the small reference machines are 25 grams and 49 grams.

Process input	Amount per kg	Source	Linked flow
Magnet wire	1.01 kg	Walter (2015)	IF, see sections 5.2.5 and 5.3.1

Table 41: Process input for the installation per 1 kg of enameled copper wire (process number 4 in Figure 27).

Solid waste	Amount per kg	Source	Linked flow
Copper scrap	0.01 kg	Walter (2015)	Copper scrap for recycling

Table 42: Waste from the installation per 1 kg of enameled copper wire (process number 4 in Figure 27).

Data for the energy use of a lacing machine was collected from Ningbo Nide (2014). The total electricity use for process steps 3 to 5 has been summarized in Table 43 with the lacing and the pressing of the end-turns providing significant contributions. There is no difference in energy input depending on the stator size for these processes as the power required to press was found to be the same, and the number of the slots are the same, for all stators produced. It was assumed that there are no losses of phase conductor insulation during these process steps. Likewise for the nylon thread.

Process input	Amount per piece	Source	Linked flow
Electricity	24 Wh	Ningbo Nide (2014), Walter (2015)	Electricity, optional

Table 43: Energy input for installation of the winding with slot and phase isolation, end-turn pressing and lacing per stator package, in processes number 3-5 of Figure 27.

5.4.4 Impregnation procedure

The main procedures for the encapsulating the stator windings are casting, dipping and trickling (Richnow et al., 2014, Tong, 2014). Casting is generally used to fully encapsulate the stator package as it is casted with resin in a mold. Dipping comes in many variants but common for all of them is that the stator is submerged into a resin during the process and this also leads to a full impregnation. In the simplest version, called dip and bake, the stator is dipped into a tank with varnish and then directly cured in an oven. However, this method leads to high dripping losses and there is a risk for air cavities inside the slots (Richnow et al., 2014). Various dipping methods have been developed to decrease dripping losses and increase the intrusion into the stator, such as hot dipping where the winding is heated, dip-rolling where the stator is only partly submerged and rolled in the resin, or the use of vacuum to eliminate the cavities (Richnow et al., 2014, Tong, 2014). Vacuum can also be used during casting. Naturally, the specific characteristics of the selected resin, for example different epoxies, also matter. Nevertheless, in most cast or dip procedures, the whole stator will be subject to impregnation and not just the windings, causing a relatively large use of resin.

In trickling, the resin is poured or sprayed onto the winding as a fine jet, often when the stator is rotating and slightly inclined, and then drawn into the cavities of the slots and end-windings by capillary action. Main benefits are that the amount of resin can be very accurately managed, short processing time, no dripping losses and reduced problems with air cavities. However, the cost of the procedure is higher than for example dip and bake (Stone et al., 2014), since advanced automation equipment and regulation is required.

Overall, the impregnation procedure is often one of the most energy demanding in the motor factory (Karlsson, 2013, Walter, 2015) due to the pre-heating before, and curing after, resin has been applied. In comparison, trickling has the advantage of being energy efficient due to the short curing time. In turn, the curing time directly links to the required winding copper temperature and consequently the heat transfer and temperature in the curing oven (Larrenduche, 2015). In an automatic continuous trickling machine there are different zones for preheat, trickling, gelling and curing. Naturally preheat and gelling conditions also matter for the power consumption per stator unit, but equally important is the loading capacity which is governed by how well the trickling machine is optimized for the specific stator design being produced (Willard, 2015, Xue, 2015). Similarly, in a batch oven it depends on how well stators are packed into the chamber.

Finally, during the curing process some of the resin mass will be lost when solvent in the resin is evaporated and polymerization is taking place, causing emissions to air as a smoke of monomers and oligomers, i.e. airborne droplets, or as volatile organic compounds (VOCs).

Data collection

The use of trickling was found to be the most representative impregnation procedure for the studied motor design. Data for electricity use was gathered for two different types of trickling machines, both continuous, in the form of the maximum rated power, maximum copper temperature achievable in the heating sections and the loading capacity for a specific stator diameter. Values were averaged from six different tunnel ring shaped trickling machines (Ningbo Haishu Nide, 2014) and three rotary table machines (Broomfield, 2014a, b, Willard, 2015). Based on observation it was found that the curing zone constitute roughly half of the machine. For the other half of the machine, about one quarter was found to be the “trickling station” with nozzles and resin supply, and the remaining three quarters were found to be preheat and gelling sections. If the zone temperatures are regulated to 130ºC for preheating, 150ºC for gelling and 170ºC for curing, then can a curing

time of 30 minutes be expected according to the resin supplier (Larrenduche, 2015). Hence, with half of the cycle time taking 30 minutes, the resulting complete cycle time for one stator was found to be 1 hour.

As a simple approximation, it was assumed that the maximum power consumption is required to accomplish the maximum rated temperature in all heating sections at the same time, including auxiliaries such as ventilation, and that the two parameters scales linearly with each other. The resulting electricity use the estimation of trickling and curing is stated in Table 44, per cm of stator diameter, and the values for the two different reference machine diameters become 0.35 kWh and 0.46 kWh. As a comparison, the energy used for the dip and batch bake procedure at Malmköpings Mekaniska Werkstad AB was also investigated for its energy use and without being dependent on the stator diameter in the same way, each stator then requires about 2 kWh for the impregnation procedure (Karlsson, 2013, Walter, 2015).

Process input	Amount per cm	Source	Linked flow
Electricity	23 Wh	Broomfield (2014a), (2014b), Ningbo Nide (2014), Willard (2015).	Electricity, optional

Table 44: Electricity input for trickling and curing the stator package per centimeter of stator diameter, in process number 6 of Figure 27.

Furthermore, 5% of the liquid epoxy resin base content was assumed to evaporate as white smoke of hydrocarbons from the curing process. The matching datasets in the Ecoinvent 3 database (Weidema et al., 2013) was identified as “hydrocarbons, aliphatic, unsaturated”. Process inputs and emissions to air for the trickling process is shown in Table 45 and Table 46.

Process input	Amount per kg	Source	Linked flow
Silica filler	250 g	Larrenduche (2015), Von Roll (2015)	E3, silica sand, see Section 4.1.5
Liquid epoxy resin	790 g		E3, epoxy resin, liquid, see Section 4.1.5

Table 45: Process input for trickling and curing the stator package per kilogram of cured epoxy resin, in process number 6 of Figure 27.

Emissions to air	Amount per kg	Source	Linked elementary flow
Hydrocarbons	40 g	Larrenduche (2015), Von Roll (2015)	E3, hydrocarbons, aliphatic, unsaturated

Table 46: Emissions from the trickling and curing of the stator package per kilogram of cured epoxy resin, in process number 6 of Figure 27.

5.4.5 Shaft preparation

The machining procedures for shaft manufacturing varies with the type of design, if it is hollow or solid, and the type of mechanical joint. Methods include both forging and welding (Tong, 2014), but the primary processing step in most shaft manufacturing is turning, forming the rod into the desired shaft geometry (Junker, 2012). For the production of solid shafts, the shaft arrives to the motor factory as a steel rod, and depending on the delivered length it may have to be cut before the turning step. The turning procedure, as well as other metal processing tools, requires a continuous spray of fluid for cooling and lubrication which is referred to as cutting fluid. It is an mixture with naphtha as the main constituent, which is diluted in water to a concentration of 5-10% before use in the machine (Statoil, 2015a, b).

Other important tools in the shaft preparation are drilling and milling machines, often with very high precision computer based control (Junker, 2012). Such machinery is used, for example, to make the shaft connection, described in Section 4.2.3. As regards manufacturing, splining is uncomplicated in terms of quality and accuracy as it is the same pattern being milled all around the shaft circumference, compared to keys or keyseats which may bring unbalance to the shaft. On the other hand, the splined section of a shaft is often heat treated at the surface to improve its mechanical properties, whereas keyseats sections are not (Tong, 2014).

Induction heating is a common method for surface hardening of motor shafts. The process is fast, only one or a few seconds, as the depth of heating necessary often is only a few millimeters (Rudnev et al., 2014). The heat is generated in the shaft surface by a magnetic field deriving from a high-frequency alternating current (Brill and Schibisch, 2015). The temperature can quickly be raised above 1000ºC and must also be followed by intensive quenching using water mixed with an oil- or polymer based quenching fluid (Rudnev et al., 2014, Tong, 2014). The case depth, i.e. the distance below the surface which becomes hardened by the heat, and energy consumed is coupled to the frequency of the induced magnetic field, but also the surface to be covered and the temperature raise required for the specific steel grade (Haimbaugh, 2001, Rudnev et al., 2014). Typically, stainless steels require among the highest temperatures, around 1100ºC. The shaft is set to rotate around its axis inside the induction coil and depending on the length of shaft section to be hardened, the induction coil and the quenching spray may have to move along the shaft to cover the whole surface.

Data collection

Data for the turning of the shaft, process number 8 in Figure 27, was collected from Walter (2015). No preceding cutting of rods into desired lengths has been included, as it was assumed to be included in the final step of the fabrication of the supplied steel. The cutting fluid use was calculated based on the yearly consumption of concentrated liquid at Malmköpings Mekaniska Werkstad AB (Walter, 2015), used by several turning, cutting, drilling and milling machines. It corresponds to a flow rate of 130-250 ml per minute when diluted[15] (Statoil, 2015a, b). Linked data in the Ecoinvent 3 database (Weidema et al., 2013) was set to naphtha as an approximation, and "waste mineral oil" for the oil share of the recollected diluted fluid. The upper flow rate value was used to calculate the amount of water that the mix requires. Typically, cutting fluid waste goes to incineration. Hence, water was omitted in the waste flow, since it does not contribute to any emissions but water vapor. The data for the energy consumption of the turning and the average generation of steel scrap were based on figures and expert estimations provided by Walter (2015), and presented in Table 47 and Table 48.

Detailed data for splining of shafts has not been available from Malmköpings Mekaniska Werkstad AB, although such machining can be conducted by multi operation machines of the plant (Walter, 2015). Therefore, data for the power consumption and the cutting fluid flow rate gathered from Walter (2015) for the machining of the housing was used, see Section 5.4.7 for more details, and combined with an estimated cycle time for the splining procedure, based on milling in two rounds, one for roughing and one for finishing. There is large variability in the cycle time depending on the milling machine capacity, but based on observation[16], a simple but reasonable milling feed rate is 1 meter per minute for a tooth depth of 1 mm, including the time for returning the milling tool to the starting position before making each new tooth. It was also assumed that doubling the tooth depth would halve the feed rate and vice versa. Hence, these assumptions result in a cycle time of roughly

Process input	Amount per kg	Source	Linked flow
Steel rod	1.25 kg	Walter (2015)	IF, see Section 5.2.1
Cutting fluid, concentrated	8 g	Walter (2015)	E3**,** naphtha
Cutting fluid, water	155 g	Statoil (2015a, b)	E3, tap water
Electricity	108 Wh	Walter (2015)	Electricity, optional

Table 47: Process input for machine turning of a steel rod into 1 kg of shaft with proper dimensions (process number 8 in Figure 27).

Waste	Amount per kg	Source	Linked flow
Steel scrap	0.25 kg	Walter (2015)	Steel scrap for recycling
Waste oil, conc. share in dilution	8 g	Walter (2015)	E3, waste mineral oil

Table 48: Waste from machine turning of a steel rod into 1 kg of shaft with proper dimensions (process number 8 in Figure 27).

[15] The upper flow value corresponds to 5% concentration and the lower flow value to 10%.

[16] Based on movie clips on Youtube of shaft splining, for example a film uploaded by Advent Tool & Manufacturing Inc. on https://www.youtube.com/user/TMFMLLC.

two minutes to spline 20 teeth of 1 mm depth or 10 teeth with 2 mm depth, over 35 mm at the shaft end, as specified by the design. Additionally, it was assumed that there are 10 splines made around the circumference for each centimeter of diameter. Correspondingly, the smallest shaft diameter of 20 mm in the model will have of cycle time of around 80 seconds and the largest shaft, 50 mm in diameter, takes 200 seconds. The extra energy necessary for splining a large shaft compared to a small shaft was accounted for by adjusting the cycle time while keeping the machine power constant, although the other way around may be more likely in reality. For simplicity, the steel removed in the splining process was accounted for in the turning process, number 8, by approximation. Table 49 and Table 50 show the compiled results for the splining process.

The energy data collection for the induction surface hardening of the splined shaft section was made from tabulated values in Haimbaugh (2001). The source states that 10 kHz is a suitable frequency for all shaft diameters in the span of 20 to 50 mm, and that for this frequency a heating time of 1.5 seconds with a power of around 30 W/mm^2 yields a case depth of 3 mm (Haimbaugh, 2001). The quenching time was set to be three times longer than the heating time based on Rudnev et al. (2014) and the quenching flow was calculated based on information from Poteet et al. (2006). The total area of all spraying holes was set to equal 10% of the splined shaft section area (5-10% is a minimum) and the flow rate to about 0.5 liters per minute and mm^2 of hole area[17], for the complete range of shafts. A typical quenching fluid was found to consist mainly of a polyalkylene glycol which is mixed with water to a concentration of about 15% (Dow, 2005a, b, 2014). This best available corresponding data in the Ecoinvent 3 database (Weidema et al., 2013) was found to be "propylene glycol" and "spent antifreezer liquid" for its waste product, in analogy with the cutting fluid waste modelling. Table 51 and Table 52 show the data summary for the surface hardening of the 35 mm shaft end.

Process input	Amount per cm	Source	Linked flow
Cutting fluid, concentrated	9 g	Walter (2015)	E3**,** naphtha
Cutting fluid, water	160 g	Statoil (2015a, b)	E3, tap water
Electricity	56 Wh	Walter (2015)	Electricity, optional

Table 49: Process input for spline milling a 3.5 cm long section of the shaft in relation to the shaft diameter (process number 9 in Figure 27).

Liquid waste	Amount per cm	Source	Linked flow
Waste oil, conc. share in dilution	9 g	Walter (2015)	E3, waste mineral oil

Table 50: Waste from spline milling a 3.5 cm long section of the shaft in relation to the shaft diameter (process number 9 in Figure 27).

Process input	Amount per cm	Source	Linked flow
Quenching fluid, concentrated	0.63 kg	Poteet et al. (2006), Dow, see text.	E3, propylene glycol
Quenching fluid, water	3.4 kg	Poteet et al. (2006), Dow, see text.	E3, tap water
Electricity	14 Wh	Haimbaugh (2001)	Electricity, optional

Table 51: Process input for induction surface hardening of a 3.5 cm long section of the shaft in relation to the shaft diameter (process number 10 in Figure 27).

Liquid waste	Amount per cm	Source	Linked flow
Waste quenching fluid, conc. share in dil.	0.63 kg	Poteet et al. (2006), Dow, see text.	E3, spent antifreezer liquid

Table 52: Waste from induction surface hardening of a 3.5 cm long section of the shaft in relation to the shaft diameter (process number 10 in Figure 27).

[17] 1.5 gallons per minute over a set of 5/32 inch diameter holes, at 20 PSI, from Figure 15 in Poteet et al. (2006).

5.4.6 Rotor assembly

Besides the preparation of the shaft, two additional steps are necessary before the rotor can be fully assembled on the shaft; the magnets should be placed and fixated within the rotor slot cavities and rotor endplates must be fabricated, i.e. process steps number 11 and 12 in Figure 27. The rotor endplates are punched from a steel sheet in a stamping machine, alike the punching of core laminations. Parts are then integrated by threading the rotor core onto the shaft and pressing in the endplates to hold everything in place, in step number 13 of Figure 27. Lastly, the rotor is balanced by removing small amounts of steel from selected points of the endplate through the drilling of minor craters, in procedure number 14 in Figure 27. It involves two steps, a balance test and the drilling, which are repeated until a satisfactory rotor balance has been achieved.

The mounting of the magnets into the rotor slots differs for pre- and post-magnetized rotors. For un-magnetized magnets, standard pick and place equipment can be used (Franke et al., 2011). However, for pre-magnetized magnets, suitable automated production equipment is difficult to acquire and the procedure is generally manual (Franke et al., 2011). Since large magnets are difficult to handle manually due their strength, they have to be mounted in smaller sections, and this coincides well with the benefits of segmentation, i.e. that losses are reduced, see Section 4.2.2. However, manual mounting of many small magnets is time consuming and labor intensive, combined with increased risks for the quality of the product, damages to the production facilities and injuries for the staff. For this reason, efforts are being made to develop suitable mounting machines (Franke et al., 2011, Franke et al., 2015, Hultman et al., 2014, Tremel et al., 2013)

A typical IPM hand mounting procedure at Motorsolver LCC in Crestwood, Kentucky, USA was described by Hendershot (2015). Magnets are delivered in, for example, 1-3 cm sections. The rotor laminations (coming from process step 1 in Figure 27) are stacked with proper alignment on a fixture up to the same height as magnets length. North Pole magnets are then hand inserted in every other slot, followed by the South Pole magnets into the remaining slots. The polarity is inspected with a pole detector. The rotor segment is then slightly heated, for instance using a hand held heat gun, before the adhesive is applied over each magnet and allowed trickle down into the small cavities around the magnets. The heat gun is then applied again to cure the adhesive, from around 30 seconds up to a minute. Finally, the core segments with installed magnets are stacked and aligned on a fixture, or directly on the shaft, before the complete package is clamped by pressing the endplates onto the shaft in a pressing machine.

Data collection

Data for the hand mounting of the magnets was gathered from Hendershot (2015), and combined with data for endplate punching and pressing, and rotor balancing from Walter (2015). Both losses of adhesives during the application and as emissions during the curing was regarded as negligible, based on the description of the procedure combined with the small amounts present in the design and a VOC content stated to be below 0.8% (Henkel, 2010).

The energy use for the punching was estimated by an extrapolation of relationship between the number of punches per minute and the sheet thickness for a certain power use compared to data compilation for the thinner electrical steel sheets, presented in section 5.4.2. The punching rate was observed to decrease with increasing thickness, but not linearly (Walter, 2015). Combined with the fact that the endplates are solid and made of a slightly heavier steel type, the energy needed per kilogram was found to be less than for the electrical steel sheets, despite the need of a larger punching force.

For the pressing, a 20 ton force applied during 5 seconds was stated by Walter (2015), and complementary data for the power consumption for such pressing was collected for an hydraulic machine from Huahong Technology (2015). The total cycle time was assumed to be double the pressing time and any leakage of hydraulic oil was neglected. Also, an estimation for the average time to balance one rotor was made by Walter (2015). The data compilation is presented in tables 53-57.

Process input	Amount per cm	Source	Linked flow
Electricity	128 Wh	Hendershot (2015)	Electricity, optional

Table 53: Process input for stacking of 1 cm rotor core (length), including the mounting and fixating the magnets into the rotor slots (process number 11 in Figure 27).

Process input	Amount per kg	Source	Linked flow
Stainless steel sheets	1.7 kg	Walter (2015)	E3, see Section 5.2.1
Electricity	9 Wh	Walter (2015)	Electricity, optional

Table 54: Process input for punching of 1 kg of stainless steel rotor endplates from a steel sheet (process number 12 in Figure 27).

Solid waste	Amount per kg	Source	Linked flow
Steel scrap	0.7 kg	Walter (2015)	Steel scrap for recycling

Table 55: Waste from punching of 1 kg of stainless steel rotor endplates from a steel sheet (process number 12 in Figure 27)

Process input	Amount per piece	Source	Linked flow
Electricity	42 Wh	Huahong Technology (2015), Walter (2015)	Electricity, optional

Table 56: Process input for assembling and pressing the rotor package onto the shaft (process number 13 in Figure 27).

Process input	Amount per piece	Source	Linked flow
Electricity	8 Wh	Walter (2015)	Electricity, optional

Table 57: Process input for balancing the rotor (process number 14 in Figure 27).

5.4.7 Preparation of die cast housing parts

The die cast aluminum housing parts, i.e. the endbells and the housing body, do not arrive to the motor factory ready-made. The fitting of the endbells with the bearings must be very precise, with a tolerance of bearing bores of around 1 µm (Walter, 2015). High precision is also required for the fitting of the housing body with the outer stator diameter, and between the endbells and the housing body. Excessive material may have to be removed from the workpiece, and holes or other types of fixation points must also be prepared. Hence, die cast parts must go through machining at the motor factory before they are apt for final assembly. Typically, this step involves multiple operations such as turning, cutting, drilling, milling and threading. In order to join all parts perfectly, several guiding edges and tightly matched surfaces must be trimmed, and the time necessary for this surface finishing depends on the total area with specific tolerance requirements. As an example, for the endbells, the bearing dimensions are more important than the endbell geometry or weight. However, for the housing body, a significant part of the processing time is coupled to other milling and drilling operations, to prepare screw holes, fixation points, and nozzles and channels for the cooling system (Walter, 2016). The finishing of the housing body's inner surface area constitute the remaining task. Aluminum scrap, mostly in the form of aluminum shavings, but also dust, is generated during this machining, and it must be removed before the assembly. The machined parts are blown clean by a compressed air spray.

Data collection

Data for the preparation of the die cast aluminum parts was collected from ELMO Malmköpings Mekaniska Werkstad AB (Karlsson, 2013, Walter, 2015, 2016) in Flen and complemented with information from Iro AB, an electrical machine manufacturer in Ulricehamn, Sweden (Magnusson, 2016). The data was established in five steps before it was compiled: the overall time to process different sized housing parts in a multi-operation machine was assessed based on existing preparation die cast parts at ELMO of an example geometry; a calculation procedure for the amount of material removed and scrapped per part was established based on the machining allowance and expert estimations; the electricity used by the multi-operation machine was assessed based on measurements made by Karlsson (2013); the flow rate of cutting fluid was estimated out of the total yearly use of cutting fluid; and the energy used for cleaning was extracted from the overall use of compressed air at the plant. By combining the processing time per part with the cutting fluid flow and the

average power use of the multi-operation machine, the amount of cutting fluid and electricity used per part was established. For further details about modelling of cutting fluid use, see section 5.4.5.

First, for process step number 15 of Figure 27, the multi-operation machine processing time for a selected housing sample in a was compared with the trimmed surface area of the same sample, including edges and bearing bores of the endbells and edges and the inner surface area of the housing body. After casting, surfaces typically have an average machining allowance of about 0.7 mm which is removed from the workpiece during turning and milling (Magnusson, 2016). The endbells of the selected housing sample required one minute of processing each, mainly for surface trimming (Walter, 2016). The machining time for the complete housing sample was 15 minutes, i.e. 13 minutes for the preparation of housing body after two minutes were spent on the endbells (Walter, 2016). Surface trimming accounted for about 50% of the time spent on preparing the body part (Walter, 2016). Based on this information, a surface trimming speed of 85 cm^2 per minute was established and used to estimate the trimming time required for the different reference machine geometries. For machining operations other than trimming, the processing time was set to be constant for both reference machines at all lengths and estimated from the time required for the housing sample, six and half minute. For the endbells, another simplification was made when the processing time was predicted to be constant for both references sizes, in contrast with the actual dependence on the bearing and bore size. Hence, the surface trimming time for the endbells was assessed to match the largest possible bore size. Also, it was assumed that the reference geometries have larger need for additional machining operations than the housing sample, and 0.5 minutes was added to each estimated surface trimming step. Hence, total processing per endbell, was calculated to 2 and 1.5 minutes for the large and small reference machines, respectively.

As regards scrap losses from surface trimming, these were found to be 2-5% for the housing body and around 1-1.5%% for the endbells, according to the same geometric calculations for the reference machines as used for the processing time assessment. Overall it was found that more robust designs have lower losses per kilogram compared to more slender housings. This is also consistent with observations of motor housing preparation in production at Iro AB(Magnusson, 2016). Hence, it was found adequate to approximate the amount of material removed from the unprocessed housing body by setting it to decrease linearly with increased final mass of the housing, from 10% for the smallest housing body mass to 5% for the largest housing body. More explicitly, the additional material input and scrap loss for the housing body of the shortest small reference machine was set to 10% of its final mass. Similarly, the added input mass, and the loss, for the longest housing of the large reference machine, was set to 5% of its final mass. Corresponding figures for the endbells were set to fixed values, 3% and 2% for the large and small reference machines, respectively.

Next, the data for processing time and scrap loss relating to the surface trimming of the housing body were combined in order to express the energy consumption and the cutting fluid use for surface trimming as functions of the amount of material removed from the housing body (once the average amount of energy used per minute of multi-operation machine processing had been decided, see below). Calculations based on the data for housing sample gave that 16 grams of mass is removed per minute of surface trimming and that it was reasonable to assume that surface trimming accounts for 50% of the total mass removal.

The data for electricity use during multi-operation machining of the die cast parts was based on the energy audit conducted by Karlsson (2013), which measured the power load of the largest multi-operation machine at the ELMO plant, both during active use and standby (see Section 5.4.9). For this machine it was found that for every 1 kWh used in active operation, another 0.4 kWh was spent during standby, calculated for the yearly operation. However, the largest of the multi-operation machines is not representative for all multi-operation machines at ELMO, in terms of the rated power. The average power rating was assessed to be half of the value measured for the largest machine. Hence, all in all, with standby taken into account, the average electric energy used to support one minute of machining was found to be 50 Wh. This was then combined with geometric analysis for the amount of material removed during a certain amount of operation time, based estimates and measurements made by Walter (2015), (2016).

As mentioned in Section 5.4.5, the yearly consumption of cutting fluid at ELMO was used to calculate a flow rate of concentrated liquid during machine operation. More precisely, the share of the total cutting fluid volume used for the machining of specific endbells was estimated and combined with the processing time and number of endbells processed for the full year (Walter, 2015). Also mentioned in Section 5.4.5, the linked flows for the Ecoinvent 3 database (Weidema et al., 2013) representation was set to naphtha for the input of concentrated fluid, and "waste mineral oil", for spent recollected fluid.

The results for process step 15 are presented in tables 58-62, with the variable process inputs and wastes coupled surface trimming of the housing body in Table 58 and Table 59. Table 60 and Table 61 show the constant values for inputs and waste coupled to other machine processing of the housing body, and Table 62 and Table 63 presented all fixed results for the two endbell sizes.

Process input	Amount per 100 g	Source	Linked flow
Cutting fluid, conc.	80 g	Magnusson (2016), Walter (2015), (2016)	E3**,** naphtha
Cutting fluid, water	1.50 kg	Statoil (2015a, b)	E3, tap water
Electricity	0.31 kWh	Karlsson (2013), Magnusson (2016), Walter (2016)	Electricity, optional

Table 58: Process input for the removal of 100 g aluminum during surface trimming of the housing body (accounting for 50% of the mass removal in process number 15 in Figure 27). The mass removed corresponds to 10% of the final mass for the smallest housing body. The removed proportion then decreases linearly and corresponds to 5% of the final mass for the largest housing body.

Waste	Amount per 100 g	Source	Linked flow
Aluminum scrap	100 g	Magnusson (2016), Walter (2015), (2016)	Aluminum scrap for recycling
Waste oil, conc. share in dilution	80 g		E3, waste mineral oil

Table 59: Waste from the removal of 100 g aluminum during surface trimming of the housing body (accounting for 50% of the mass removal in process number 15 in Figure 27). The mass removed corresponds to 10% of the final mass for the smallest housing body. The removed proportion then decreases linearly and corresponds to 5% of the final mass for the largest housing body.

Process input	Amount per piece	Source	Linked flow
Cutting fluid, conc.	85 g	Magnusson (2016), Walter (2015), (2016)	E3**,** naphtha
Cutting fluid, water	1.56 kg	Statoil (2015a, b)	E3, tap water
Electricity	0.33 kWh	Karlsson (2013), Magnusson (2016), Walter (2016)	Electricity, optional

Table 60: Process input per housing body for other machining operations (accounting for 50% of the mass removal in process number 15 in Figure 27). The mass removed corresponds to 10% of the final mass for the smallest housing body. The removed proportion then decreases linearly and corresponds to 5% of the final mass for the largest housing body.

Waste	Amount per piece	Source	Linked flow
Aluminum scrap	Variable	Magnusson (2016), Walter (2015), (2016)	Aluminum scrap for recycling
Waste oil, conc. share in dilution	85 g		E3, waste mineral oil

Table 61: Waste per housing body from other machining operations (accounting for 50% of the mass removal in process number 15 in Figure 27). The mass removed corresponds to 10% of the final mass for the smallest housing body. The removed proportion then decreases linearly and corresponds to 5% of the final mass for the largest housing body.

Process input	Amount per piece	Source	Linked flow
Small endbell, from die casting	1.03 kg	Magnusson (2016), Walter (2015), (2016)	IF, see Section 5.2.4
Large endbell, from die casting	2.55 kg		
Cutting fluid, conc., small endbell	20 g		E3**,** naphtha
Cutting fluid, conc., large endbell	25 g		
Cutting fluid, water., small endbell	0.36 kg		E3**, tap water**
Cutting fluid, water, large endbell	0.48 kg		
Electricity, small endbell	75 Wh	Karlsson (2013), Magnusson (2016), Walter (2015), (2016)	Electricity, optional
Electricity, large endbell	100 Wh		

Table 62: Process input for machining one aluminum endbell (process number 15 in Figure 27).

Waste	Amount per piece	Source	Linked flow
Aluminum scrap, small endbell	30 g	Magnusson (2016), Walter (2015), (2016)	Aluminum scrap for recycling
Aluminum scrap, large endbell	50 g		
Waste oil, conc. share, small endbell	20 g		E3, waste mineral oil
Waste oil, conc. share, large endbell	25 g		

Table 63: Waste from machining one aluminum endbell (process number 15 in Figure 27).

In process step number 16 of Figure 27, the machined parts are cleaned using compressed air blowers. The data collection and analysis made on the compressed air system and various use of pneumatics at the manufacturing site, is further described in Section 5.4.9. Still, as a starting point, electricity consumption measurements for the central compressor had been provided by Karlsson (2013). Compressed air use in specific processes was then approximated in the form of "unit operations" based on typical flow rates and time estimates for open blow, e.g. cleaning, in comparison with spray painting and pneumatic press-fitting, taken from tabulated type data for different typical compressed air applications (Appleton, 2016, SWP, 2016). For example, it was assumed that cleaning one endbell takes about 20 seconds and one house body just over one minute. The yearly production output of electrical machines and other machined products was also accounted for (Walter, 2016). Notably, compressed air use was found to be very energy demanding, since relatively short active operations carry a load of losses from compressor heat and some air leakage, caused also during standby. However, for the final calculations, the peak power load of the compressor was assumed for the full workday and combined with the full production capacity output of the factory, instead of the measured values, in order to model a situation of high volume production and full use of the compressed air system. In doing so, standby time was set to be negligible. The energy used for the cleaning of housing parts is shown in Table 64.

Process input	Amount per piece	Source	Linked flow
Electricity, one endbell	170 Wh	Appleton (2016), Eret et al. (2010) Karlsson (2013), SWP (2016), Walter (2016)	Electricity, optional
Electricity, housing body	0.52 kWh		

Table 64: Electricity for generation of compressed air used in cleaning of housing parts after machining (process number 16 in Figure 27).

Finally before the complete housing goes to final assembly, the terminal block is mounted onto the cylindrical body. This operation, number 17 in Figure 27, was assumed to be manual, without losses or energy consumption.

In a last comment on this section, it is important to point out that the machine processing and cleaning of the housing parts are the only processes in the motor factory where stand-by energy was included and directly linked to each part. There are two reasons for this. First, data was available. Second, since the housing parts optionally can be excluded in the LCI model, this was found more important for these two process steps than for any other of the processes shown in Figure 27.

5.4.8 Wire termination, unit assembly and painting

In the end assembly, process number 18 in Figure 27, the complete electrical machine is put together in several steps. The stator package is fitted into the housing body, and the winding connectors are coupled to the terminal block. In parallel, the bearings are press-fitted onto the balanced shaft. At last, the rotor and stator packages can be merged into one unit by placing the bearings into the bores of the endbells and then secure the endbell and body parts of the housing into one unit using fasteners such as bolts and nuts, or screws. Alongside, the stator part of the resolver is connected to one of the endbells, and the rotor part to the end of the shaft. Subsequently, the complete machine goes through a test sequence in a rig, checking, for example, that the windings and connection cables are undamaged and fully functioning. Most of these operations can be assumed to be made by hand, possibly with the assistance of automated hand-held tools. However, two assembly operation requires machine assistance, when then bearings are pressed onto the shaft and when the stator is fitted into the housing body.

However, before the final assembly can take place, the stator connection wires must be equipped with the designated copper lugs, i.e. process number 7 in Figure 27, which has not been previously described. According to Walter (2015), this is done by hot crimping, i.e. the copper in the wire and in the connector are joined into piece using a form of welding. Wires are stripped and placed compactly inside a lug or a sleeve. The connector is then pressed mechanically and simultaneously resistance heated using electricity. The metal parts anneal and join strongly owing to the high temperature.

Finally, in the last process, number 19 in Figure 27, after the complete assembly, the housing is spray painted and the machine set aside to cure at room temperature before delivery to the customer.

Data collection

The electric energy used for hot crimping was calculated based on data from Amada Miyachi (2015) and TES Vsetín (2015). A small amount of copper is commonly scrapped in the wire termination procedure as wires are cut to fit into the lug (Walter, 2015). The electric energy used was found to depend on the crimping time rather than the size of the lugs, and was assessed to be the same for both reference machines. For simplicity, the magnet wire loss and related additional process input of magnet wire compared to that specified by the design, were also established as fixed values per stator package, based on the geometry of the large reference machine. Results are shown in Table 65 and Table 66.

Process input	Amount per piece	Source	Linked flow
Magnet wire, to cover for loss	36 g	Walter (2015)	IF, see Section 5.4.3.
Electricity	170 Wh	Amada Miyachi (2015), TES Vsetín (2015)	Electricity, optional

Table 65: Process input for the wire termination of the phase conductors with copper lugs (process number 7 in Figure 27) before the end assembly of the complete electrical machine.

Solid waste	Amount per piece	Source	Linked flow
Copper scrap	36 g	Walter (2015)	Copper scrap for recycling

Table 66: Waste from the wire termination of the phase conductors with copper lugs (process number 7 in Figure 27) before the end assembly of the complete electrical machine.

Process input	Amount per piece	Source	Linked flow
Electricity	170 Wh	Huahong Technology (2015), Karlsson (2013), Walter (2016)	Electricity, optional

Table 67: Electricity input for the press fitting of the stator into the housing body and the bearings onto the shaft during end assembly of the complete electrical machine (process number 18 in Figure 27).

The mounting steps in the end assembly were assumed to be manual, except for the pressing of the stator package into the housing body and the press-fitting of the bearings onto the shaft. The electricity used for the stator package fitting was calculated based on the same type of hydraulic press as used for the rotor assembly (Huahong Technology, 2015), see Section 5.4.6, but with a doubled cycle time to account for the increased stroke length compared to the rotor pressing. The bearing press procedure was included in the form of a pneumatic press machine operation, and based on the overall assessment of the compressed air system (described in Section 5.4.9), in a similar unit operation approach as described for the cleaning in process step 16, see Section 5.4.7. The sum of the electric energy used for the pressing operations is presented in Table 67. For the testing step last in the end assembly, no electricity use has been accounted for here, but instead it was taken as a part of the technical building services, presented in Section 5.4.9, since it is conducted with computers and other general tools.

Data for the process input to and emissions from painting was gathered from supplier of the selected varnish (Von Roll, 2013, Larrenduche, 2015) and the solvent sub supplier (ExxonMobil, 2007, 2014). It was combined with the overall assessment of the compressed air system (Karlsson, 2013, Appleton, 2016, SWP, 2016, Walter, 2016), since the spray painting equipment was found to be pneumatically propelled. In addition,

the air flow rate for the spray painting was set to 200 liters per minute, based on the typical flow rate identified and used for spray painting in the unit operation comparison. The "air to paint ratio" was assumed to be 1:1000, taken from observations of standard spray gun properties (Meiji, 2015), which gave a paint flow rate of 200 ml per minute.

Furthermore, the varnish mass calculation presented in Section 4.3.4 was based on dried matter. The solid mass content of the varnish is 52% and the liquid density is 0.9 grams per liter (Von Roll, 2013). The remaining 48% of the mass consists of solvent which evaporates as VOCs during the curing (ExxonMobil, 2014). The compilation of the data is shown in Table 68 and Table 69.

Process input	Amount per 100 g	Source	Linked flow
Liquid varnish, solid share	100 g	Von Roll (2013)	E3, alkyd resin, long oil, w/o solvent
Liquid varnish, solvent share	92 g	Von Roll (2013)	E3, naphtha
Electricity	0.56 kWh	Karlsson (2013), Von Roll (2013), Meiji (2015), Appleton (2016), SWP (2016), Walter (2016)	Electricity, optional

Table 68: Process input for the painting procedure corresponding to 100 g dried varnish on the electrical machine housing (process number 19 in Figure 27).

Emissions to air	Amount per 100 g	Source	Linked elementary flow
VOC	92 g	Von Roll (2013), ExxonMobil (2014)	E3, NMVOC

Table 69: Emissions to air from the painting procedure corresponding to 100 g dried varnish on the electrical machine housing (process number 19 in Figure 27).

5.4.9 Technical building services

Additional to the specific manufacturing processes presented so far in Chapter 4, there are also several basic functions which are necessary in order to operate a motor factory, referred to as technical building services. Maintaining these services in operation requires energy, and may cause emissions, just like the processes presented in Figure 27. However, unlike the specific production processes, this environmental load does not have a direct physical link to each electrical machine, e.g. no amount of mass being removed or reshaped, and no surface area to be processed. Instead, the energy used relates to the total activity and size of the motor plant, and the burden carried by each electrical machine produced, must be decided by means of allocation.

Technical building services include heating, ventilation, and lighting, for example. Moreover, computers for administrative work, logic control of the machinery and for testing, are also necessary. Some machines require start up procedures and energy to hold them at standby. In cold climates, such as Sweden, heating may constitute a significant share of the energy consumption whereas in other countries, air-cooling systems may be more important. Anyhow, both external factors such as the local climate, and process specific conditions governed by the product design and coupled required machinery, determine the need for various technical building services (Bonvoisin et al., 2013). Often there is a substantial energy demand for these services, e.g. to start-up and maintain the equipment ready to operate (Gutowski et al., 2006). In fact, it is common that non-productive machine time, computer use and other technical building services constitute the major share of the total factory energy consumption (Bonvoisin et al., 2013).

The compressed air system typically also belongs to the technical building services. As mentioned in previous sections, it is used in machines based on pneumatic force, in spray and blow applications, and also for pneumatic control of machinery. In pneumatic control, actuators are used to control the movement or positioning of a workpiece or a sensor on a machine. Compressed air systems generally suffer both from large heat losses from the compressor and large leakage losses (U.S. Department of Energy, 2003). Proactive detection and mending of leaks can considerably reduce the energy used by the compressed air system.

Data collection

The assessment of electric energy used for technical building services was based on figures for the hourly electricity consumption during 2013 from ELMO Malmköpings Mekaniska Werkstad AB, provided by Walter (2016), and the energy audit conducted at the plant the same year (Karlsson, 2013). The combined assessment of these two sources indicated that more than half of the electricity used at ELMO during 2013 was coupled to building services. However, in order to sort out useful information for the user of LCI model about the different types of building services and motivate an allocation procedure, the activities at the plant had to be analyzed in more detail. As an important first step, the energy used for technical building services had to be separated from that used for specific production processes, out of the total.

The ELMO factory manufactures both electrical machines of different kinds and singular metal parts of steel or aluminum to be used as mechanical components, shaped and worked by a set of multi-operation machines, as mentioned in Section 5.4.7. The electrical machine manufacturing mobilizes most of the work at the plant, compared to the metal components fabrication. For the set of multi-operation machines about 60% of the throughput are electrical machine parts, according to Walter (2016). Similarly, roughly 70% of the compressed air use is coupled to the electrical machine manufacturing (Walter, 2016). The number of working days during 2013, with production at the plant, was counted to 250, and this figure was used to differentiate between productive and non-productive time for all calculations based on daily averages.

ELMO's main product is an induction motor for washing machines. In 2013 roughly 10000 such machine units were produced at the plant, accounting for 90% of all electrical machines produced in the factory (Walter, 2016). However, the actual capacity of the factory is larger, about 200 units per day, and a total of 50000 units yearly, according to the official customer information from ELMO (2016). It could likely even be increased further, with minor adoptions. In order to be in line with the methodological selection of modelling large scale production, as stated in Section 2.4, the maximum production capacity was used for calculations of technical building services per unit.

The energy audit by Karlsson (2013) showed that two of the most energy consuming individual manufacturing processes of the plant are used in the fabrication of this washing machine motor. These are the casting of aluminum in the rotors (see Section 3.3 about induction machines) and the batch bake procedure following the varnish dipping. Together these two processes account for 10% of the yearly electricity use of the plant. However, since neither of them are representative for the PMSM design selected for the LCI model, both were excluded from further assessment and discounted from the total electricity use. Finally, all heating at of the plant is conducted with electrical air to air heat pumps, so heating has been a part of the overall assessment of electricity use. On the plant level, the average heating over the year was found to demand more energy than any other support system, and therefore it also becomes the biggest load when calculated per unit.

In the previous description of the specific production procedures at the motor factory, in sections 5.4.2-5.4.8, standby energy consumption was considered for production processes using compressed air and when the multi-operation machines are used. This was done since non-active electricity consumption for these two types of processes was included and measured in the energy audit (Karlsson, 2013). It showed that the largest of the multi-operation machines on average require around half of its active operating power to be held in standby mode, yielding that over a complete year, a little less than a third of its total energy use goes to standby operation. The stand-by energy consumption of other machines at the factory, solely used to produce electrical machines, was not possible to separate from other daily use of electricity.

For the compressed air system, one main compressor runs 14 hours per workday with an average power consumption of 17 kW (Karlsson, 2013). The majority of the energy, 80% goes to upholding the system pressure during stand-by and to compensate for leakage, i.e. each compressed air driven operation carries a significant load of non-active energy consumption. However, since the compressed air-system is dimensioned for a higher production rate, the active operation was scaled up to 100% of active operation, i.e. without standby, to account for increased use at full plant capacity, and in line with high volume manufacturing as argued for in Section 2.4. This was accounted for in a "unit operations" analysis of the compressed air system, established based on type data from Appleton (2016), SWP (2016), previously brought up in the descriptions of some of the specific manufacturing processes. However, additional to the unit operations, the compressed air system was also found to be a part of the building services. Compressed air is used as open blow for all sorts of cleaning and in pneumatic control of most machinery (Walter, 2016). These two types of compressed air use has not been possible to link to any specific manufacturing processes. Instead, they were included as a part of the building services. Together they were estimated to represent a majority of the total electricity used by compressed air system, 50% out of the total for the cleaning and 5% for the pneumatic control, based on Eret et al. (2010).

Finally, a summary of the electricity use for technical building services valid for PMSM manufacturing was compiled based on the data discussed so far in this section, by combining the hourly electricity consumption for 2013 at ELMO Malmköpings Mekaniska Werkstad AB with the energy audit results, and dividing the result with the number units for the current maximum plant capacity. 70% of the total electricity coupled to technical building services was then allocated to the electrical machine manufacturing, and the remaining part to the metal components fabrication. This allocation was based on the split between the two product types in the use of compressed air, as it was the best available indicator for how activities and energy use couple to the two different product types. Another important assumption was that the overall time to produce one electrical machine, gate to gate at the factory, is roughly the same regardless of machine type, specific design and size. Hence, it was found reasonable that each electrical machine unit produced carries the same load as regards technical building services. The building services have been divided into four categories, as can be seen in Table 70.

Process input	**Amount per piece**	**Source**	**Linked flow**
Electricity for heating using electrical heat pumps, average over the year	3.6 kWh	Eret et al. (2010) Karlsson (2013) Walter (2016)	Electricity, optional
Electricity for basic use, i.e. functions which are never shut down such as hot water and ventilation	2.9 kWh		Electricity, optional
Electricity for general work[1], e.g. most computers, tools, lighting and machine stand-by[2]	1.7 kWh		Electricity, optional
Electricity for compressed air use, i.e. the share for general cleaning and pneumatic control[3]	0.7 kWh		Electricity, optional

Note 1: Electricity turned on during workdays, and turned off during nights and weekends.
Note 2: Standby machine operation, excluding multi-operation machines and functions using compressed air.
Note 3: Scaled up to 100% of active operation, i.e. no standby, to account for increased use at full plant capacity.

Table 70: Electricity input per piece (i.e. complete PMSM) for different types of technical building services.

References

ABB (2002). *Environmental Product Declaration: AC Low voltage cast iron motor, type M3BP 315*. Release/version May 2002. Vaasa, Finland: ABB Oy / BA Electrical Machines, LV Motors. (Document code: LV Motors/EPD M3BP315 GB 05-2002 3GZF500931-22).

AK Steel (2007). *304/304L Stainless steel data sheet*. USA: AK Steel Corporation. (Product data sheet).

AK Steel (2014). *Hot Dip Galvanized Steel*. USA: AK Steel Corporation. (Product data bulletin).

Althaus, H.-J., Hischier, R., Osses, M., Primas, A., Hellweg, S., Jungbluth, N. & Chudacoff, M. (2007). Life Cycle Inventories of Chemicals. 2007, Dübendorf, Switzerland: Swiss Centre for Life Cycle Inventories. Ecoinvent report No. 8. (Data v2.0).

Amada Miyachi (2015). *Hot Crimping*. Release/version January 2015. Puchheim, Germany: Amada Miyachi Europe Gmbh. (Technical specification for hot crimping/welding power supply. TDS RW M2-M4 Series RW 01-2015 EN).

AMG Vanadium (2015). *Silicon* [Online]. USA: AMG Vanadium Inc. Available: http://amg-v.com/siliconpage.html Accessed 21 May 2015. (Silicon metal products information page)

ANSYS (2011). *Study of a Permanent Magnet Motor with MAXWELL 3D:Example of the 2004 Prius IPM Motor*. Ansoft Maxwell Field Simulator: Topic – Motor Application Note 1.1, Maxwell 3D, version 11. Accessed 2015. ANSYS, Inc. (Tutorial example from Ansoft Maxwell).

ANSYS (2015). *ANSYS® Electromagnetic Suite, Maxwell 2015.1.0.* Release number 16.1.0. ANSYS, Inc. (Electrical machine design and evaluation software).

Appleton (2016). *Air Tool or Equipment CFM Requirement* [Online]. USA: Appleton Compressor Service & Supply, Inc. Available: http://webtest.appletoncompressor.com/wp-content/uploads/2011/04/Air-Tool-or-Equipment-CFM-Requirement.pdf Accessed 2016-02-08.

Arnell, S. (2012). *Personal communication with GREGER, K. October 31:th 2012*. Principal engineer, ABB Sustainability Reporting, ABB AB, Västerås, Sweden.

Barré, O. & Napame, B. (2016). Concentrated Windings in Compact Permanent Magnet Synchronous Generators: Managing Efficiency. *Machines*, 4(1)**,** pp. 2.

Barsoum, I. & Khan, F. (2012). Strength Optimization of Induction Hardened Splined Shaft – Material and Geometric Aspects. *International Journal of Mechanical, Aerospace, Industrial, Mechatronic and Manufacturing Engineering*, 6(3)**,** pp. 676-679.

Baumüller (2014). *Three-phase synchronous motors DSP1-045-100*. Germany: Baumüller Nürnberg GmbH. (Product catalogue).

Beckley, P. (2002). *Electrical Steels for Rotating Machines*. London, United Kingdom: The Institution of Energy and Engineering. ISBN: 978-0-85296-980-9.

Bonvoisin, J., Thiede, S., Brissaud, D. & Herrmann, C. (2013). An implemented framework to estimate manufacturing-related energy consumption in product design. *International Journal of Computer Integrated Manufacturing*, 26(9)**,** pp. 866-880.

Brenn, G., Steiner, H. & Baric, E. (2012). *WIRE NEWS 12: High Quality Wire Coating in MAG Magnet Wire Machines*. Austria: MAG Maschinen- und Apparatebau AG. (Technical information brochure).

Breyden (2015). *Product Data Sheet*. United States of America: Breyden Products, Inc. (Product datasheet for nylon cord for lacing, part number 112-1).

Brill, S. & Schibisch, D. M. (2015). *Induction hardening versus case hardening – a comparison*. Heat processing. Vulkan-Verlag.

Broomfield (2014a). *TM-25 Trickle impregnation machine*. Release/version 15 December. United States of America: Broomfield Laboratories. (Machine specification datasheet for electric machine impregnation equipment).

Broomfield (2014b). *TM-50 Trickle impregnation machine*. Release/version 15 December. United States of America: Broomfield Laboratories. (Machine specification datasheet for electric machine impregnation equipment).

Brown, D., Ma, B.-M. & Chen, Z. (2002). Developments in the processing and properties of NdFeb-type permanent magnets. *Journal of Magnetism and Magnetic Materials,* 248(3)**,** pp. 432-440.

Burress, T. (2013) Benchmarking State-of-the-Art Technologies Project ID: APE006. *2013 U.S. DOE Hydrogen and Fuel Cells Program and Vehicle Technologies Program Annual Merit Review and Peer Evaluation Meeting*, May 14 2013. Electrical and Electronics Systems Research Division, Oak Ridge National Laboratory, US Department of Energy. (PowerPoint conference presentation).

Burress, T. & Campbell, S. (2013) Benchmarking EV and HEV Power Electronics and Electric Machines. *Transportation Electrification Conference and Expo (ITEC), 2013 IEEE* 16-19 June 2013, Detroit, MI, USA. IEEE, pp. 1 - 6.

Burress, T. A., Campbell, S. L., Coomer, C. L., Ayers, C. W., Wereszczak, A. A., Cunningham, J. P., Marlino, L. D., Seiber, L. E. & Lin, H. T. (2011). *Evaluation of the 2010 Toyota Prius Hybrid Synergy Drive System*. Editor: OLSZEWSKI, M. March. USA: Electrical and Electronics Systems Research Division, Oak Ridge National Laboratory, US Department of Energy. ORNL/TM-2010/253.

Burress, T. A., Coomer, C. L., Campbell, S. L., Seiber, L. E., Marlino, L. D., Staunton, R. H. & Cunningham, J. P. (2008). *Evaluation of the 2007 Toyota Camry Hybrid Synergy Drive System*. Editor: OLSZEWSKI, M. April. USA: Electrical and Electronics Systems Research Division, Oak Ridge National Laboratory, US Department of Energy. ORNL/TM-2007/190.

Burress, T. A., Coomer, C. L., Campbell, S. L., Wereszczak, A. A., Cunningham, J. P., Marlino, L. D., Seiber, L. E. & Lin, H. T. (2009). *Evaluation of the 2008 Lexus LS 600H Hybrid Synergy Drive System*. Editor: OLSZEWSKI, M. Janaury. USA: Electrical and Electronics Systems Research Division, Oak Ridge National Laboratory, US Department of Energy. ORNL/TM-2008/185.

Campbell, J. (2011). *Complete Casting Handbook - Metal Casting Processes, Metallurgy, Techniques and Design*. Amsterdam, Netherlands: Elsevier B.V. ISBN: 978-1-85617-809-9.

Carbex (2015a). *Carbex Inside - Produktinformation: Isolerslang silikon-gummi klass C 180°C*. Sweden: Carbex AB. (Product datasheet from local supplier).

Carbex (2015b). *Carbex Inside - Produktinformation: Polyesterfilm MYLAR A*. Sweden: Carbex AB. (Product datasheet from local supplier).

Chan, C. C. (2007). The state of the art of electric, hybrid, and fuel cell vehicles. *Proceedings of the IEEE,* 95(4)**,** pp. 704-718.

Chang Chun Plastics (2012). *Material Safety Data Sheet - Phenolic Resin PF8090M65*. Taiwan: Chang Chun Plastics Co., Ltd. (MSDS for resin recommened to use on electric laminates).

Chen, S. L., Liu, W., Geng, D. Y., Zhao, X. G. & Zhang, Z. D. (2006). Decomposition of B4C and magnetic properties of Nd–Fe–(B,C) alloys synthesized by mechanical alloying. *Journal of Alloys and Compounds,* 415(1–2)**,** pp. 271-275.

Choe, Y.-Y., Oh, S.-Y., Ham, S.-H., Jang, I.-S., Cho, S.-Y., Lee, J. & Ko, K.-C. (2012). Comparison of Concentrated and Distributed Winding in an IPMSM for Vehicle Traction. *Energy Procedia,* 14**,** pp. 1368-1373.

Classen, M., Althaus, H.-J., Blaser, S., Scharnhorst, W., Tuchschmid, M., Jungbluth, N. & Emmenegger, M. F. (2009). Life Cycle Inventories of Metals. March 2009, Dübendorf, Switzerland: Swiss Centre for Life Cycle Inventories. Ecoinvent report No. 10. (Data v2.1).

Croat, J. J. (1992). *High energy product rare earth magnet alloys*. UNITED STATES PATENT AND TRADEMARK OFFICE. Assinged for General Motors Corporation, Detroit, Michigan. United States of America. Patent application: US 75,261. Patent number: US 5172751.

Czaputa, K. (2012). *WIRE NEWS 12: The Serious Idea Behind the Incredible Mozart Zero*. Austria: MAG Maschinen- und Apparatebau AG. (Technical information brochure).

Dalquist, S. & Gutowski, T. (2004). Life cycle analysis of conventional manufacturing techniques: Die casting. December 2004, Boston, USA: Environmentally Benign Manufacturing group, Laboratory for Manufacturing and Productivity, Massachusetts Institute of Technology. LMP-MIT-TGG-03-12-09-2004.

Dawsey, R. T., Stancu, C. C., Ostrom, E. R. & Doo, Y. (2009). *Permanent magnet machine rotor*. UNITED STATES PATENT AND TRADEMARK OFFICE. Assinged for GM Global Technology Operations Inc., Detroit, MI. United States of America. Patent application: US 11/668,910. Patent number: US 7,479,723 B2.

Del Duce, A., Gauch, M. & Althaus, H.-J. (2014). Electric passenger car transport and passenger car life cycle inventories in ecoinvent version 3. *The International Journal of Life Cycle Assessment*.

DIN (2006). *Splined connections with involute splines based on reference diameters — Part 1: Principles*. Germany: DIN Deutsches Institut für Normung e. V. (German splining standard DIN 5480-1)

Dorrell, D. G., Hsieh, M., Popescu, M., Evans, L., Staton, D. A. & Grout, V. (2011). A Review of the Design Issues and Techniques for Radial-Flux Brushless Surface and Internal Rare-Earth Permanent-Magnet Motors. *IEEE Transactions on Industrial Electronics*, 58(9)**,** pp. 3741-3757.

Dow (2005a). *Selection Guide for UCON Quenchants*. United States of America: The Dow Chemical Company. (Guide for the use of UCON™ quenchants during steel hardening. Form No. 118-01588-1005).

Dow (2005b). *UCON™ Quenchant RL*. United States of America: The Dow Chemical Company. (Technical data sheet UCON™ Quenchant RL. Form No. 118-01291-0205-rlr).

Dow (2014). *Product Safety Assessment - UCON™ Quenchants and Metalworking Lubricants*. United States of America: The Dow Chemical Company. (Product safety description for UCON™ quenchants. Form No. 233-000808-MM-0614X).

Dupont (2004). *Material Data Safety Sheet - MYLAR polyester film*. Release/version 27 April. USA: DuPont Teijin Films, U.S. Limited Partnership. (OEM MSDS for insulation foil).

Dupont (2005). *Crastin® PBT thermoplastic polyester resin - Crastin® 6130 NC010*. Release/version 22 April. USA: DuPont Company. (Product information datasheet).

Dutta, R., Chong, L. & Rahman, F. M. (2013). Analysis and experimental verification of losses in a concentrated wound interior permanent magnet machine. *Progress In Electromagnetics Research B*, 48**,** pp. 221-248.

ELMO (2016). *Om ELMO* [Online]. Sweden: Malmköpings Mekaniska Werkstad AB. Available: http://www.elmo.nu/about-elmo Accessed 2016-01-28.

Eret, P., Harris, C., Lasa, T. d., Meskell, C. & O'Donnell, G. (2010) Industrial Compressed Air Usage – Two Case Studies. *7th International Fluid Power Conference*, March 22nd to 24th 2010, Aachen, Germany.

Essex Brownwell (1998). *Motor Repair Supplies*. United States of America: Essex Group, Inc. (Product catalogue for electric motor parts and accessories).

ExxonMobil (2007). *Material safety data sheet: Aromatic 100 Fluid*. Release/version October 4th. United States of America: Exxon Mobil Corporation. (Product MSDS).

ExxonMobil (2014). *Product Safety Summary: Aromatic 100 Fluid; Solvesso™ 100 Fluid*. Release/version Janaury. United States of America: Exxon Mobil Corporation. (Product safety datasheet).

Fang, Z. Z. (ed.) (2010). *Sintering of advanced materials - Fundamentals and processes*. Cambridge, UK: Woodhead Publishing Limited. ISBN: 978-1-84569-562-0.

Franke, J., Hofmann, B., Tremel, J. & Meyer, A. (2015). Innovative Methods for Automated Assembly and Fixation of Permanent Magnets in Electrical Machines. *Procedia CIRP 26, 12th Global Conference on Sustainable Manufacturing*, 22– 24 September, 2014, Johor Bahru, Malaysia. pp. 724-728.

Franke, J., Tremel, J. & Kuhl, A. (2011) Innovative developments for automated magnet handling and bonding of rare earth magnets. *Assembly and Manufacturing (ISAM), 2011 IEEE International Symposium on*, 25-27 May 2011, Tampere, Finland. pp. 1-5.

Fuller (2013). *Fuller Metric Parts Ltd. - Quality Products and Services Since 1976*. Canada: Fuller Metric Parts Ltd. (Product catalogue).

Fyhr, P., Stahl, J. & Andersson, M. (2012) The scale of permanent magnet materials for automotive traction motors. *Electric Drives Production Conference (EDPC), 2012 2nd International*, 15-18 Oct. 2012 2012, Nuremberg, Germany. pp. 1-7.

Ghosh, A. (2000). *Secondary Steelmaking: Principles and Applications*. United States of America: CRC Press. ISBN: 978-0-8493-0264-0.

Gieras, J. F. (2010). *Permanent Magnet Motor Technology: Design and Applications*. 3:rd ed, Boca Raton, FL, USA: CRC Press, Taylor & Francis Group. ISBN: 978-1-4200-6440-7.

Grunditz, E. A. & Thiringer, T. (2016a). Characterizing BEV Powertrain Energy Consumption, Efficiency and Range during Official and Drive Cycles from Gothenburg/Sweden. *IEEE Transactions on Vehicular Technology*, 65(6)**,** pp. 3964-3980.

Grunditz, E. A. & Thiringer, T. (2016b). Performance Analysis of Current BEVs - Based on a Comprehensive Review of Specifications. *IEEE Transactions on Transportation Electrification*.

Gutfleisch, O., Willard, M. A., Brück, E., Chen, C. H., Sankar, S. G. & Liu, J. P. (2011). Magnetic Materials and Devices for the 21st Century: Stronger, Lighter, and More Energy Efficient. *Advanced Materials*, 23(7)**,** pp. 821-842.

Gutowski, T., Dahmus, J. & Thiriez, A. (2006) Electrical Energy Requirements for Manufacturing Processes. *13th CIRP International Conference of Life Cycle Engineering*, May 31:st - June 2:nd 2006, Lueven, Belgium.

Habermacher, F. (2011). *Modeling Material Inventories and Environmental Impacts of Electric Passenger Cars.* Master Thesis, Department of Environmental Sciences, ETH Zurich, Switzerland.

Haimbaugh, R. E. (2001). *Practical Induction Heat Treating*. Materials Park, Ohio, USA: ASM International. ISBN: 0-87170-743-8.

Hampton, N., Hartlein, R., Lennartsson, H., Orton, H. & Ramachandran, R. (2007) Long-life XLPE Insulated Power Cable. *JICABLE'07 - 7th International Conference on Power Insulated Cables*, June 24th-28th 2007, Versailles , France.

Hawkins, T., Gausen, O. & Strømman, A. (2012). Environmental impacts of hybrid and electric vehicles – a review. *The International Journal of Life Cycle Assessment*, 17(8)**,** pp. 997-1014.

Haynes, W. M. (2015). *CRC Handbook of Chemistry and Physics*. 96th ed, Boca Raton, FL, United States of America: CRC Press, Taylor and Francis Group, LLC ISBN: 978-1-4822-6097-7

Heinemann, T. (2016). *Energy and Resource Efficiency in Aluminium Die Casting*. Switzerland: Springer International Publishing. ISBN: 978-3-319-18814-0.

Hendershot, J. R. (2015). *Personal communication with NORDELÖF, A. December 26:th 2015*. President & CEO of Motorsolver LCC, SAE & ASME member, IEEE life fellow.

Hendershot, J. R. & Miller, T. J. E. (2010). *Design of Brushless Permanent-Magnet Machines*. 2:nd ed, USA: Motor Design Books LLC. ISBN: 9780984068708.

Henkel (2010). *Loctite® Threadlocker, Red 271™*. Release/version 22 May. United States: Henkel Corporation. (Product datasheet, ref. no. 120271).

Henkel (2015). *Safety Data Sheet - Loctite® Threadlocker, Red 271™*. Release/version 15 July. United States: Henkel Corporation. (MSDS for anaerobic sealant).

Hischier, R. (2007). Life Cycle Inventories of Packagings and Graphical Papers. – Part II, Plastics. 2007, Dübendorf, Switzerland: Swiss Centre for Life Cycle Inventories. Ecoinvent report No. 11. (Data v2.0).

Hitachi (2014). Special Issue "Hitachi Technology 2014". *Hitachi Review*, 63(3).

Hitachi Chemical (2015). *Insulating Varnishes* [Online]. Japan: Hitachi Chemical Co., Ltd. . Available: http://www.hitachi-chem.co.jp/english/products/eim/001.html Accessed 23 June 2015. (Electrical Insulating Materials)

Hitachi Metals (2014a). *NEOMAX® Series - Demagnitization Curve*. Japan: Hitachi Metals, Ltd. (Demagnitization datasheet for Neomax series).

Hitachi Metals (2014b). *Permanent Magnets*. Japan: Hitachi Metals, Ltd. (Product catalogue for Neomax series).

Hitachi Metals (2015a). *Magnet Wire - Selection and Use Directions for Magnet Wire*. CAT. no. 15-5 (D). Japan: Hitachi Metals, Ltd. (Product catalogue).

Hitachi Metals (2015b). *Neodymium-iron-boron magnets NEOMAX® - Properties* [Online]. Japan: Hitachi Metals, Ltd. Available: http://www.hitachi-metals.co.jp/e/products/auto/el/p03_21.html Accessed September 24 2015. (Product specifications under "Electric- and Electronics-Related Products (Magnets, Harnesses, and Sensors)")

Huahong Technology (2015). *Q43-1200A* [Online]. China: Jiangsu Huahong Technology Stock Co., Ltd. Available: http://www.asiabaler.com/Q43.php Accessed 2016-02-05.

Hultman, E., Salar, D. & Leijon, M. (2014). Robotized Surface Mounting of Permanent Magnets. *Machines,* 2(4)**,** pp. 219.

IPPC (2001). Integrated Pollution Prevention and Control (IPPC) - Best Available Techniques Reference Document on the Production of Iron and Steel. December 2001: EUROPEAN COMMISSION.

Johansson, J. (2015). *Personal communication with NORDELÖF, A. June 10:th, 11:th and 12:th 2015*. Technical specialist of electrical machine mechnical design , Aros Electronics AB and IRO AB, Van de Wiele Group, Ulricehamn, Sweden.

Johansson, J. (2015). *Personal communication with NORDELÖF, A. April 9:th 2015*. Technical Specialist Power Electronics, Volvo Group Trucks Technology, Volvo Group.

Junker, S. (2012). Highly flexible and efficient shaft manufacture for customized electric machines. *Electric Drives Production Conference (EDPC), 2012 2nd International*, 15-18 Oct. 2012. pp. 1-4.

Karlsson, P. (2013). *Mätning vid Malmköpings Mekaniska Werkstad AB*. 2013-09-10 - 2013-09-16. Industriell Laststyrning. (Measurement charts for energy and power consumption as part of an energy survey at Malmköpings Mekaniska Werkstad AB).

Kauppinen, J. (2014). *Redesigning the Coil End Insulation of Electrical Motor.* Thesis for the degree of Bachelor, Vasa University of Applied Sciences, Finland.

Kellenberger, D., Althaus, H.-J., Künniger, T., Lehmann, M., Jungbluth, N. & Thalmann, P. (2007). Life Cycle Inventories of Building Products. 2007: Swiss Centre for Life Cycle Inventories. Ecoinvent report No. 7. (Data v2.0).

Kisner, R., A. Melin, T. Burress, D. Fugate, D. Holcomb, J. Wilgen, J. Miller, D. Wilson, P. Silva, L. Whitlow, a. & Peretz, F. (2012). *Embedded Sensors and Controls to Improve Component Performance and Reliability Conceptual Design Report*. September. USA: Measurement Science and Systems Engineering Division, Oak Ridge National Laboratory, US Department of Energy. ORNL/TM-2012/433.

Kolehmainen, J. (2007) Machine with a Rotor Structure Supported only by Buried Magnets. *ISEF 2007 - XIII International Symposium on Electromagnetic Fields in Mechatronics, Electrical and Electronic Engineering*, September 13-15 2007, Prague, Czech Republic. pp. 6.

Kolehmainen, J. & Ikäheimo, J. (2008). Motors with buried magnets for medium-speed applications. *IEEE Transactions on Energy Conversion,* 23(1)**,** pp. 86-91.

Koltun, P. & Tharumarajah, A. (2014). Life Cycle Impact of Rare Earth Elements. *ISRN Metallurgy*, 2014**,** pp. 10.

Krishnan, R. (2010). *Permanent Magnet Synchronous and Brushless DC Motor Drives*. Boca Raton, FL, USA: CRC Press, Taylor & Francis Group. ISBN: 978-0-8247-5384-9.

Kwon, S.-O., Kim, S.-I., Zhang, P. & Hong, J.-P. (2006). Performance comparison of IPMSM with distributed and concentrated windings. *Conference Record of the 2006 IEEE Industry Applications Conference Forty-First IAS Annual Meeting*, 8-12 Oct. 2006. vol. 4**,** pp. 1984-1988.

Lagneborg, R. & Waltersson, E. (2004). *Guide för legeringsmetaller och spårelement i stål*. Rapport nr D811. 2 ed. Stockholm, Sweden: Jernkontoret. ISSN 0280-249X.

Lahd Geagea, M., Stille, P., Gauthier-Lafaye, F. & Millet, M. (2008). Tracing of Industrial Aerosol Sources in an Urban Environment Using Pb, Sr, and Nd Isotopes. *Environmental Science & Technology*, 42(3)**,** pp. 692-698.

Larrenduche, D. (2015). *Personal communication with NORDELÖF, A. September 5:th and 7:th, and October 28:th 2015*. Global Product Line Manager, Vice President Product Line Management, Von Roll Isola France SA.

Lenz, M. (2011) Individual E-Mobility System Solutions for Automotive and Off-Highway Applications. *Eco-mobility 2011, Austrian Association for Advanced Propulsion Systems 6:th International Conference*, November 15 2011, Vienna, Austria. Bosch Engineering GmbH. (PowerPoint conference presentation).

Leoni (2014). *LEONI Automotive Cables*. Germany: Leoni Kabel GmbH. (Product catalogue for automotive cables).

Lewis, C. J. & Boynton, R. S. (1999). *Acid Neutrilization with Lime for Environmental Control and Manufacturing Processes*. Bulletin No. 216. United States of America: The National Lime Association.

Li, W. F., Sepehri-Amin, H., Ohkubo, T., Hase, N. & Hono, K. (2011). Distribution of Dy in high-coercivity (Nd,Dy)–Fe–B sintered magnet. *Acta Materialia,* 59(8)**,** pp. 3061-3069.

Li, X. (2016). *Apparatus and Process for delivering molten steel to a continuous casting mold*. UNITED STATES PATENT AND TRADEMARK OFFICE. Assinged for Moltenideas LCC, Commerce Township, Michigan, USA. United States of America. Patent application: US 14/466,014. Patent number: US 20160052049 A1.

Lindenmo, M. (2012). *Personal communication with GREGER, K. December 4:th 2012*. Manager Development and Technical Customer Support, Cogent Power / Surahammars Bruk AB.

Lindenmo, M. (2015). *Personal communication with NORDELÖF, A. June 21:st and 25:th, and August 21:st 2015*. Manager Development and Technical Customer Support, Cogent Power / Surahammars Bruk AB.

Lindström, J. (1999). *Development of an Experimental Permanent-Magnet Motor Drive.* Licentiante Thesis at the School of Electrical and Computer Engineering, Chalmers University of Technology, Göteborg. (Technical Report No. 312L)

Liu, N. C. & Stadelmaier, H. H. (1986). High coercivity permanent magnet materials based on iron-rare-earth-carbon alloys. *Materials Letters,* 4(8–9)**,** pp. 377-380.

Lucas, J., Lucas, P., Le Mercier, T., Rollat, A. & Davenport, W. G. I. (2015). *Rare Earths - Science, Technology, Production and Use* Amsterdam, Netherlands: Elsevier B.V. ISBN: 978-0-444-62735-3.

Luvata (2015). *Oxygen-free Copper Cu-OF*. Finland: Luvata Pori Oy. (Copper product data sheet - magnet windings and electrical motors).

Låftman, L. (2012). *Personal communication with GREGER, K. November 11:th 2012*. Senior technical specialist of electric motors, Danaher Motion Stockholm AB / Kollmorgen Corporation; Danaher Corporation.

Löfgren, B., Tillman, A.-M. & Rinde, B. (2011). Manufacturing actor's LCA. *Journal of Cleaner Production,* 19(17–18)**,** pp. 2025-2033.

MAG (2016). *Mozart Zero H5 - Horizontal Single Line Copper Wire Enamelling Machine* [Online]. Austria: MAG Maschinen- und Apparatebau AG. Available: http://www.mag.at/products/horizontal-machines/Mozart-H5.php Accessed 2016-02-23. (Undated datasheet for magnet wire enamelling machine)

Magcraft (2007). *Permanent Magnet Selection and Design Handbook*. Vienna, VA, USA: National Imports LCC. (Design handbook from Magcraft - Advanced Magnetic Materials).

Magnusson, P. (2016). *Personal communication with NORDELÖF, A. February 9:th 2016*. Product Manager, Mechanics, at IRO AB, Van de Wiele Group, Ulricehamn, Sweden. *(Manager at electric machine production facility).*

McCallum, R. W. & Branagan, D. J. (1996). *Carbide/nitride grain refined rare earth-iron-boron permanent magnet and method of making*. UNITED STATES PATENT AND TRADEMARK OFFICE. Assinged for Iowa State University Research Foundation, Inc., Ames, Iowa. United States of America. Patent application: US 232,837. Patent number: US 5486240.

Meiji (2015). *Spray Gun Painting Equipment*. Japan: Meiji Air Compressor MFG CO., LTD. (Product catalogue for air spray painting equipment. Catalog number 151002KS.).

Miller, J. M. (2013a) Electric Motor R&D Project ID: APE051. *2013 U.S. DOE Hydrogen and Fuel Cells Program and Vehicle Technologies Program Annual Merit Review and Peer Evaluation Meeting*, May 15 2013a. Electrical and Electronics Systems Research Division, Oak Ridge National Laboratory, US Department of Energy. (PowerPoint conference presentation).

Miller, J. M. (2013b). Oak Ridge National Laboratory Annual Progress Report for the Power Electronics and Electric Motors Program. *Annual Progress Report - Advanced Power Electronics and Electric Motors*. November 2013b, USA: US DEPARTMENT OF ENERGY: Electrical and Electronics Systems Research Division, Oak Ridge National Laboratory. ORNL/TM-2013/498.

Miller, R. (2009). *Ten Technologies to Watch in 2009*. Industrial Heating. January 8. Troy, Michigan, USA: BNP Media Manufacturing Group, BMP Media.

Moing, A., Vardelle, A., Legoux, J. G. & Themelis, N. J. (2009) LCA Comparison of Electroplating and Other Thermal Spray

Processes. *Thermal Spray 2009: Expanding Thermal Spray Performance to New Markets and Applications (ASM International),* 2009, Las Vegas, NV, USA. ASM International.

Momentive (2016). *SilGrip* PSA5080 Technical Data Sheet*. Release/version 29 January. United States of America: Momentive Performance Materials Inc. (Technical data sheet for silicone pressure sensitive adhesive, HCD-10838).

Muller, S., Lesage, P., Ciroth, A., Mutel, C., Weidema, B. P. & Samson, R. (2014). The application of the pedigree approach to the distributions foreseen in ecoinvent v3. *The International Journal of Life Cycle Assessment*, [online]**,** pp. 1-11.

Nagasaki, Y. & Shimao, M. (2015). *Production method for rare earth permanent magnet*. UNITED STATES PATENT AND TRADEMARK OFFICE. Assinged for Shin-Etsu Chemical Co, Ltd. United States of America. Patent application: US 14/424,647. Patent number: US 20150211138 A1.

Nakada, T., Ishikawa, S. & Oki, S. (2014). *Development of an Electric Motor for a Newly Developed Electric Vehicle*. SAE Technical Paper 2014-01-1879. SAE International.

Namiki, S. & Sakamoto, K. (2005). *Method of molding resin to protect a resolver winding*. UNITED STATES PATENT AND TRADEMARK OFFICE. United States of America. Patent application: 10/826,135.

NETL (2014a) NETL Life Cycle Inventory Data – Unit Process: Metallothermic Reduction of Rare Earth Oxides [Online]. Last updated: June 10 2014. Version 01. United Stated of America: U.S. DEPARTMENT OF ENERGY, NATIONAL ENERGY TECHNOLOGY LABORATORY. Available: www.netl.doe.gov/LCA. Accessed Ocotber 29 2015. (Gate-to-gate process - metallothermic reduction of a rare earth oxide through calcium chloride and sodium.)

NETL (2014b) NETL Life Cycle Inventory Data – Unit Process: NdFeB Permanent Magnet Manufacturing [Online]. Last updated: July 3 2014. Version 01. United Stated of America: U.S. DEPARTMENT OF ENERGY, NATIONAL ENERGY TECHNOLOGY LABORATORY. Available: www.netl.doe.gov/LCA. Accessed October 29 2015. (Gate-to-gate manufacturing process for 1kg plated NdFeB permanent magnet)

NETL (2014c) NETL Life Cycle Inventory Data – Unit Process: Rare Earth Oxide Electrolysis [Online]. Last updated: June 5 2014. Version 01. United Stated of America: U.S. DEPARTMENT OF ENERGY, NATIONAL ENERGY TECHNOLOGY LABORATORY. Available: www.netl.doe.gov/LCA.

Accessed October 29 2015. (Gate-to-gate process - electrolysis of a rare earth oxide using a fluoride-based process.)

NETL (2015). *NETL Unit Process Library* [Online]. United States of America: U.S. Department of Energy, National Energy Technology Laboratory. Available: http://www.netl.doe.gov/research/energy-analysis/life-cycle-analysis/unit-process-library Accessed October 29 2015.

Ningbo Haishu Nide (2014). *Varnish machine catalogue*. China: Ningbo Haishu Nide International Co., Ltd. (Product catalogue for electric machine impregnation equipment).

Ningbo Nide (2014). *Induction machine catalogue*. China: Ningbo Nide Mechanical Equipment Co., Ltd. (Product catalogue for electric machine manufacturing equipment).

Nordelöf, A. (2016) Scalable IPMSM LCI Model.xlsm [Online]. Version 1.0. Gothenburg, Sweden: ENVIRONMENTAL SYSTEMS ANALYSIS; CHALMERS UNIVERSITY OF TECHNOLOGY. Distributed by The Swedish Life Cycle Center. Available: http://cpmdatabase.cpm.chalmers.se/Scripts/sheet.asp?ActId=JT-2016-06-21-39. (Gate to gate life cycle inventory in Microsoft Excel Macro-Enabled Worksheet)

Nordelöf, A. (2017) Scalable IPMSM LCI Model v1.01.xlsm [Online]. Version 1.01. Gothenburg, Sweden: ENVIRONMENTAL SYSTEMS ANALYSIS; CHALMERS UNIVERSITY OF TECHNOLOGY. Distributed by The Swedish Life Cycle Center. Available: http://cpmdatabase.cpm.chalmers.se/Scripts/sheet.asp?ActId=JT-2016-06-21-39. (Gate to gate life cycle inventory in Microsoft Excel Macro-Enabled Worksheet)

Nordelöf, A., Messagie, M., Tillman, A.-M., Ljunggren Söderman, M. & Van Mierlo, J. (2014). Environmental impacts of hybrid, plug-in hybrid, and battery electric vehicles—what can we learn from life cycle assessment? *The International Journal of Life Cycle Assessment*, 19(11)**,** pp. 1866-1890.

NSi (2010). *NSi Electrical Catalog 2010*. United States of America: NSi Industries, LLC. (Product catalogue for electrical connector parts).

NSK (2013). *Roller Bearings*. CAT. no. E1102m. Tokyo, Japan: NSK Ltd. (Product catalogue).

Nuss, P. & Eckelman, M. J. (2014). Life Cycle Assessment of Metals: A Scientific Synthesis. *PLOS ONE*, 9(7)**,** pp. 12.

Oeters, F. & Ottrow, M. (2012). Production of pure and high purity iron. *Ullmann's Encyclopedia of Industrial Chemistry*, Electronic Release. Chapter 5. Volume 20. Weinheim: Wiley-VCH Verlag GmbH & Co. Online ISBN 978-3-5273-0673-2.

Ozpineci, B. (2011). Oak Ridge National Laboratory Annual Progress Report for the Power Electronics and Electric Machinery Program. *Annual Progress Report - Power Electronics and Electric Machines*. October 2011, USA: US DEPARTMENT OF ENERGY: Energy and Transportation Science Division, Oak Ridge National Laboratory. ORNL/TM-2011/263.

Ozpineci, B. (2014). Oak Ridge National Laboratory Annual Progress Report for the Power Electronics and Electric Motors Program. *Annual Progress Report - Advanced Power Electronics and Electric Motors*. November 2014, USA: US DEPARTMENT OF ENERGY: Electrical and Electronics Systems Research Division, Oak Ridge National Laboratory. ORNL/SPR-2014/532.

Polynt Composites (2015). *Polymac 220-1935*. Release/version April. USA: Polynt Composites USA, Inc. (Technical specification for thermosetting polyester resin intended for coil coating).

Poteet, D., Totten, G. E. & Canale, L. C. F. (2006). Basic principles of quench system design for induction hardening. *In:* HERRING, D., ed. *Heat Treating : Proceedings of the 23rd Heat Treating Society Conference*, September 25-28, 2005, David L. Lawrence Convention Center, Pittsburgh, Pennsylvania, USA. Published: Materials Park, OH, USA: ASM International.

Pyrhönen, J., Jokinen, T. & Hrabovcova, V. (2008). *Design of Rotating Electrical Machines*. United Kingdom: John Wiley & Sons, Ltd. ISBN: 978-0-470-69516-6.

Richnow, J., Stenzel, P., Renner, A., Gerling, D. & Endisch, C. (2014). Influence of different impregnation methods and resins on thermal behavior and lifetime of electrical stators. *4:th International Electric Drives Production Conference (EDPC), 2014* Sept. 30 - Oct. 1 2014. pp. 1-7.

Roberts, M. J. (2003). *Modified life cycle inventory of aluminium die casting.* Thesis for the degree of Master of Engineering, Deakin University, Victoria, Australia.

Rudnev, V., Fett, G. A., Griebel, A. & Tartaglia, J. (2014). Principles of Induction Hardening and Inspection. *In:* RUDNEV, V. & TOTTEN, G. E. (eds.) *ASM Handbook, Induction Heating and Heat Treatment.* Vol. 4C. ASM International. ISBN: 978-1-62708-012-5.

Sagawa, M. (2013). *Method for producing sintered NdFeB magnet*. UNITED STATES PATENT AND TRADEMARK OFFICE. Assinged for Intermetallics Co., Ltd., Kyoto. United States of America. Patent application: US 12/441,124. Patent number: US 8420160 B2.

Sagawa, M. (2014). *Method for making NdFeB sintered magnet*. UNITED STATES PATENT AND TRADEMARK OFFICE. Assinged for Intermetallics Co., Ltd., Kyoto. United States of America. Patent application: US 12/595,872. Patent number: US 8801870 B2.

Sato, Y., Ishikawa, S., Okubo, T., Abe, M. & Tamai, K. (2011). *Development of High Response Motor and Inverter System for the Nissan LEAF Electric Vehicle*. SAE Technical Paper 2011-01-0350. SAE International.

Saveway Isolierstoffe (2008). *Safirex Material Safety Data Sheet*. Germany: Saveway Isolierstoffe GmbH. (MSDS for mica paper).

Saveway Isolierstoffe (2015). *Safirex Technical Data Sheet*. Germany: Saveway Isolierstoffe GmbH. (Technical data sheet for mica paper).

Schlesinger, M. & Paunovic, M. (eds.) (2010). *Modern Electroplating.* 5th ed, Hoboken, NJ, USA: John Wiley & Sons, Ltd. ISBN: 978-0-470-16778-6.

Schwartz, J. (2014). *Electric motor installation for improved vehicle noise characteristics.* Thesis for the degree of Master of Science, Lund University, Lund, Sweden.

Sharma, R. A. (1986). *Metallothermic reduction of rare earth oxides*. UNITED STATES PATENT AND TRADEMARK OFFICE. Assinged for General Motors Corporation. United States of America. Patent application: US 627,737. Patent number: US 4,578,242.

Shimizu, H., Okubo, T., Hirano, I., Ishikawa, S. & Abe, M. (2013). *Development of an Integrated Electrified Powertrain for a Newly Developed Electric Vehicle*. SAE Technical Paper 2013-01-1759. SAE International.

Sprecher, B., Xiao, Y., Walton, A., Speight, J., Harris, R., Kleijn, R., Visser, G. & Kramer, G. J. (2014a). Life Cycle Inventory of the Production of Rare Earths and the Subsequent Production of NdFeB Rare Earth Permanent Magnets. *Environmental Science & Technology,* 48(7)**,** pp. 3951-3958.

Sprecher, B., Xiao, Y., Walton, A., Speight, J., Harris, R., Kleijn, R., Visser, G. & Kramer, G. J. (2014b). *Life cycle inventory of the production of rare earths and the subsequent production of NdFeB rare earth permanent magnets - Supporting Information*. The Netherlands: Institute of Environmental Sciences (CML), Leiden University. (Supporting Information for Environmental Science & Technology).

Statoil (2015a). *Produktdatablad Coolway HD 25*. Release/version 14 September. Sweden: Statoil Fuel and Lubricants Sweden AB. (Cutting fluid technical specification).

Statoil (2015b). *Säkerhetsdatablad: COOLWAY HD 25*. Release/version 3 September. Sweden: Statoil Fuel & Retail Lubricants Sweden AB. (Cutting fluid MSDS).

Steiner, R. & Frischknecht, R. (2007). Metals Processing and Compresses Air Supply. 2007, Uster, Switzerland: Swiss Centre for Life Cycle Inventories. Ecoinvent report No. 23. (Data v2.0).

Stone, G. C., Culbert, I., Boulter, E. A. & Dhirani, H. (2014). *Electrical Insulation for Rotating Machines: Design, Evaluation, Aging, Testing, and Repair*. Second ed: John Wiley & Sons, Inc. ISBN: 978-1-118-05706-3.

Suppan, G., Ruehrig, M., Kanitz, A. & Gores, H. J. (2015). Electroplating Dysprosium from IL-Based Solutions: A Promising Electrochemical Step to Produce Stronger High Performance Nd(Dy)-Fe-B Sintered Magnets. *Journal of The Electrochemical Society,* 162(8)**,** pp. D382-D388

Surahammars Bruk (2014a). *Hi-Lite - Electrical steel for next generation designs*. COGENT POWER INC.: Tata Steel Europe, Tata Group. (Product catalogue).

Surahammars Bruk (2014b). *Non oriented electrical steel*. COGENT POWER INC.: Tata Steel Europe, Tata Group. (Product catalogue).

Surahammars Bruk (2015a). *Hi-Lite - NO30*. Release/version April. COGENT POWER INC.: Tata Steel Europe, Tata Group. (Datasheet).

Surahammars Bruk (2015b). *SURALAC® 9000*. COGENT POWER INC.: Tata Steel Europe, Tata Group. (Datasheet).

SWP (2016). *Air Tool Consumption Guide* [Online]. UK: Specialised Welding Products Ltd. Available: http://www.specialisedwelding.co.uk/manuals/Air_Compressor_Manuals/Air%20Tool%20Consumption%20Guide.pdf Accessed 2016-02-08.

Tamagawa (2014). *VR Type Resolver Singlsyn - Super-thin Angle Sensor (Absolute Type)*. Japan: Tamagawa Seiki CO., Ltd. (Product catalogue T12-1570N13).

TES Vsetín (2015). *Hot Crimping*. Release/version 2015-10-13. Czech Republic: TES Vsetín s.r.o. (Technical catalogue for hot crimping system).

Tessarolo, A., Mezzarobba, M. & Menis, R. (2014) A New Rotor Design for Flux Weakening Capability Improvement in Spoke-Type Interior Permanent Magnet Synchronous Machines. *Ninth International Conference on Ecological Vehicles and Renewable Energies (EVER)*, 25-27 March 2014, Monte-Carlo. pp. 1-9.

The National Lime Association (2015). *Iron and Steel* [Online]. USA: Creativo Inc. Available: http://www.hitachi-chem.co.jp/english/products/eim/001.html Accessed 29 July 2015. (Lime use in steel product treatment)

Tong, W. (2014). *Mechanical Design of Electric Motors*. Boca Raton, FL, USA: CRC Press, Taylor & Francis Group. ISBN: 978-1-4200-9144-1.

Towne, A. N. & Bombicino, T. A. (1975). *Process for manufacturing mica sheet composites*. UNITED STATES PATENT AND TRADEMARK OFFICE. Assinged for New England Mica Company, Needham Heights, Massachusetts. United States of America. Patent application: US 299,880. Patent number: US 3880972.

Tremel, J., Hofmann, B. & Risch, F. (2013). Handling and Fixation of Permanent Magnets. *Advanced Materials Research*, 769**,** pp. 3-10.

U.S. Department of Energy (2003). *Improving Compressed Air System Performance: A Sourcebook for Industry*. Washington, D.C., United States of America: U.S. Department of Energy, Energy Efficiency and Renewable Energy. (Industrial energy source book, DOE/GO-102003-1822).

U.S. Geological Survey (2014). *Mineral Commodoties Summaries 2014*. February. USA: U.S. Department of the Interior & U.S. Geological Survey. 978–1–4113–3765–7.

US EPA (2012). Rare Earth Elements: A Review of Production, Processing, Recycling, and Associated Environmental Issues. December 2012, Cincinnati, OH: The U.S. Environmental Protection Agency (EPA), Office of Research and Development. EPA 600/R-12/572.

Vaimann, T., Kallaste, A., Kilk, A. & Belahcen, A. (2013). Magnetic properties of reduced Dy NdFeB permanent magnets and their usage in electrical machines. *AFRICON, 2013*, 9-12 Sept. . pp. 1-5.

Walraven (2011). *Data Sheet Surface Treatment*. Release/version March. United Kingdom: Walraven Better Installation Systems, Walraven Ltd.

Walter, M. (2015). *Personal communication with NORDELÖF, A. August 27:th, October 10:th and November 4:th 2015*. CEO and owner, ELMO, Malmköpings Mekaniska Werkstad AB, Flen, Sweden.

Walter, M. (2016). *Personal communication with NORDELÖF, A. January 29:th, and February 2:nd and 8:th 2016*. CEO and owner, ELMO, Malmköpings Mekaniska Werkstad AB, Flen, Sweden.

Weidema, B. P., Bauer, C., Hischier, R., Mutel, C., Nemecek, T., Reinhard, J., Vadenbo, C. O. & Wernet, G. (2013). *The ecoinvent database: Overview and methodology, Data quality guideline for the ecoinvent database version 3* [Online]. Switzerland: The Centre for Life Cycle Inventories. Available: www.ecoinvent.org 2014-2017.

Wilhelmsen (2016). *Argon E-50 filling*. Norway: Wilhelmsen Maritime Services AS. (Technical data sheet for a 50 L 200 bar argon bottle, product number 905174).

Willard, S. (2015). *Personal communication with NORDELÖF, A. December 18:th 2015*. Sales Manager at Broomfield Laboratories.

Von Roll (2007). *Low voltage materials and systems*. USA: Von Roll USA, Inc. (Product catalogue).

Von Roll (2012). *Winding Wires and Litz Wires*. Switzerland: Von Roll Holding AG. (Product catalogue).

Von Roll (2013). *Varnish - Damicoat® 2405-2 Natural*. Release/version 21 March. France: Von Roll France SA. (Product datasheet).

Von Roll (2015). *Resin - Damisol® 3500 HTC*. Release/version 7 September. France: Von Roll France SA. (Product datasheet).

Worrell, E., Blinde, P., Neelis, M., Blomen, E. & Masanet, E. (2010). Energy Efficiency Improvement and Cost Saving Opportunities for the U.S. Iron and Steel Industry. *An ENERGY STAR® Guide for Energy and Plant Managers*. October 2010, Berkeley, California, USA: Ernest Orlando Lawrence Berkeley National Laboratory, University of California. LBNL-4779E.

Xue, A. (2015). *Personal communication with NORDELÖF, A. December 17:th 2015*. Marketing & Sales Manager at Ningbo Nide Mechanical Equipment Co., Ltd.

Yan, G., McGuiness, P. J., Farr, J. P. G. & Harris, I. R. (2010). Optimisation of the processing of Nd–Fe–B with dysprosium addition. *Journal of Alloys and Compounds,* 491(1–2)**,** pp. L20-L24.

Zakotnik, M. & Tudor, C. O. (2015). Commercial-scale recycling of NdFeB-type magnets with grain boundary modification yields products with ‘designer properties’ that exceed those of starting materials. *Waste Management,* 44**,** pp. 48-54.

Överstam, U. (2013). *Personal communication with GREGER K. AND NORDELÖF A. February 20:th and March 7:th 2013*. LCA Scientist, ABB AB Corporate Research, ABB AB, Västerås, Sweden.

Appendix A: Qualitative uncertainty assessment

A qualitative data uncertainty assessment was conducted for the individual flows on the unit process level of the model, based on the Ecoinvent pedigree matrix approach as presented in the overview and methodology report for Ecoinvent version 3 (Weidema et al., 2013). Thus, uncertainty estimations are given for individual data points of each unit process and presented in the table on the following pages. The data points refer to the design and production data presented in the tables of chapters 4 and 5 of this report, but conforming to the format used in model file where all flows are included and correctly linked. Unlike the model file, the tables of Chapter 5 (mainly section 5.4 describing the motor factory) do not fully report all input flows specified by the design data of Chapter 4 or internal flows between processes. The model file also presents the resulting geometric standard deviations, for the unit process data points, but not for aggregated results.

Lognormal uncertainty distributions were assumed for all flows in line with the "simplified standard procedure" (Weidema et al., 2013). A lognormal distribution is defined by two parameters: the geometric mean (μ_g) and the geometric standard deviation (GSD). The geometric mean equals the deterministic value of each flow (i.e. the determined amount), whereas the GSD captures the information on the uncertainty (Muller et al., 2014). Basic uncertainty factors (marked with note A in the column heading, see table below) were taken from Table 10.3 of Weidema et al. (2013) (except in two cases, the mass of the finalized housing and shaft, see below) and additional quality uncertainty factors (marked with B in the column heading) were generated by evaluating all data according to the pedigree matrix (Table 10.4) and extract corresponding tabulated factors (Table 10.5). All factors were then summarized to form an estimated log-transformed variance σ^2 of each underlying normal distribution (to the lognormal distributions), in accordance Weidema et al. (2013). The geometric standard deviation of each lognormal distribution was calculated using the following definition:

$$\mathrm{GSD} = e^{\sigma} = e^{\sqrt{\sigma^2}}$$

As indicated in Figure 3 of this report, some material flows goes through activities within the extended system boundaries and further into the regular system boundaries as parts. Such flows passing through the extended system have not been assessed for uncertainty to avoid double counting when these flows enter the regular system. Instead, they have been assessed at the point in the system where they were measured or estimated. However, the data for silicon steel alloy composition is an exception since it stipulates an aggregation of three flows into one before any further processing is executed in the extended system. Hence, this alloying process has been treated as taking place when these flows cross the extended system boundary, during steel making (based on the Ecoinvent dataset for unalloyed steel).

Furthermore, flows specified by the ANSYS Maxwell calculations have been assessed with zero variance, i.e. a GSD of 1. The reason is that this design data is electromagnetically correlated and it constitutes the starting point for all model calculations by specifying the magnet, copper and electrical steel masses. Additionally, there are also internal flows marked as "unaltered subpart input". Similar to the flows passing through the extended system these flows have not been for assessed for uncertainty to avoid multiple assessment of the same data. The precondition is that the flow represents a subpart which remains computationally unaltered within a unit process, although merged with other flows into a more complete part. For example, once the stator core has been stacked and welded it remains unaltered despite that it continues throughout several process steps to become a part of the final motor.

Two exceptions were made from the use of tabulated default values for the basic uncertainty factor, for the design data of the housing ("Housing, ready for assembly") and the shaft. In both cases the model relies on curve fitting to scattered data points, and instead of using the default factors, the actual variance was calculated for the log-transformed ratios between each original data point observed in literature and the models' estimated curve (expressed in kg of total mass per kW of maximum power for the housing and mm of cross section diameter per Nm of maximum torque for the shaft). This real variance of log-transformed data is italicized in the column for basic uncertainty factors.

In order to account for error propagation throughout cumulative results, inventory data for the desired power and torque requirements has to be implemented on the unit process level and calculated in a Monte Carlo simulation tool, by the user. This was not possible to include in the model file as the size of many flows change when the motor size is scaled depending on the input parameters.

Overall, this qualitative assessment of data uncertainty was added to the LCI model to assist users who wish to include uncertainty evaluation based on the Ecoinvent pedigree matrix approach, as a follow-up to the recommendations for how to link all data to Ecoinvent version 3. However, it was never a main goal to build a full pedigree matrix based uncertainty assessment into the aggregated inventory list of the model file.

Internal reference			***Uncertainty assessment***							
Unit process in model file	**Flow name**	**Report table no.**	**Basic factor[A]**	**Reliability[B]**	**Completeness[B]**	**Temporal correlation[B]**	**Geographical correlation[B]**	**Further technical correlation[B]**	**Log-transformed total variance – sum of all factors (σ^2)**	**Geometric standard deviation (GSD)**
Production of 1 kg neodymium metal through fused-salt electrolysis.	Neodymium oxide	21	0.0006	1	3	1	2	2	0.001825	1.0436
	Electricity	21	0.0006	1	3	1	2	2	0.001825	1.0436
	Lithium fluoride	21	0.0006	1	3	1	2	2	0.001825	1.0436
	Lime	21	0.0006	1	3	1	2	2	0.001825	1.0436
	Graphite anodes	21	0.0006	1	3	1	2	2	0.001825	1.0436
	Carbon dioxide	22	0.0006	1	3	1	2	2	0.001825	1.0436
	Hydrogen fluoride	22	0.0006	1	3	1	2	2	0.001825	1.0436
	Dust (Nd_2O_3)	22	0.12	1	3	1	2	2	0.121225	1.4165
	Sludge, dry content	22	0.0006	1	3	1	2	2	0.001825	1.0436
Production of 1 kg electrolytic iron	Unalloyed steel	23	0.0006	2	3	2	1	2	0.0026	1.0523
	Electricity	23	0.0006	2	3	2	1	2	0.0026	1.0523
	Sludge, dry content	24	0.0006	2	3	2	1	2	0.0026	1.0523
Production of 1 kg of Nd(Dy)FeB nickel coated magnet	Electrolytic iron	25	0.0006	2	1	1	1	2	0.0018	1.0433
	Neodymium	25	0.0006	2	1	1	1	2	0.0018	1.0433
	Boron carbide	25	0.0006	2	5	1	1	2	0.0098	1.1041
	Nickel	25	0.0006	2	1	3	1	2	0.0038	1.0636
	Dysprosium oxide	25	0.0006	2	2	1	1	2	0.0019	1.0446
	Electricity, for heating	25	0.0006	3	2	5	1	2	0.0433	1.2313
	Electricity, other	25	0.0006	3	2	5	1	2	0.0433	1.2313
	Hydrogen	25	0.0006	2	1	5	1	2	0.0418	1.2269
	Caustic soda	25	0.0006	2	1	3	2	2	0.003825	1.0638
	Sulfuric acid	25	0.0006	2	1	3	2	2	0.003825	1.0638
	Water	25	0.0006	2	1	3	2	2	0.003825	1.0638
	Nickel (to air)	26	0.65	2	1	3	2	2	0.653225	2.2439
	Nickel sulfamate (to water)	26	0.65	2	1	3	2	2	0.653225	2.2439
	Neodymium-iron-boron scrap	26	0.0006	2	1	5	1	2	0.0418	1.2269
	Sludge, dry content	26	0.0006	2	1	3	1	2	0.0038	1.0636
1 ton of silicon steel alloy	Unalloyed steel	27	0.0006	1	4	1	1	1	0.0026	1.0523
	Ferrosilicon	27	0.0006	1	4	1	1	1	0.0026	1.0523
	Aluminum	27	0.0006	1	4	1	1	1	0.0026	1.0523

Continued from previous page

Internal reference			***Uncertainty assessment***							
Unit process in model file	**Flow name**	**Report table no.**	**Basic factor[A]**	**Reliability[B]**	**Completeness[B]**	**Temporal correlation[B]**	**Geographical correlation[B]**	**Further technical correlation[B]**	**Log-transformed total variance – sum of all factors (σ^2)**	**Geometric standard deviation (GSD)**
Production of 1 ton electrical steel sheets	Silicon steel, hot rolled	28	0.0006	1	4	2	1	1	0.0028	1.0543
	Phenolic resin	28	0.0006	1	4	1	1	1	0.0026	1.0523
	Electricity	28	0.0006	1	4	2	1	1	0.0028	1.0543
	Propane/LPG	28	0.0006	1	4	1	1	1	0.0026	1.0523
	Sulfuric acid	28	0.0006	1	4	1	1	1	0.0026	1.0523
	Rolling/lubricating oil	28	0.0006	1	4	1	1	1	0.0026	1.0523
	Quicklime powder	28	0.0006	1	4	1	1	1	0.0026	1.0523
	Carbon dioxide	29	0.0006	1	4	1	1	1	0.0026	1.0523
	Nitrogen oxides	29	0.04	2	4	1	1	1	0.0426	1.2292
	Sulfur oxides	29	0.0006	2	4	1	1	1	0.0032	1.0582
	Steel scrap	29	0.0006	1	4	2	1	1	0.0028	1.0543
	Sludge, dry content	29	0.0006	3	4	1	1	1	0.0046	1.0702
Die casting of 1 kg of aluminum	Aluminum	30	0.0006	1	1	1	2	1	0.000625	1.0253
	Heat, from natural gas	30	0.0006	1	1	1	2	1	0.000625	1.0253
	Electricity	30	0.0006	1	1	1	2	1	0.000625	1.0253
	Lubricating oil	30	0.0006	3	1	4	3	1	0.0107	1.1090
	Aluminum (to air)	31	0.65	1	1	1	2	1	0.650025	2.2395
	VOC	31	0.04	1	1	4	2	1	0.048025	1.2450
	Waste aluminum	31	0.0006	1	1	1	2	1	0.000625	1.0253
Enameling 1 kg of magnet wire	Copper wire, uncoated	32	0.0006	2	4	1	1	1	0.0032	1.0582
	Liquid enamel, polyester share	32	0.0006	2	4	1	1	1	0.0032	1.0582
	Liquid enamel, xylene solvent share	32	0.0006	2	4	1	1	1	0.0032	1.0582
	Electricity	32	0.0006	2	4	1	1	1	0.0032	1.0582
	Xylene (to air)	33	0.12	2	4	1	1	1	0.1226	1.4193
Assembly of resolver including punching of 1 kg resolver core laminations	PBT resolver case	-	0.0006	2	2	1	1	1	0.0013	1.0367
	Magnet wire in resolver	-	0.0006	2	2	1	1	1	0.0013	1.0367
	Electrical steel sheet, for resolver	34	0.0006	2	2	1	1	1	0.0013	1.0367
	Steel scrap	35	0.0006	4	2	1	1	1	0.0087	1.0978
(1.) Punching of 1 kg of core laminations	Electrical steel sheet	36	0.0006	3	4	1	1	1	0.0046	1.0582
	Electricity	36	0.0006	2	4	1	1	1	0.0032	1.0702
	Steel scrap	37	0.0006	3	4	1	1	1	0.0046	1.0582
(2.) Stacking and welding per cm of stator core length (electricity and argon input), and per kg of stacked stator core (other)	Electricity	38	0.0006	3	4	1	1	1	0.0046	1.0702
	Argon shielding gas	38	0.0006	4	4	1	1	1	0.0106	1.0702
	Stator laminations	39	0.0006	4	4	1	1	1	0.0106	1.1084
	Steel scrap	40	0.0006	3	4	1	1	1	0.0046	1.1084
(3.) Installation of slot insulation	Stator core	-	ANSYS Maxwell calculation.							1.0000
	PET foil	-	0.0006	2	4	1	1	1	0.0032	1.0582

Continued from previous page

Internal reference			***Uncertainty assessment***							
Unit process in model file	**Flow name**	**Report table no.**	**Basic factor[A]**	**Reliability[B]**	**Completeness[B]**	**Temporal correlation[B]**	**Geographical correlation[B]**	**Further technical correlation[B]**	**Log-transformed total variance – sum of all factors (σ^2)**	**Geometric standard deviation (GSD)**
(4.) Winding and phase isolation installation, per kg of installed magnet wire (total magnet wire and copper scrap), and per kg of stator package with winding, ready for pressing (other)	Magnet wire	(41)	0.0006	4	4	1	1	1	0.0106	1.1084
	Copper scrap	42	0.0006	4	4	1	1	1	0.0106	1.1084
	Magnet wire, installed as designed	-	ANSYS Maxwell calculation.							1.0000
	Stator core with slot insulation	-	Unaltered subpart input							1.0000
	Silicone cable isolation/tubing	-	0.0006	4	4	1	1	1	0.0106	1.1084
	Mica tape, glass fiber cloth content	-	0.0006	4	4	1	1	1	0.0106	1.1084
	Mica tape, mica content	-	0.0006	4	4	1	1	1	0.0106	1.1084
	Mica tape, silicone bond content	-	0.0006	4	4	1	1	1	0.0106	1.1084
(5.) Bandaging and pressing per piece	Stator package w winding, for pressing	-	Unaltered subpart input							1.0000
	Nylon lacing cord	-	0.0006	4	4	1	1	1	0.0106	1.1084
	Electricity	43	0.0006	3	4	1	1	1	0.0046	1.0702
(6.) Impregnation and curing per cm of stator diameter (electricity), per kg of cured resin (resin-related), per kg of stator package (unaltered input)	Electricity	44	0.0006	2	2	1	3	2	0.002	1.0457
	Silica filler in epoxy resin	45	0.0006	2	2	1	1	1	0.0013	1.0367
	Liquid epoxy resin	45	0.0006	2	2	1	1	1	0.0013	1.0367
	Hydrocarbons	46	0.12	4	2	1	1	1	0.1281	1.4303
	Stator package, bandaged	-	Unaltered subpart input							1.0000
(7.) Wire termination, per piece	Stator package, impregnated	-	Unaltered subpart input							1.0000
	Magnet wire, cutaway in wire term.	65	0.0006	4	4	1	1	1	0.0106	1.1084
	Copper lugs, tin plated	-	0.0006	3	4	1	1	1	0.0046	1.0702
	Electricity	65	0.0006	3	4	1	3	2	0.0053	1.0755
	Copper scrap	66	0.0006	3	4	1	1	1	0.0046	1.0702
(8.) Machine turning of a steel rod into 1 kg of shaft with proper dimensions	Steel rod	47	0.0006	4	4	1	1	1	0.0106	1.1084
	Cutting fluid, concentrated	47	0.0006	2	4	1	1	1	0.0032	1.0582
	Cutting fluid, water	47	0.0006	2	4	1	1	1	0.0032	1.0582
	Electricity	47	0.0006	2	4	1	1	1	0.0032	1.0582
	Steel scrap	48	0.0006	4	4	1	1	1	0.0106	1.1084
	Waste oil, conc. share in dilution	48	0.0006	2	4	1	1	1	0.0032	1.0582
(9.) Spline milling a 3.5 cm long section per cm of shaft diameter	Shaft, ready for splining	-	Unaltered subpart input							1.0000
	Cutting fluid, concentrated	49	0.0006	3	4	1	1	4	0.0446	1.2351
	Cutting fluid, water	49	0.0006	3	4	1	1	4	0.0446	1.2351
	Electricity	49	0.0006	3	4	1	1	4	0.0446	1.2351
	Waste oil, conc. share in dilution	50	0.0006	3	4	1	1	4	0.0446	1.2351
(10.) Induction surface hardening of a 3.5 cm long section of the shaft per cm of shaft diameter	Shaft in progress, ready for hardening	-	Unaltered subpart input							1.0000
	Quenching fluid, concentrated	51	0.0006	3	3	1	1	4	0.0432	1.2310
	Quenching fluid, water	51	0.0006	3	3	1	1	4	0.0432	1.2310
	Electricity	51	0.0006	3	3	1	1	4	0.0432	1.2310
	Waste quenching fluid, conc. share	52	0.0006	3	3	1	1	4	0.0432	1.2310

Continued from previous page

Internal reference			***Uncertainty assessment***							
Unit process in model file	**Flow name**	**Report table no.**	**Basic factor[A]**	**Reliability[B]**	**Completeness[B]**	**Temporal correlation[B]**	**Geographical correlation[B]**	**Further technical correlation[B]**	**Log-transformed total variance – sum of all factors (σ^2)**	**Geometric standard deviation (GSD)**
(11.) Stacking of rotor laminations, magnet mounting and fixation, per cm (electricity) and per kg (other) of stacked rotor core	Electricity	53	0.0006	3	4	1	1	2	0.0052	1.0748
	Rotor laminations/core	-	ANSYS Maxwell calculation.							1.0000
	Nd(Dy)FeB nickel coated magnet	-	ANSYS Maxwell calculation.							1.0000
	Magn. fix. resin, methacrylate ester	-	0.0006	2	4	1	1	2	0.0038	1.0636
(12.) Punching of 1 kg of stainless steel rotor endplates	Stainless steel sheets	54	0.0006	2	4	1	1	1	0.0032	1.0582
	Electricity	54	0.0006	2	4	1	1	1	0.0032	1.0582
	Steel scrap	55	0.0006	2	4	1	1	1	0.0032	1.0582
(13.) Assembling and pressing the rotor package onto the shaft, per piece	Stacked rotor core with magnets	-	Unaltered subpart input							1.0000
	Shaft	-	*0.06*	4	4	1	1	1	0.07	1.3029
	Stainless steel rotor endplates	-	0.0006	4	4	1	1	1	0.0106	1.1084
	Electricity	56	0.0006	3	4	1	1	1	0.0046	1.0702
(14.) Balancing the rotor, per piece	Rotor package on shaft, unbalanced	-	Unaltered subpart input							1.0000
	Electricity	57	0.0006	3	4	1	1	1	0.0046	1.0702
(15.) Machining of housing parts, per 100 g of aluminum removed during surface trimming of the housing body (accounting for 50% of the material removed)	Die cast, unfinished housing body	-	0.0006	4	4	1	1	2	0.0112	1.1116
	Cutting fluid, concentrated	58	0.0006	2	4	1	1	1	0.0032	1.0582
	Cutting fluid, water	58	0.0006	2	4	1	1	1	0.0032	1.0582
	Electricity	58	0.0006	2	4	1	1	1	0.0032	1.0582
	Aluminum scrap	59	0.0006	4	4	1	1	2	0.0112	1.1116
	Waste oil, conc. share in dilution	59	0.0006	2	4	1	1	1	0.0032	1.0582
(15.) Machining of housing parts, per housing body (piece) for other machining operations (accounting for 50% of the material removed)	Housing body, surface trimmed	-	0.0006	4	4	1	1	1	0.0112	1.0582
	Cutting fluid, concentrated	60	0.0006	2	4	1	1	1	0.0032	1.0582
	Cutting fluid, water	60	0.0006	2	4	1	1	1	0.0032	1.0582
	Electricity	60	0.0006	2	4	1	1	1	0.0032	1.0582
	Aluminum scrap	61	0.0006	2	4	1	1	1	0.0032	1.0582
	Waste oil, conc. share in dilution	61	0.0006	2	4	1	1	1	0.0032	1.0582
(15.) Machining of housing parts, per endbell (piece) subject to both surface trimming and other machining operations	Die cast, unfinished endbells	-	0.0006	4	4	1	1	1	0.0106	1.1084
	Cutting fluid, concentrated	62	0.0006	2	4	1	1	1	0.0032	1.0582
	Cutting fluid, water	62	0.0006	2	4	1	1	1	0.0032	1.0582
	Electricity	62	0.0006	2	4	1	1	1	0.0032	1.0582
	Aluminum scrap	63	0.0006	4	4	1	1	1	0.0106	1.1084
	Waste oil, conc. share in dilution	63	0.0006	2	4	1	1	1	0.0032	1.0582
(16.) Cleaning, per piece	Housing, to cleaning	-	Unaltered subpart input							1.0000
	Electricity	64	0.0006	3	4	1	1	1	0.0046	1.0702
(17.) Mounting, per piece	Housing, ready for assembly	-	*0.07*	3	3	1	1	1	0.0726	1.3092
	PBT part, terminal block	-	0.0006	3	4	1	1	1	0.0046	1.0702

Continued from previous page

Internal reference			***Uncertainty assessment***							
Unit process in model file	**Flow name**	**Report table no.**	**Basic factor[A]**	**Reliability[B]**	**Completeness[B]**	**Temporal correlation[B]**	**Geographical correlation[B]**	**Further technical correlation[B]**	**Log-transformed total variance – sum of all factors (σ^2)**	**Geometric standard deviation (GSD)**
(18.) End assembly, per piece	Stator package, complete, for ass.	-	Unaltered subpart input							1.0000
	Rotor package, on shaft, for assembly	-	Unaltered subpart input							1.0000
	Housing and PBT terminal block	-	Unaltered subpart input							1.0000
	Bearings	-	0.0006	2	4	1	1	1	0.0032	1.0582
	Galvanized fasteners and plates	-	0.0006	4	4	1	1	1	0.0106	1.1084
	Electricity	67	0.0006	2	4	1	1	1	0.0032	1.0582
(19.) Painting, per 100 g of dried varnish on the electrical machine housing	Assembled motor, ready for painting	-	Unaltered subpart input							1.0000
	Liquid varnish, solid share	68	0.0006	2	4	1	1	1	0.0032	1.0582
	Liquid varnish, solvent share	68	0.0006	2	4	1	1	1	0.0032	1.0582
	Electricity	68	0.0006	3	4	1	1	1	0.0046	1.0702
	VOC	69	0.04	2	4	1	1	1	0.0426	1.2292
Technical building services, motor factory	Electricity for heating	70	0.0006	2	4	1	1	1	0.0032	1.0582
	Electricity for basic functions	70	0.0006	2	4	1	1	1	0.0032	1.0582
	Electricity for general work	70	0.0006	2	4	1	1	1	0.0032	1.0582
	Electricity for compressed air	70	0.0006	2	4	1	1	1	0.0032	1.0582